



**HAL**  
open science

# Carbonylation Reactions Using Single-Atom Catalysts

Lole Jurado, Sergio Posada-pérez, M. Rosa Axet

► **To cite this version:**

Lole Jurado, Sergio Posada-pérez, M. Rosa Axet. Carbonylation Reactions Using Single-Atom Catalysts. ChemCatChem, In press, pp.e202400543. 10.1002/cctc.202400543 . hal-04666537

**HAL Id: hal-04666537**

**<https://hal.science/hal-04666537v1>**

Submitted on 1 Aug 2024

**HAL** is a multi-disciplinary open access archive for the deposit and dissemination of scientific research documents, whether they are published or not. The documents may come from teaching and research institutions in France or abroad, or from public or private research centers.

L'archive ouverte pluridisciplinaire **HAL**, est destinée au dépôt et à la diffusion de documents scientifiques de niveau recherche, publiés ou non, émanant des établissements d'enseignement et de recherche français ou étrangers, des laboratoires publics ou privés.



Distributed under a Creative Commons Attribution - NonCommercial - NoDerivatives 4.0 International License

# Carbonylation Reactions Using Single-Atom Catalysts

Lole Jurado,<sup>[a]</sup> Sergio Posada-Pérez,<sup>[b]</sup> and M. Rosa Axet<sup>\*,[c]</sup>

The development of highly efficient and selective catalysts for carbonylation reactions represents a significant challenge in catalysis. Single-atom catalysts (SACs) have postulated as promising candidates able to combine the strengths of both homogeneous and heterogeneous catalysts. In this paper, we review recent advances in tailoring solid supports for SACs to enhance their catalytic performance in carbonylation reactions. We first discuss the effect of supports on the hydroformylation

reaction catalysed by SACs, followed by recent advances for methanol, ethanol, and dimethyl ether carbonylation reactions, focusing on the design of halide-free catalysts with improved activity and stability. Finally, oxidative carbonylation is discussed. Overall, this review highlights the importance of tailoring solid supports for SACs to achieve highly active and selective catalysts in carbonylation reactions, paving the way for future developments in sustainable catalysis.

## Introduction

The introduction of a carbonyl group in an organic molecule, known generally as carbonylation reaction, is a versatile methodology to produce aldehydes, ketones, esters, amides and other derivatives. The first examples of carbonylation reactions are transition-metal-catalysed, but other types of carbonylative transformations also exist, such as, free-radical and transition-metal radical, and cationic or anionic carbonylation reactions. Among them, transition-metal-catalysed carbonylations are the most common due to their versatility and the use of mild reaction conditions.<sup>[1–4]</sup>

The carbonylation of propylene was discovered by Otto Roelen in 1938.<sup>[5]</sup> He found that propylaldehyde and diethylketone were produced when adding ethylene to a Fischer-Tropsch reaction.<sup>[6]</sup> Nowadays, this reaction is known as hydroformylation or oxo synthesis,<sup>[7–12]</sup> and it is among the homogeneously catalysed reactions that find applications in industry, generating aldehydes and alcohols from alkenes, with production exceeding 12 million tons annually.<sup>[12]</sup> The carbonylation of methanol to produce acetic acid is a widely used industrial process as well, also homogeneously catalysed by transition metals. W. J. Reppe, in 1941, discovered this carbonylation reaction using iron, cobalt, and nickel carbonyls or halides under harsh reactions conditions (50–70 MPa and 250–270 °C).<sup>[2]</sup> Later, more

efficient processes have been described for the synthesis of acetic acid from methanol, using a Rh- or Ir-based catalysts. The Monsanto process operates from 1967 using a Rh-based catalyst in mild reaction conditions (3–4 MPa and 180–220 °C). The Cativa process, using an Ir-based catalyst, less expensive than Rh, was introduced in 1996.<sup>[13]</sup> Pivalic acid is also obtained industrially by the hydrocarboxylation of isobutene via the Koch reaction. Besides their industrial impact, carbonylation reactions are nowadays a powerful tool to obtain carbonyl-containing compounds from a plethora of substrates including organic halides, alkenes, alkynes, or even simply C–H, C–C, and C–N bonds.<sup>[14,15]</sup> Given the industrial importance of these carbonylation reactions and their future applications, and considering the general use of costly and scarcely metals, several strategies have been proposed over the years in order to decrease the economic and environmental impact of these processes. The biphasic system for hydroformylation is an excellent example of keeping a high activity and selectivity of homogeneous catalysis while overcoming the issue of catalyst separation inherent to homogeneous catalysed processes.<sup>[16,17]</sup> Heterogeneous catalysts could be a solution to overcome metal and ligand losses, although usually at the cost of activity and selectivity, and proceeding as well, at harsher reaction conditions. Specifically, in carbonylation reactions, which often require the use of scarce and expensive transition metals, the research of new and low-cost heterogeneous catalyst alternatives is of high interest. The use of heterogeneous catalysts has been described for carbonylation reactions, mainly for hydroformylation.<sup>[18–20]</sup> Yet, the true catalytic species operating in these catalysed reactions not being deeply investigated in many cases. For instance, under hydroformylation conditions is very common to produce unmodified hydridorhodium carbonyl species from rhodium complexes,<sup>[9]</sup> or clusters,<sup>[21]</sup> and most probably from single-atom catalysts (SACs).<sup>[22–25]</sup> SACs have emerged as an approach that could be described as a bridging gap between homogeneous and heterogeneous catalysis.<sup>[26–36]</sup> SACs combine the use of isolated metal atoms, as in homogeneous catalysis, which are highly dispersed on a support, enabling recyclability as in heterogeneous catalysis. In other words, SACs mimic the reactivity and selectivity of homogeneous catalysts with the

[a] L. Jurado  
 Instituto de Ciencia de Materiales de Sevilla, Centro Mixto CSIC-Universidad de Sevilla, Av. Américo Vespucio 49, 41092 Sevilla, Spain

[b] S. Posada-Pérez  
 Institut de Química Computacional i Catàlisi and Departament de Química, Universitat de Girona, c/ Maria Aurèlia Capmany 69, 17003 Girona, Catalonia, Spain

[c] M. R. Axet  
 CNRS, LCC (Laboratoire de Chimie de Coordination), Université de Toulouse, UPS, INPT, 205 route de Narbonne, F-31077 Toulouse Cedex 4, France  
 E-mail: rosa.axet@lcc-toulouse.fr

© 2024 The Authors. ChemCatChem published by Wiley-VCH GmbH. This is an open access article under the terms of the Creative Commons Attribution Non-Commercial NoDerivs License, which permits use and distribution in any medium, provided the original work is properly cited, the use is non-commercial and no modifications or adaptations are made.

advantages of the supported ones. SACs demonstrate highly catalytic efficiency owing to their singular metal atoms dispersed onto support materials since it maximizes the catalytic activity per metal atom,<sup>[26]</sup> in contrast to metal nanoparticles (NPs) based catalysts where only surface atoms participate in the catalytic process. This enhanced reactivity is attributable to the greater accessibility of the isolated metal atoms, the higher metallic surface available, and different mechanism that may operate.<sup>[37–40]</sup> In the development of SACs, it is important to consider the robustness, the nature of the metal-support interaction and the surrounding chemical environment to prevent leaching issues and to provide to the metal the desired electronic structure. It is also crucial to consider the non-innocent role of the support to the reaction mechanism. SACs can leverage the metal utilization due to the low coordination of single metal atoms and offer tunability of catalytic sites on the support. They are sensitive to the structural and electronic properties of the support, which play a crucial role on the performance of the catalysts. Understanding and controlling the local coordination environment of SACs on the support is essential to elucidate and optimize catalytic activity and selectivity, minimizing undesired side reactions. Thus, SACs represent a promising frontier in catalysis, offering superior atom efficiency, reactivity, selectivity, stability, and tailored electronic structure compared to NP catalysts. These attributes render SACs invaluable for a plethora of catalytic applications, particularly for carbonylation reactions. The potential of SACs for applications in carbonylation reactions has been identified in recent years, and research on this area is emerging, however, it is still in its infancy and further research is needed to elucidate the mechanisms operating in carbonylation reactions. To reach this aim the combination of theoretical

calculations<sup>[41]</sup> together with advanced (in situ and operando) characterization techniques<sup>[29,42]</sup> is essential. In this review, we discuss recent trends in carbonylation reactions catalysed by isolated metallic single sites. While existing reviews have covered the use of single sites for catalysis,<sup>[26–36]</sup> and particularly focusing on hydroformylation<sup>[18–20]</sup> and methanol carbonylation,<sup>[2]</sup> none have specifically addressed the use of this family of catalysts for carbonylation reactions, despite these reactions sharing some mechanistic similarities and utilizing similar methodologies such as synthesis, catalysis, theoretical calculations and characterisation. Hydroformylation is the carbonylation reaction that has been more studied up to now using SACs, for this reason, recent publications review the topic,<sup>[18–20]</sup> therefore, below only representative and recent examples are detailed. Furthermore, recent examples on the use of SACs for alcohol carbonylation are detailed. A relatively recent review deals with the production of acetic acid from methanol catalysed by homogeneous and heterogeneous catalysts,<sup>[2]</sup> yet several recent examples of SACs for this application are not included. Oxidative carbonylation of methane<sup>[14,43, 44]</sup> is latter discussed together with other kinds of carbonylation reactions. Finally, a summary in which the accomplishments on the field are succinctly presented with some emerging strategies and challenges of SACs for carbonylation reactions.

## Hydroformylation

The hydroformylation reaction allows the insertion of CO and H<sub>2</sub> into an unsaturated compound producing aldehydes or its derivatives (Figure 1). The reaction is typically catalysed with



Lole Jurado completed her PhD in Chemistry at the University of Strasbourg in 2020, under the supervision of Profs. Anne-Cécile Roger and Sébastien Thomas. She has worked as a postdoctoral researcher in France (LCC-CNRS, Toulouse) and Spain (ICIQ, Tarragona). Currently, she is working at ICMSE (CSIC) in Sevilla. Her research interests focus on the design and development of heterogeneous catalysts to make industrial processes more eco-friendly and cost-effective. Her experience spans from the synthesis of catalysts for use in biomass gasification pilot plants to the design of single-atom catalyst for producing highly valuable products.



Sergio Posada Pérez is a Marie Curie postdoctoral researcher at Institut de Química Computacional i Catalisi (IQCC) at the University of Girona. He obtained his PhD in Theoretical Chemistry and Computational modelling from the University of Barcelona in 2018. His current research mainly focuses on the application of density functional theory in catalytic processes, both heterogeneous and homogeneous, and in materials modelling for energy conversion and storage.



M. Rosa Axet specializes in the study of catalytic nanomaterials, including multimetallic, supported, colloidal, shape-controlled, and single-site. She has been a CNRS researcher at LCC-CNRS in Toulouse since 2010. She received her PhD in 2006 from Universitat Rovira i Virgili under the supervision of C. Claver and S. Castillon, focusing on chiral homogeneous catalysis. She pursued postdoctoral research in organometallic chemistry and catalysis (in Trieste with B. Milani and in Paris with H. Amouri), as well as in nanomaterials (in Toulouse with B. Chaudret and K. Philippot). She has co-authored over 50 publications in these fields.

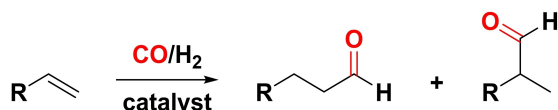


Figure 1. Hydroformylation reaction.

homogeneous catalysts based on Rh and Co, which are typically modified with phosphorous ligands.<sup>[7–11]</sup> Due to the use of an expensive metal, ligands with no negligible economic value, and the fact that in homogeneous catalysis their recovery is difficult after reaction, several strategies have been developed over the years, including homogeneous biphasic systems<sup>[16,17]</sup> and heterogeneous catalysts.<sup>[18–20]</sup> Recently, SACs have been postulated as powerful catalytic tool for hydroformylation, and a clear trend seems to be materializing in recent works, focussing on the engineering of the supports to accommodate metal atoms, mainly Rh, but also Co and Ru, providing them stability and specific electronic configurations. Indeed, the stability and catalytic performance of single centres in SACs are strongly influenced by their chemical environment, i.e. surrounding atoms or surface functional groups, inherent to the surface of the support.<sup>[45]</sup> Understanding the influence of the local environment in the catalytic performances is, thus, crucial. The properties that supports confer to the single sites can be compared, to a certain extent, to the role of ligands in homogeneous catalysis: supports supply anchoring sites for stabilizing single centres, and significantly impact their catalytic behaviour, mainly modulating the metal-support interaction, but also participating during catalysis. For hydroformylation reactions using SACs a wide-range of supports such as metal oxides,<sup>[22,40, 46–55]</sup> zeolites,<sup>[56–58]</sup> metal-organic frameworks (MOFs),<sup>[59]</sup> porous organic polymers (POPs),<sup>[20,60–65]</sup> carbon-based materials,<sup>[23,38, 66]</sup> supported ionic liquid phase (SILP),<sup>[67–71]</sup> and other supports such phosphates<sup>[72]</sup> and carbides<sup>[73]</sup> have been recently reported. Recent examples on SACs for hydroformylation are discussed below regarding the role of support in the stabilization, local coordination environment, and their catalytic performance.

### Non-Reducible Metal Oxides

The electronic properties of single sites, and subsequently their catalytic properties, can be adjusted by charge transfer, electron polarization, and/or electronic confinement, when supported on metal oxides. Despite the low concentration of defects, the presence of unsaturated coordination sites and -OH groups on the surface of non-reducible oxides such as Al<sub>2</sub>O<sub>3</sub> and SiO<sub>2</sub> could potentially contribute to effectively stabilizing isolated metal centres.<sup>[74,75]</sup> Active metals may react with oxygen ions on the surface, forming metal-oxo/hydroxyl groups, leading to highly dispersed single metal centres. Unfortunately, these features may be insufficient to enhance the metal-support interaction and stabilize isolated metal centres, requiring additional modifications of the supports.<sup>[75]</sup> For hydroformylation, the use of non-reducible oxides as supports has been described

as a good strategy to provide performant catalysts; nevertheless, recent works use additional modifications to improve the stability and catalytic performance of single metal centres on those supports (Table 1). For instance, the modification of the local electronic environment of Rh single sites on Al<sub>2</sub>O<sub>3</sub> (Rh/Al<sub>2</sub>O<sub>3</sub>) by adding ReO<sub>x</sub> (Rh-ReO<sub>x</sub>/Al<sub>2</sub>O<sub>3</sub>) did result in an improvement in the catalytic performances in the hydroformylation of ethylene.<sup>[49]</sup> The impact of ReO<sub>x</sub> on the electronic properties of Rh sites was confirmed by a blue shift in the CO stretching frequencies of the Rh gem-dicarbonyl species (–Rh(CO)<sub>2</sub>) in IR. These shifts, attributed to electron withdrawal by Lewis acidic ReO<sub>x</sub> species, intensified by increasing ReO<sub>x</sub> loading and pointed to a greater cationic character of Rh sites due to the dispersion of Rh near ReO<sub>x</sub> species. The presence of ReO<sub>x</sub> (Rh-ReO<sub>x</sub>/Al<sub>2</sub>O<sub>3</sub>) enhanced the turnover frequency (TOF) of the reaction by approximately 44 times with respect to the unmodified Rh/Al<sub>2</sub>O<sub>3</sub>. Moreover, a linear correlation between TOF and CO stretching of Rh gem-dicarbonyl species (depending on Re loading) was found. Lee et al.<sup>[51]</sup> studied at the theoretical level the influence of ReO<sub>x</sub> as promoter in the Rh/γ-Al<sub>2</sub>O<sub>3</sub> system for the hydroformylation of ethylene. Density functional theory (DFT) was employed to unveil the effect of ReO<sub>x</sub> combined with single Rh atoms. It was found that without ReO<sub>x</sub> the CO insertion step is the key step for the reaction rate, while the presence of ReO<sub>x</sub> reduces the Rh-CO interaction and ReO<sub>x</sub> improved the selectivity of propanal by blocking the main hydrogenation through steric effects. Similarly to Rh-ReO<sub>x</sub>/Al<sub>2</sub>O<sub>3</sub>, Rh-WO<sub>x</sub> isolated pairs on Al<sub>2</sub>O<sub>3</sub> and SiO<sub>2</sub> have demonstrated enhanced catalytic performance in ethylene hydroformylation and remarkable stability.<sup>[54]</sup> Specifically, Rh-0.7WO<sub>x</sub>/Al<sub>2</sub>O<sub>3</sub> exhibited a higher TOF for propanal formation, surpassing Rh/Al<sub>2</sub>O<sub>3</sub> by 18 times; also higher selectivity towards propanal (53 %) compared to unmodified Rh/Al<sub>2</sub>O<sub>3</sub> (16 %). Mechanistic insights revealed that the presence of WO<sub>x</sub> reduced the apparent activation barrier for propanal formation and showed a positive order with CO concentration, which is in contrast with the negative order in CO observed on Rh/Al<sub>2</sub>O<sub>3</sub>. In addition, kinetic isotope effect (KIE, rate<sub>H2</sub>/rate<sub>D2</sub>) for Rh-0.7WO<sub>x</sub>/Al<sub>2</sub>O<sub>3</sub> (KIE of 2.02) compared to Rh/Al<sub>2</sub>O<sub>3</sub> (KIE of 1.04) revealed modifications in the reaction mechanism due to the local interaction of Rh with WO<sub>x</sub>. Taking into consideration these observations, the authors proposed a bifunctional mechanism involving Rh-WO<sub>x</sub> pairs dynamically reconfiguring their coordination during the catalytic cycle facilitated high-selectivity hydroformylation, enabling elevated rates. For hydroformylation, modification of SiO<sub>2</sub> as a support with other oxides for SACS is still lacking. Yet, recently the introduction of Al into previously modified Rh/SiO<sub>2</sub> catalysts with tethered diphenylphosphinopropyl (DPPPTS) led to an improvement of the catalytic performance, regardless of the Al/Rh ratio, in the hydroformylation of ethylene.<sup>[46]</sup> An Al/Rh ratio of 1 was, by far, the most active catalyst, reaching a TOF of about four times higher, 134 h<sup>-1</sup>, than the bare Rh, TOF of 34 h<sup>-1</sup>, over a reaction time of 144 h. The role of Al was to improve the Rh dispersion, and also, to provide weak Brønsted and Lewis acid sites, as ascertained by pyridine absorbed FT-IR and NH<sub>3</sub>-TPD, which impacted in the reaction outcome. An excellent Rh SAC for styrene hydroformylation based in ZnO

**Table 1.** Hydroformylation using single-atom catalysts based on solid supports.

Catalyst	Substrate	TOF (h <sup>-1</sup> )	Selectivity (%)	l:b	Reaction conditions	Ref.
0.20%Rh/2.9%ReO <sub>x</sub> -Al <sub>2</sub> O <sub>3</sub>	ethylene	10.8	45	–	C <sub>2</sub> H <sub>4</sub> /CO/H <sub>2</sub> 1:1:1, total flow of 30 mL min <sup>-1</sup> , 150 °C; fixed bed reactor	49
0.23%Rh-0.7%WO <sub>x</sub> /Al <sub>2</sub> O <sub>3</sub>	ethylene	37.4	95	–	420 mg of catalyst, 0.1 MPa C <sub>2</sub> H <sub>4</sub> /CO/H <sub>2</sub> 1:1:1, total flow of 30 mL min <sup>-1</sup> , 150 °C; fixed bed reactor	54
0.10%Rh/SnO <sub>2</sub>	ethylene	225	> 95	–	2 MPa C <sub>2</sub> H <sub>4</sub> /CO/H <sub>2</sub> 1:1:1, 150 °C; fixed bed reactor	40
0.20%Rh/CoO	propene	2065	94.4	15	50 mg of catalyst, 3 MPa CO/H <sub>2</sub> 1:1, 0.16 MPa C <sub>3</sub> H <sub>6</sub> , isopropanol, 2 h, 100 °C	48
0.06%Rh/CeO <sub>2</sub> -V <sub>0</sub>	propene	5072	100	0.7	20 mg of catalyst, 3 MPa CO/H <sub>2</sub> 1:1, 0.2 MPa C <sub>3</sub> H <sub>6</sub> , n-heptane, 0.5 h, 100 °C	55
0.07%Rh/1%MnO <sub>x</sub> -CeO <sub>2</sub>	propene	7200	100	0.7	20 mg of catalyst, 3 MPa CO/H <sub>2</sub> 1:1, 0.2 MPa C <sub>3</sub> H <sub>6</sub> , n-heptane, 0.5 h, 100 °C	78
0.06%Rh/Xantphos(P) <sub>3</sub> -CeO <sub>2</sub>	propene	476	100	13	0.6 MPa CO/H <sub>2</sub> 1:1, 0.2 MPa C <sub>3</sub> H <sub>6</sub> , n-heptane, 2 h, 100 °C	79
0.06%Rh/Xantphos(P) <sub>3</sub> -CeO <sub>2</sub>	1-octene	407	31	36	4.6 mmol of substrate, 0.6 MPa CO/H <sub>2</sub> 1:1, n-heptane, 2 h, 100 °C	79
0.06%Rh/Xantphos(P) <sub>3</sub> -CeO <sub>2</sub>	styrene	127	84	1.6	4.6 mmol of substrate, 0.6 MPa CO/H <sub>2</sub> 1:1, n-heptane, 2 h, 100 °C	79
0.006%Rh/ZnO-w	styrene	3333	99	1	10 <sup>-5</sup> mmol Rh, 2.5 mmol of substrate, 1.6 MPa CO/H <sub>2</sub> 1:1, toluene, 12 h, 100 °C	47
0.24%Rh-Co-P/ZnO	styrene	1457	80	1.6	12.5 mg of catalyst, 2 mmol of substrate, 4 MPa CO/H <sub>2</sub> 1:1, THF, 4 h, 100 °C	53
Rh/CeO <sub>2</sub>	styrene	130	97	1.1	Rh/styrene 1:500, 1 MPa CO/H <sub>2</sub> 1:1, benzene, 12 h, 90 °C	50
Rh <sub>1</sub> /CeO <sub>2</sub>	styrene	4.5	98	3	0.007 mmol of Rh, 50 mg of substrate, 3 MPa CO, dioxane + H <sub>2</sub> O, 12 h, 120 °C	22
0.81%Rh <sub>1</sub> /Y	1-hexene	106	100	2.2	50 mg of catalyst, 3 mmol of substrate, 6 MPa CO/H <sub>2</sub> 1:1, toluene, 1 h, 60 °C	88
Rh <sub>1</sub> /MFI-cal	ethylene	99	92	–	100 mg of catalyst, 0.1 MPa C <sub>2</sub> H <sub>4</sub> /CO/H <sub>2</sub> /N <sub>2</sub> 1:1:1:0.5, total flow of 35 mL min <sup>-1</sup> , 90 °C; fixed bed reactor	58
Rh <sub>1</sub> /MFI-cal	propene	18.3	68	4.2	30 mg of catalyst, 0.1 MPa C <sub>3</sub> H <sub>6</sub> /CO/H <sub>2</sub> /N <sub>2</sub> 0.6:0.6:0.6:1, total flow of 14 mL min <sup>-1</sup> , 120 °C; fixed bed reactor	58
0.50%Rh/PNP-ND	1-octene	103	90	1.5	50 mg of catalyst, 3 mmol of substrate, 3 MPa CO/H <sub>2</sub> 1:1, toluene, 12 h, 60 °C	23
0.50%Rh/PNP-ND	1-decene	77.3	80	1.28	50 mg of catalyst, 3 mmol of substrate, 3 MPa CO/H <sub>2</sub> 1:1, toluene, 16 h, 70 °C	23
0.50%Rh/PNP-ND	styrene	95	> 99	0.08	50 mg of catalyst, 3 mmol of substrate, 3 MPa CO/H <sub>2</sub> 1:1, toluene/H <sub>2</sub> O, 10 h, 50 °C	23
0.0125%Ru@NC	1-hexene	208.3	100	3.2	100 mg of catalyst, 3.2 mmol of substrate, 4 MPa CO/H <sub>2</sub> 1:1, 2 h, 150 °C	38
0.10%Rh/ECN	styrene	125	82	1.6	2×10 <sup>-3</sup> mmol of Rh, 1 mmol of substrate, 2 MPa CO/H <sub>2</sub> 1:1, THF, 2 h, 90 °C	66
5%Co/β-Mo <sub>2</sub> C	propene	66	89	1.3	50 mg of catalyst, 0.6 MPa C <sub>3</sub> H <sub>6</sub> , 4 MPa CO/H <sub>2</sub> 1:1, toluene, 10 h, 160 °C	73
15%CoZrP-2.0	1-octene	2.3	92	1.6	50 mg of catalyst, 4 MPa CO/H <sub>2</sub> 1:1, toluene, 6 h, 160 °C	72

was described by Zang et al. (Figure 2 (a)).<sup>[47]</sup> The authors describe a turnover number (TON) of 40000 h<sup>-1</sup>, 99% aldehyde selectivity displaying a linear-to-branched ratio (l:b) of 1, outperforming the homogeneous [RhCl(PPh<sub>3</sub>)<sub>3</sub>], at 100 °C in toluene under 16 bar of CO/H<sub>2</sub> 1:1. X-ray photoelectron spectroscopy (XPS) analyses in Rh/ZnO samples consisting in single sites pointed that a mixture of Rh<sup>3+</sup>/Rh<sup>+</sup> species coexist in the material. A latter work using Rh as SAC on ZnO describes the effect of modification of the support on its catalytic properties.<sup>[53]</sup> ZnO was doped with Co and/or P to produce Co/ZnO, P/ZnO and Co-P/ZnO (Figure 2 (b)). XPS and diffuse

reflectance infrared Fourier transform spectroscopy (DRIFTS) after CO exposure show that in the absence of P, Rh NPs are formed, and the atomically dispersed Rh in Rh-P/ZnO and Rh-Co-P/ZnO display an oxidation state of Rh<sup>3+</sup>. Upon testing all catalysts in hydroformylation of a wide range of olefins (including 1-decene, styrene, among others), a remarkable increase in the regioselectivity was observed for the Co modified catalysts (Co/ZnO and Co-P/ZnO). The highest l:b, reaching a value of 2.1, was achieved using Rh-Co-P/ZnO. After further mechanistic studies, the authors suggest that Co altered the electronic environment of Rh modifying the coordination



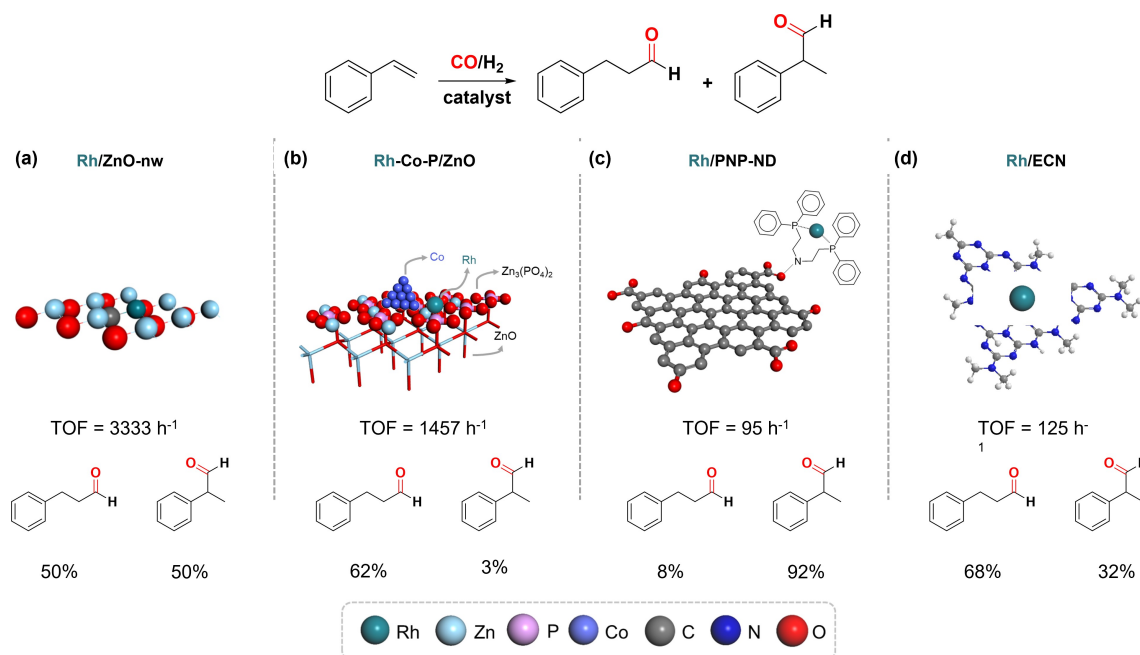


**Figure 2.** Styrene hydroformylation using Rh single atoms supported on (a) ZnO-w,<sup>[47]</sup> (b) Co-P/ZnO,<sup>[53]</sup> (c) PNP-ND,<sup>[23]</sup> and (d) ECN.<sup>[66]</sup>

mode of the alkene in turn, thus increasing selectivity towards the lineal aldehyde, while P is responsible of the dispersibility of Rh on the support, avoiding the formation of NPs.

### Reducible Metal Oxides

Reducible oxides host several types of defects in their structure, such as oxygen and metal vacancies, edges, steps, or terraces, which serve as suitable anchor sites for stabilizing single centres. However, controlling the direct chemical environment in reducible oxides-supported SACs remains challenging as any of the aforementioned defects can serve as anchor centre.<sup>[76,77]</sup> In recent years, significant efforts have been made to understand how the chemical environment of single atoms supported on reducible oxides influences the catalytic performance in hydroformylation reactions (Table 1). These examples include the work of Wang et al. in which Rh single atoms supported on CoO displayed an exceptional catalytic performance in propylene hydroformylation, with comparable reactivity as its homogeneous counterpart.<sup>[48]</sup> At low Rh loading (0.2 wt%), Rh was incorporated in the CoO structure by replacing two Co atoms in which a Co vacancy was involved (Figure 3), while Rh clusters were observed at higher loadings (> 1 wt%). K-edge X-ray absorption near edge structure (XANES) profiles of Rh revealed the formation of Rh–O shell for 0.2%Rh/CoO, leading to a well dispersed Rh atoms on the support. An additional new peak associated to Rh–Rh bonds was observed at higher Rh loadings (1.0% and 4.8% Rh NPs/CoO), attributed to Rh nanoclusters. XANES and XPS results revealed the existence of Rh in higher oxidation state for Rh single atoms (0.2%Rh/CoO) than Rh nanoclusters (1.0% and 4.8% Rh NPs/CoO). Only Rh<sup>3+</sup> species were found in the former, while in the later Rh<sup>3+</sup>

coexisted with metallic Rh species. The Rh single atom catalyst exhibited the best catalytic performances, achieving the highest TOF, 2065 h<sup>-1</sup>, with a remarkable chemoselectivity to the formation of butyraldehyde (94%), which was preserved even after five catalytic rounds. Interestingly, a notable regioselectivity (l:b about 16), favouring the formation of linear aldehyde, was observed for Rh single atoms. Contrary, Rh nanoclusters led to a decrease in TOF (1000 h<sup>-1</sup> for 1%Rh/CoO and < 500 h<sup>-1</sup> for 4.8%Rh/CoO) and chemoselectivity (68.7% for 1%Rh/CoO and 53.9% for 4.8%Rh/CoO), without apparent improvement in the regioselectivity. The reconstruction of the environment of Rh single atoms upon exposure to the reaction mixture promoted the adsorption and activation of the reactant, thereby enhancing the catalytic performance in hydroformylation of propylene. As revealed by in situ DRIFTS and XPS measurements, the interaction between propylene and CO with Rh single atoms was enhanced during the use of the reaction gas mixture. DFT calculations demonstrated that deviations of Rh single atoms towards the centre of the unit cell and displacement out of the plane in the atmosphere containing both H<sub>2</sub> and CO resulted in an increase in the adsorption energy of propene (from –0.46 to 0.80 eV). The regioselectivity in the hydroformylation reaction appears to be influenced by the site of H addition to the C=C bond of the olefin. Co-adsorbed configurations of reactants and catalysts were also established. Discrete Rh single atoms restrict the H adsorption configuration and, consequently, limit the variety of addition pathways. Analysis of the reaction paths derived from the two most stable co-adsorbed configurations indicates that the formation of linear aldehyde was kinetically favourable, explaining the high regioselectivity observed for Rh single atoms compared to their nanocluster counterparts.

Recent studies have evaluated the impact of various metal oxide-based supports on both the activity and selectivity of Rh-

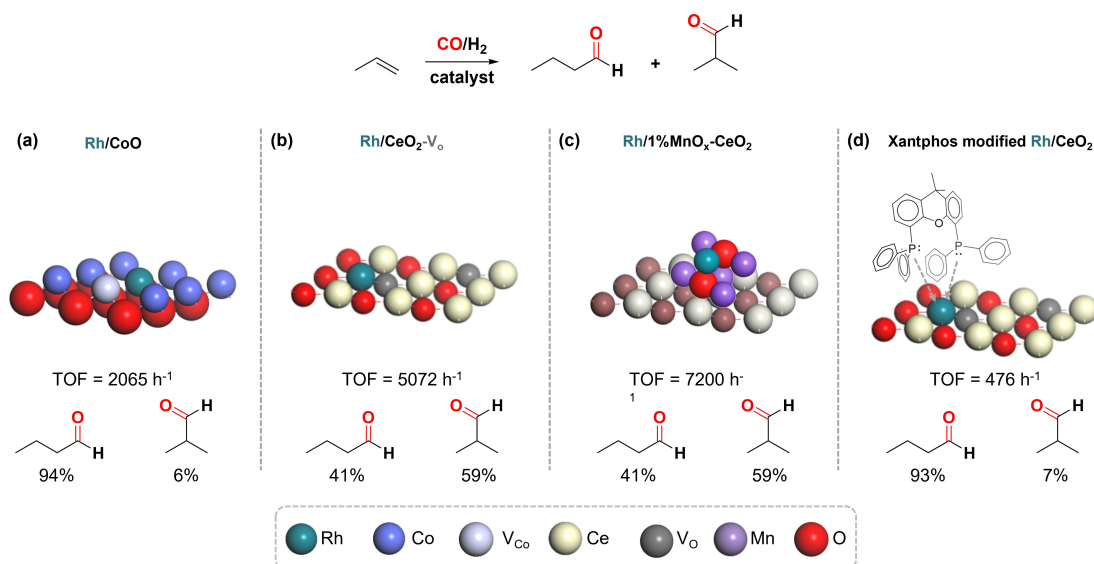


**Figure 3.** Propene hydroformylation using Rh single atoms supported on (a) CoO,<sup>[48]</sup> (b) CeO<sub>2</sub>-V<sub>o</sub>,<sup>[55]</sup> (c) 1%MnO<sub>x</sub>-CeO<sub>2</sub>,<sup>[78]</sup> and (d) Xantphos modified CeO<sub>2</sub> (V<sub>co</sub> cobalt vacancy; V<sub>o</sub>, oxygen vacancy).<sup>[79]</sup>

based SACs. Amsler et al.<sup>[50]</sup> compared Rh SACs based on MgO and CeO<sub>2</sub> experimentally and at a theoretical level for styrene hydroformylation. Rh/CeO<sub>2</sub> was found highly active displaying a TOF 130 h<sup>-1</sup>, with a 97% of aldehyde selectivity, I:b 1.1 (at 90 °C in octane under 1 MPa of CO/H<sub>2</sub> 1:1); outperforming Rh/MgO. The coordination of Rh to the support was found key to explain these results; in Rh/CeO<sub>2</sub>(111) the CO insertion, considered the rate-determining step, displays lower activation energy than high-confined Rh/MgO(301). They also indicate that the desorption process of the active carbonyl species is the most probable deactivation pathway. Willing to change the coordination environment of Rh single atoms on CeO<sub>2</sub>, as well as their electronic properties, to improve catalytic performances of Rh/CeO<sub>2</sub> as hydroformylation catalyst, Zheng et al.<sup>[55]</sup> introduced oxygen vacancies onto the support by calcinating CeO<sub>2</sub> (Figure 3 (b)). The temperature of calcination tuned the number of vacancies and a temperature of 800 °C was found the optimal to reach higher activity in propene hydroformylation (Figure 4). XPS, Raman, and electron paramagnetic resonance (EPR) results revealed that Rh promoted the desorption of oxygen from the CeO<sub>2</sub> surface at high calcination temperatures (700–800 °C), resulting in the creation of oxygen vacancies and increase the electronic density of Ce<sup>4+</sup> and Rh<sup>3+</sup>, leading to their reduction. Additional characterization (CO-FTIR, XANES, and extended X-ray absorption fine structure (EXAFS)) revealed the existence of Rh single atoms with higher electronic density and lower Rh–O coordination number when subjected to higher calcination temperatures. It resulted in a stronger adsorption strength of CO on Rh/CeO<sub>2</sub> as it was evidenced by FTIR coupling with temperature programmed desorption (TPD) analysis. DFT calculations confirmed that the formation of a single oxygen vacancy near to a Rh single atom (Rh-V<sub>o</sub>) was the most stable configuration for Rh/CeO<sub>2</sub> calcined at high temperature. The variations in electronic properties and local coordination of Rh single atoms significantly affected their catalytic performance in

propene hydroformylation. Remarkable enhancements in TOF values were observed for Rh/CeO<sub>2</sub> calcined at 700 °C (2393 h<sup>-1</sup>) and 800 °C (5072 h<sup>-1</sup>), in stark contrast to the TOF of less than 500 h<sup>-1</sup> recorded for low calcination temperatures (400–600 °C) (0.2 MPa of propene, at 100 °C in n-heptane under 3 MPa of CO/H<sub>2</sub> 1:1, stirring at 300 rpm). All catalysts displayed 100% of chemoselectivity to the formation of the aldehydes and low regioselectivity, with an I:b of about 0.67. The effect of MnO<sub>x</sub> clusters (Figure 3 (c))<sup>[78]</sup> and the addition of phosphine ligands (Figure 3 (d))<sup>[79]</sup> on Rh/CeO<sub>2</sub> systems have been also investigated by the same authors. MnO<sub>x</sub> were used as a promoter in order to modulate the CO adsorption strength on Rh/CeO<sub>2</sub> systems and aid the CO insertion in propene hydroformylation. At MnO<sub>x</sub> loading of 1 wt%, Mn was partially inserted in CeO<sub>2</sub> structure (Rh/1%MnO<sub>x</sub>-CeO<sub>2</sub>), increasing the formation of oxygen vacancies. Advanced characterization techniques revealed the formation of Rh<sup>3+</sup> single atoms located on MnO<sub>x</sub> clusters (Figure 3 (c)). A blue shift in the CO stretching mode of -Rh(CO)<sub>2</sub> species was observed for Rh/1%MnO<sub>x</sub>-CeO<sub>2</sub> when compared with Rh/CeO<sub>2</sub>, highlighting that Rh with more cationic character was attained in the former. Kinetic studies revealed an increase in the CO reaction order coupled with a decrease in the propene reaction order for Rh/1%MnO<sub>x</sub>-CeO<sub>2</sub> (-0.44 for CO and 0.52 for propene) compared to bare Rh/CeO<sub>2</sub> (-1.2 for CO and 0.94 for propene). This shift indicated that the presence of MnO<sub>x</sub> weakened CO adsorption strength and promoted propene adsorption, thus enhancing the catalytic performance of Rh/1%MnO<sub>x</sub>-CeO<sub>2</sub> in propene hydroformylation (TOF of 7200 h<sup>-1</sup>). The use of MnO<sub>x</sub> as a promoter did not improve the regioselectivity of Rh/CeO<sub>2</sub>, remaining in a I:b ratio of 0.67. In situ XPS and FTIR studies revealed that Rh-MnO<sub>x</sub> pairs, formed under reaction atmosphere, were the catalytic active centres. Building upon the success of POPs-supported Rh single atoms in achieving excellent regioselectivity, they recently modified Rh/CeO<sub>2</sub> by incorporating multiple phosphine ligands.<sup>[79]</sup> Xantphos-modified

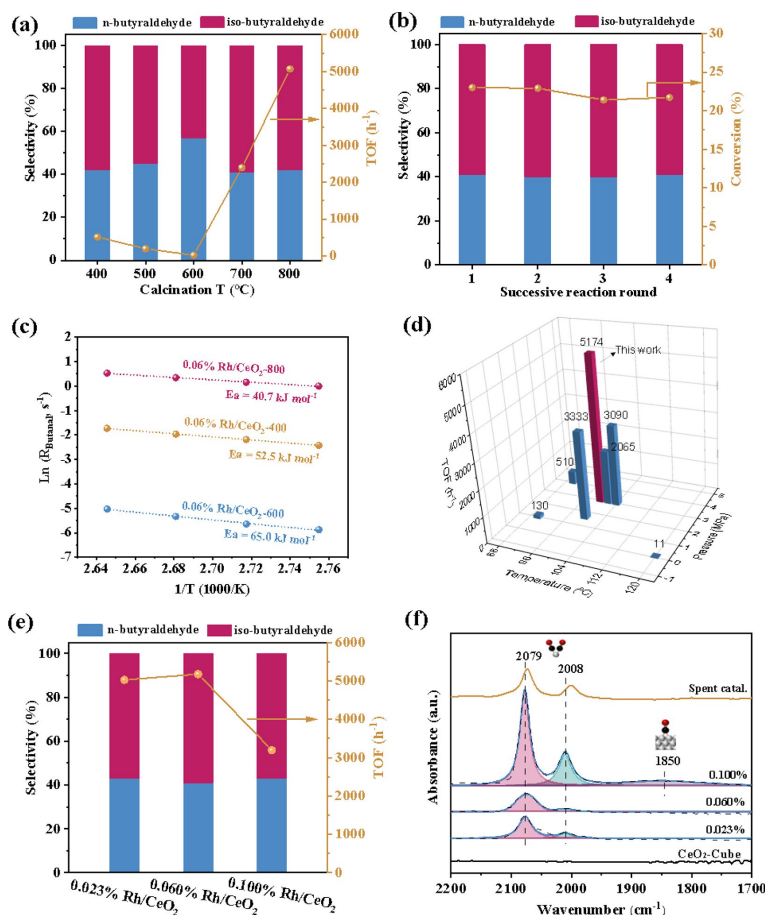


**Figure 4.** (a) Effect of the calcination temperature on the TOF and selectivity for the 0.06%Rh/CeO<sub>2</sub>. (b) Recycling performance of 0.06%Rh/CeO<sub>2</sub> calcined at 800 °C for the hydroformylation of propylene. (c) Arrhenius plots of 0.06%Rh/CeO<sub>2</sub> calcined at different temperatures. (d) Activity comparison with reported single-atom Rh. (e) TOF and selectivity on CeO<sub>2</sub> supported Rh catalysts with different loadings of Rh. (f) CO-FTIR spectra for Rh/CeO<sub>2</sub> with different Rh loadings and spent 0.06%Rh/CeO<sub>2</sub>. Reaction conditions: 100 °C, 3 MPa CO/H<sub>2</sub> 1:1, 0.2 MPa propylene, 20 mg of the catalyst, 0.5 h, 300 rpm. Arrhenius plots were examined under the conversions < 25% by varying the catalyst amount. Reprinted with permission *ACS Catal.* 2023, 13, 11, 7243–7255. Copyright 2023 American Chemical Society.<sup>[55]</sup>

Rh/CeO<sub>2</sub> (Figure 3 (d)), with a P/Rh ratio of 3, demonstrated a superior catalytic performance in propene hydroformylation (0.6 MPa of propene, 100 °C, 3 MPa of CO/H<sub>2</sub> 1:1 for 2 h), achieving a TOF of 476 h<sup>-1</sup> and exhibiting high regioselectivity towards the formation of linear aldehydes, with a l:b ratio of 13. The high regioselectivity was attributed to the unique structure of the Xantphos ligand. This structural feature conveyed significant steric hindrance during alkene adsorption, thereby promoting the linear adsorption mode of propene. This preference for linear adsorption contributed to the observed high regioselectivity to the formation of linear aldehydes during propene hydroformylation. Although high regioselectivity (l:b ratio of 36) was achieved when using 1-octene as a substrate in the presence of Xantphos ligand, chemoselectivity was compromised, favouring isomerization as a side reaction. Furthermore, lower catalytic performance was observed when styrene was used (TOF of 127 h<sup>-1</sup>, l:b ratio of 1.6, and chemoselectivity of 86%), which was clearly attributed to the high steric hindrance posed by the ligand.

The ability of a support to produce oxygen vacancies has been exploited by M.G. Farpón et al. to synthesise highly active

catalysts for ethylene hydroformylation.<sup>[40]</sup> Different oxide supports (m-ZrO<sub>2</sub>, CeO<sub>2</sub>, and SnO<sub>2</sub>) with identical cation M valency, but differing in their oxygen vacancy formation energies were used with this aim. SiO<sub>2</sub> was used as reference support on which Rh was also dispersed. While isolated Rh single atoms were produced on the three selected supports through oxidative metal dispersion and atom trapping, poly-nuclear Rh aggregates formed on SiO<sub>2</sub>. The metal-support interaction, thus, stabilization of single atoms centres, was found to decrease as follows: Rh/SnO<sub>2</sub> > Rh/ZrO<sub>2</sub> > Rh/CeO<sub>2</sub> > Rh<sub>n</sub>/SiO<sub>2</sub> (Figure 5). Among the catalysts, isolated Rh on SnO<sub>2</sub> exhibited an outstanding catalytic performance in gas-phase hydroformylation of ethylene, reaching a TOF values of 225 h<sup>-1</sup>, with the highest chemoselectivity to propanal formation (95%) at temperatures of 150 °C. TOF values of two orders of magnitude lower were reached for Rh/CeO<sub>2</sub> (0.6 h<sup>-1</sup>), Rh/ZrO<sub>2</sub> (1.4 h<sup>-1</sup>), and Rh/SiO<sub>2</sub> (3.7 h<sup>-1</sup>), displaying around 55–68% of hydroformylation selectivity. The partial aggregation of Rh on CeO<sub>2</sub> and ZrO<sub>2</sub>, proven their poor stability due to their weak metal-support interaction, spelt out their low catalytic activity in hydroformylation of ethylene. In contrast, Rh remained



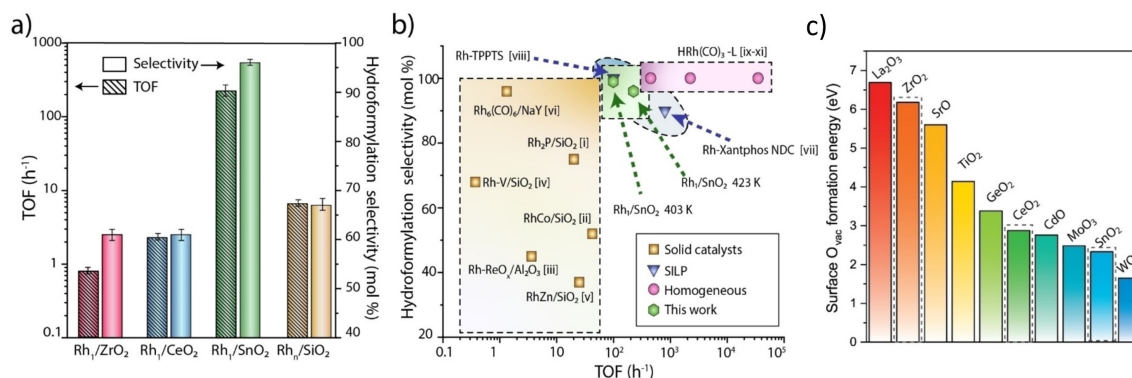


**Figure 5.** Gas-phase hydroformylation of ethylene. (a) Initial ethylene hydroformylation turnover frequency (TOF) and selectivity for single-atom catalysts supported on the series of MO<sub>2</sub> supports (M = Zr, Ce, Sn). The performance of a reference Rh<sub>1</sub>/SiO<sub>2</sub> catalyst has also been included for comparison. Reaction conditions: gas feed Ar/CO/H<sub>2</sub>/C<sub>2</sub>H<sub>4</sub> 1 : 5 : 1 : 1 (vol), 423 K, 2 MPa. (b) Comparison of the catalytic performance for the Rh/SnO<sub>2</sub> single-atom catalyst (this work) with the state-of-the-art. (c) Surface oxygen vacancies (O<sub>vac</sub>) formation energies for selected metal oxides. Adapted with permission *Angew. Chem. Int. Ed.* 2023, 62, e202214048.<sup>[40]</sup>

mainly as single sites on SnO<sub>2</sub> under reaction conditions and displayed indeed comparable catalytic performance in ethylene hydroformylation to those of homogeneous counterparts. Additional DFT calculations provided insights into these catalytic systems, revealing that Rh was preferably stabilized in six-fold coordinated sites on the SnO<sub>2</sub> (110) surface. Oxygen vacancies formed by removing bridging O atoms from the SnO<sub>2</sub> surface under the reducing atmosphere led to four-fold coordinated Rh, releasing two coordination sites to which two CO molecules strongly bonded. A reconstruction of Rh single atoms occurred, transitioning from six-fold coordination, with two CO molecules and four lattice O atoms, to four-fold coordination by detachment from the lattice O atoms, providing an energetically favourable route. Subsequently, H<sub>2</sub> dissociation was favoured at the Rh-oxide interface, generating the HRh<sup>+</sup>(CO)<sub>2</sub> active complex for hydroformylation and the adsorption of a hydride on the SnO<sub>2</sub> (110) surface. The free energy barrier found for hydrogenation of ethylene (105 kJ mol<sup>-1</sup>) was substantially higher than for CO adsorption (57 kJ mol<sup>-1</sup>), reinforcing the high selectivity to hydroformylation experimentally achieved for Rh/SnO<sub>2</sub>. Thus, the authors conclude that oxygen vacancy plays an important role in the activity and stability of Rh SACs, and specifically, SnO<sub>2</sub> confers to Rh single sites a coordination flexibility which translates to an improved catalytic performance for hydroformylation.

Besides the support effects on hydroformylation catalysed by single sites, the modification of the reaction conditions can also be an effective strategy for modulating the catalytic performance of a described system. Li et al. reported that regioselectivity toward linear aldehydes can be enhanced by coupling the hydroformylation of styrene with low-temperature water gas shift (LWGS), which generates hydrogen in situ.<sup>22</sup> CeO<sub>2</sub>-supported Rh single atoms were used as catalysts in the hydroformylation of styrene, under a CO/H<sub>2</sub> mixture, or employing CO and H<sub>2</sub>O. Under syngas, Rh/CeO<sub>2</sub> exhibited low regioselectivity toward linear aldehydes, with a l:b ratio of 0.9, despite achieving full styrene conversion and high chemoselectivity for phenylpropyl aldehydes. Using only CO in H<sub>2</sub>O,

the l:b ratio increased to 3, while displaying slightly lower conversion. These results were further confirmed using other homogeneous (RhCl<sub>3</sub> and RhCl(PPh<sub>3</sub>)<sub>3</sub>) and heterogeneous catalysts (Rh NPs/CeO<sub>2</sub>, Rh/FeO<sub>x</sub>, Rh/ZnO, and Rh/TiO<sub>2</sub>). While homogeneous catalysts showed high regioselectivity toward linear aldehydes, their conversion rates were relatively low compared to Rh/CeO<sub>2</sub>, attributed to their low activity in LWGS. CeO<sub>2</sub>-supported Rh NPs exhibited similar conversion rates and regioselectivity, but their high activity in hydrogenation of C=O bonds resulted in phenylpropanols as dominant products. Rh/FeO<sub>x</sub> and Rh/TiO<sub>2</sub> showed similar l:b ratios as Rh/CeO<sub>2</sub>, although with lower conversion, approximately 50%, suggesting that high regioselectivity could still be achieved through this new route. The lower conversion rates observed for Rh/FeO<sub>x</sub> and Rh/TiO<sub>2</sub> compared to Rh/CeO<sub>2</sub> indicate that Rh/CeO<sub>2</sub> interfacial sites are the most active in LWGS. The proposed mechanism involves the addition of the hydrogen generated in situ, existing as formic acid or bidentate formate generated from LWGS, to the unsubstituted end of the C=C bond. This favours carbonyl insertion at the end of the C=C bond, leading to the formation of linear aldehydes. ZnO-supported Rh single atoms displayed low activity in LWGS, leading to a lack of activity in the hydroformylation of styrene in these conditions. Thus, reducible oxides or other supports active in the LWGS reaction are required for achieving optimal catalytic performance, as high activity in WGS enhances in situ hydrogen concentration, thereby improving conversion rates. The large scope of the approach, reaching high regioselectivity with many catalytic formulations, proved that the unusual regioselectivity primarily arises from the in situ generation of hydrogen rather than the inherent activity of the catalyst, offering a novel route in which easily separable heterogeneous catalysts, without the need for additional ligands, offer comparable performance to their homogeneous counterparts.

## Zeolites

The encapsulation of isolated single atoms and modulation of their microenvironment within zeolite cages have been reported as another successful strategy for achieving highly stable and active single-atom catalysts.<sup>[35]</sup> Zeolites offer a wide range of cage dimensions and varying degrees of acidity, bringing an extensive range of possibilities in single-atom engineering. The synergistic catalytic effect resulting from the combination of metallic single atoms, mainly Rh, and acidic sites on zeolites is expected to significantly enhance not only the hydroformylation reaction but also other carbonylation reactions. The low coordination degree of cations in zeolites and their high electrophilicity allow for high coordination flexibility, tuning the Lewis acid properties of the metal cation, particularly important for reactions like hydroformylation, involving intermediates with multiple coordinate ligands. Single-site solid-based catalysts, such as Rh/faujasite,<sup>[56]</sup> K–Rh/S-1,<sup>[56]</sup> Y zeolite,<sup>[80]</sup> and Rh/MFI zeolite<sup>[58]</sup>, have shown promising activity in hydroformylation reactions (Table 1). However, the nature of active sites remains debated, highlighting the importance of multiple operando spectroscopic tools, and calculations for catalyst understanding. Hydroformylation can be seen as an example of a chemical process greatly affected by the local environment of active sites. Acidic sites facilitate the adsorption of reactants onto the surface of the catalyst. By means of the protonation or polarization of the reactant, these sites activate the olefins and facilitate their interaction with the dispersed metal centres, where commonly the reactions take place. For example, the acidic sites may activate the olefin by protonation, facilitating its interaction with the metal centre of the catalyst. In this sense it is important to highlight the role of silanol groups (–Si–OH), hydroxyl groups attached to silicon atoms in the zeolite framework. These hydroxyl groups can act as Brønsted acid sites, capable of donating protons in acidic catalysis. The acidity of silanol groups depends on factors such as their concentration, the structure of the zeolite framework, and the local environment. In many cases, the presence of silanol groups contributes to the acidic nature of zeolite catalysts, enabling them to facilitate various acid-catalysed reactions. Silanol groups play a crucial role in promoting the adsorption and activation of reactant molecules. Liu et al.,<sup>[81]</sup> demonstrated the key role of these species towards the hydroformylation reaction. Larger silanol concentration showed larger styrene conversions in commercial siliceous MFI zeolite. DFT simulations revealed that ethylene and 1-hexene have stronger binding energies on zeolite containing silanol groups with respect the silanol-free zeolite. The acidic centres were revealed as one of the keys of the catalytic activity of Rh dispersed on DeAlBEA zeolite with Zn and Co atoms in silanol nests. On the one hand, at the same concentration of Rh, less concentration of Zn enhances the propanal selectivity because of the weak hydrogenation activity of Zn Lewis acid centres. Acidic sites facilitate proton transfer and activation of reactant molecules. Probably, the major concentration of Zn does not help silanol groups in the adsorption and activation of olefin substrates. On the other hand, at the same concentration of Zn and Co, the latter show

larger activity, and it is attributed to the effectiveness of that silanol nest containing Co favour the dispersion of Rh, since it implies that number of accessible Rh active sites increase. Furthermore, the lower hydroformylation activity of DeAlBEA containing Zn compared with Co-DeAlBEA system can be influenced by the higher electron density on Rh in the former catalyst. It implies strong Rh–CO interaction hence inhibiting ethyl group migration to CO to form acyl groups. This electron density on Rh is lower than on Co-DeAlBEA DeAlBEA, facilitating the formation of acyl groups, which benefit the hydroformylation activity. Rh single atoms on a faujasite structure with a 0.8% of Rh loading demonstrated an excellent catalytic performance in alkene hydroformylation under mild reaction conditions. Shang et al.<sup>[57]</sup> revealed that this Rh/faujasite catalysts outperform most homogeneous and heterogeneous catalysis for the 1-hexene hydroformylation, avoiding the Rh leaching. Moreover, they use DFT simulations to unveil the reaction mechanism of 1-hexene hydroformylation to heptanal. The H<sub>2</sub> activation was found as a very feasible step, since only requires 32.80 kJ mol<sup>−1</sup>, and two different pathways were predicted for the formation of the linear aldehyde. The lowest in energy implies the attack of the hydride on the β-C and the attack of the adsorbed CO on α-C, being the latter the largest energy barrier (96.50 kJ mol<sup>−1</sup>). The branched mechanism presents slightly higher barriers, in agreement with the experimental results. For both mechanisms, the most relevant step is the desorption, since the product interacts strongly with the catalysts. Zhao et al.<sup>[58]</sup> demonstrated the impact of the structural rearrangement of Rh/zeolite catalyst, Rh/MFI, under reaction conditions, depending in turn on the catalyst pre-activation conditions, on the catalytic performances in the ethylene hydroformylation reaction. Both unreduced and reduced MFI-encapsulated Rh clusters were tested resulting in a highly active catalyst for propanal formation for the former, including at relatively low temperatures, yielding 2.2 mmol<sub>propanal</sub> g<sub>cat</sub><sup>−1</sup> at 90 °C, with selectivity above 95%. Moreover, apparent activation energy (E<sub>a</sub>) for propanal formation of unreduced catalyst was found to be the lowest (19.5 kJ mol<sup>−1</sup>). However, a decrease in propanal yields and an increase in apparent activation energy for propanal formation was observed for both the reduced catalyst under syngas (yield of 1.4 mmol<sub>propanal</sub> g<sub>cat</sub><sup>−1</sup> at 90 °C; E<sub>a</sub> of 25.6 kJ mol<sup>−1</sup>) and under H<sub>2</sub> (yield of 1.3 mmol<sub>propanal</sub> g<sub>cat</sub><sup>−1</sup> at 90 °C; E<sub>a</sub> of 31.6 kJ mol<sup>−1</sup>). These differences in catalytic performance were attributed to the oxidation state of Rh sites formed when catalysts were either reduced or not. In unreduced samples, mainly Rh<sup>3+</sup> single sites were formed through the oxidative disruption of encapsulated Rh<sub>2</sub>O<sub>3</sub> clusters, leading to the formation of monocarbonyl Rh(CO)L species interacting with OH groups of the zeolite under reaction conditions. Meanwhile, Rh<sup>0</sup> sites were primarily generated in the reduced catalysts, resulting from the disruption of Rh<sup>0</sup> clusters formed during the reducing treatment. According to these authors, oxidized Rh<sup>3+</sup> site behaves as a more effective precursor for low-temperature propanal formation than commonly reported Rh<sup>+</sup>(CO)<sub>2</sub> species.<sup>[55,82]</sup> This affirmation diverges from the conventional findings in the literature which typically suggest that Rh<sup>+</sup> in the form of Rh<sup>+</sup>(CO)<sub>2</sub> or Rh<sup>0</sup> serve as the

active sites in hydroformylation. The formation of dicarbonyl  $\text{Rh}^+(\text{CO})_2$  species under reaction conditions in the reduced catalysts requires high temperatures to desorb one CO molecule to subsequently absorb the olefin. This phenomenon explains their low catalytic performance in the hydroformylation of ethylene compared with the unreduced catalysts. At high reaction temperatures (200 °C), agglomeration of Rh into Rh NPs was observed, resulting in decreased activity in propanal formation and increased activity in the hydrogenation of ethylene. To prevent the sintering, phosphorus was added as a dopant; the formation of Rh-(O)-PMFI catalysts, in which phosphorus is in a  $\text{P}^{5+}$  oxidation state. This modification promoted a high concentration of  $\text{Rh}^{3+}$  sites in the reduced catalyst under a syngas atmosphere, and increased the activity and stability of the catalyst. Propylene was also used as a substrate to investigate the regioselectivity promoted by the unreduced (Rh-MFI) and P-doped catalysts (Rh-(O)-PMFI). Due to the steric hindrance of zeolite channels, high regioselectivity for the formation of linear aldehyde was attained for the undoped catalyst, with a l:b ratio of 4.1 and a chemoselectivity of 67%. Doping with P did not improve either the regioselectivity or chemoselectivity, suggesting that not only steric hindrance determines regioselectivity, but also the electronic properties of Rh single sites.

Overall, zeolites offer a versatile platform for SACs engineering due to their varied cage dimensions and degrees of acidity. The acidic sites on zeolites play a multifaceted role in hydroformylation reactions, clearly evidencing that the single metal or small metal clusters are not the only aspect to take into account for the design of new catalyst with improved activity and selectivity. The collaborative efforts of acidic sites and metal single atoms within zeolite cages offer a promising avenue for designing highly active and selective catalysts for hydroformylation and related reactions. To put the focus only on the size and charge of Rh single atoms (and Rh clusters) is interesting to shed light on the debate about which is the active species for this reaction. Nevertheless, for the future design of active zeolite catalysts for carbonylation reactions, the role of acidic sites on the activation of substrate and the dispersion of the single atom must be consciously evaluated, since all the results seem to corroborate the relevance of the acidic sites and metal atoms (or clusters) for the catalysts performance.

### Carbon-Based Supports

The modification of carbon supports with other heteroatoms or pending groups is a good strategy to anchor firmly metals to their surface and to modify the catalytic properties of the materials, in heterogeneous catalysis<sup>[83–86]</sup> or in SACs.<sup>[87]</sup> For hydroformylation applications, examples using this strategy have demonstrated the importance of the modification of the support (Table 1). Gao et al.<sup>[23]</sup> described a Rh phosphorus complex supported on nanodiamonds that outperformed similar Rh supported catalysts and was close to the performances of homogeneous Rh catalyst analogue, obtaining an

excellent regioselectivity to the branched aldehydes with respect to the linear ones. DFT simulations unveil a very low energy barrier (18.33  $\text{kJ mol}^{-1}$ ) for the styrene coordination to the catalytic complex, being linked to the Rh single atom. The preference for the branched aldehyde was demonstrated since the barrier is slightly lower (4.80  $\text{kJ mol}^{-1}$ ) with respect to the linear pathway. Ru isolated single atoms and clusters were supported in a N-doped carbon matrix and the materials used as catalysts in the hydroformylation of 1-hexene.<sup>[88]</sup> Similarly, as observed before in other catalysts, the addition of a dopant, here N, increased the catalyst stability and activity. The characterization of the materials showed that isolated single atoms and clusters of Ru coexist in the sample, and isolated single atoms are responsible for the high catalytic activity, which corresponds to  $\text{Ru}^{2+}\text{-N}$  species. At lower Ru loading, catalysts displayed the highest percentage of Ru single atoms; as a consequence, these were the most active catalysts for the hydroformylation of 1-hexene (at 150 °C under 4 MPa  $\text{CO}/\text{H}_2$  1:1, 750 rpm).

The use on nitrogen as an anchoring site of the support has also been used by Jurado et al.<sup>[66]</sup> as strategy to obtain robust catalysts for the liquid-phase hydroformylation of styrene. Carbon nitride,  $\text{C}_3\text{N}_4$ , a medium band gap semiconductor with a tuneable electronic structure that displays triazine rings in its structure, was used as support to synthesize Rh SACs (Figure 6). DRIFTS after CO exposure showed *gem*-dicarbonyl  $\text{Rh}^{\delta+}(\text{CO})_2$  species (2090 and 2024  $\text{cm}^{-1}$ ) as a main Rh contribution along with some minor signals attributed to Rh NPs. A TOF of 125  $\text{h}^{-1}$  at 2 h of reaction and a l:b of 1.6 was observed for the hydroformylation of styrene in THF at 90 °C under 2 MPa of  $\text{CO}/\text{H}_2$  1:1 using a low Rh loading (0.1 wt%). DFT calculations demonstrated that at low metal coverage, Rh atoms were stably coordinated in the pockets displayed by the structure, and not in between the sheets, and also that  $\text{HRh}(\text{CO})_x$  species were stably coordinated to the surface in the presence of ethylene.

The use of doping heteroatoms in carbonaceous supports for SACs in hydroformylation has been relatively unexplored. Initial findings suggest that their presence positively impacts stability and activity, as seen with metal oxide-based SACs. However, further efforts in this area are needed to fully understand their influence and enhance their effectiveness in hydroformylation reactions.

### Other Solid Supports

Zirconium phosphate-supported Co-based catalysts, named  $\text{ZrP-x}$ , where  $x$  represents the P/Zr ratio (0.5–2), were described for the hydroformylation of olefins.<sup>[72]</sup> The P/Zr ratio determined the stability and activity of the catalysts:  $\text{Co}/\text{ZrP-2.0}$  catalyst demonstrated almost complete conversion of 1-octene with an aldehyde selectivity of 91% and proved recyclable for up to six cycles without apparent catalytic deactivation (at 160 °C in toluene under 4 MPa of  $\text{CO}/\text{H}_2$  1:1, 6 h, 1000 rpm). Additionally, several olefins were selectively converted into the corresponding alcohols by increasing the temperature to 190 °C and the partial  $\text{H}_2$  pressure ( $\text{CO}/\text{H}_2$  1:2), reaching a selectivity of up to

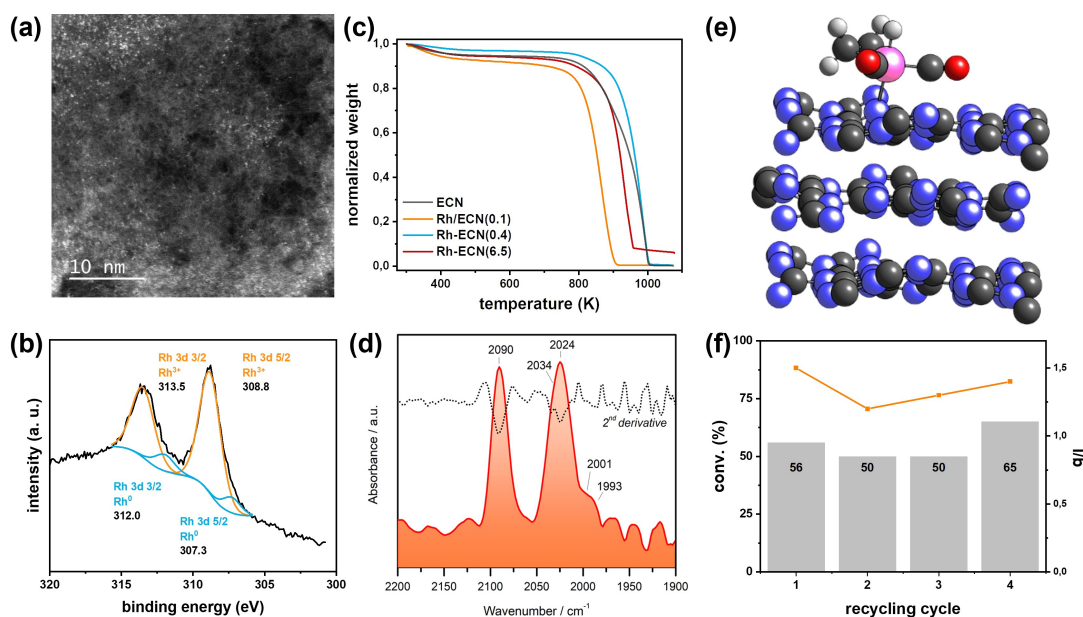


**Figure 6.** (a) HAADF-STEM image of Rh/ECN(0.1) (scale bar = 10 nm). (b) High-resolution XPS spectra of Rh 3d Rh/ECN(0.1). (c) Thermogravimetric analysis curves under  $N_2$  for ECN, Rh/ECN(0.1), Rh-ECN(0.4), and Rh-ECN(6.5). (d) DRIFT spectra recorded on Rh/ECN(0.1) sample after CO adsorption (20 min) and Ar purging (5 min) at 50 °C. The inclusion of second derivative curve facilitates the identification of the bands. (e) Sketch of the optimized  $HRh(CO)_2(C_2H_4)$  species supported on ECN (grey, blue, pink, red, and white balls represent carbon, nitrogen, rhodium, oxygen, and hydrogen atoms respectively). (f) Conversion (grey bars) and I:b ratio (orange line) of recycling tests performed with Rh/ECN(0.1) ( $5 \times 10^{-12}$  mmol of metal, 0.6 mmol of styrene, 0.25 mmol of octane (internal standard), 2 MPa of syngas ( $CO/H_2$  1:1), 5 mL of THF, 20 h, 70 °C, 1200 rpm). Reproduced from *Catal. Sci. Technol.*, 2023,13, 1425–1436 with permission from the Royal Society of Chemistry.<sup>[66]</sup>

90%, without notable hydrogenation of the C=C bond of the olefin. Characterization revealed that atomically dispersed  $Co^{2+}$  species were intricately bonded to the phosphate group of ZrP-2.0, replacing H from the Brønsted acid sites, resulting in the formation of oxygen-bonded isolated  $Co^{2+}$  atoms. This distinctive configuration facilitated electron transfer from the atomically dispersed  $Co^{2+}$  species to the ZrP support, leading to electron-deficient  $Co^{2+}$  sites with increasing P/Zr ratio. The strong electronic interaction was found to effectively mitigate the leaching of active Co species, thereby enhancing as well the stability of the catalyst. In the case of molybdenum carbide, the  $\beta$  phase was used to support cobalt clusters for the hydroformylation of propene.<sup>[73]</sup> The  $\beta$ - $Mo_2C$  support was classified as non-innocent support since the Co- $\beta$ - $Mo_2C$  interface demonstrated enhanced activity and less leaching than the experiments carried out with Co clusters. DFT simulations associated these results with a decrease of the energy barriers.

### Metal-Organic Frameworks and Porous Organic Polymers

Rhodium supported on porous materials like MOFs have been also utilized as hydroformylation catalysts. In particular, Hou et al.<sup>[59]</sup> studied the deposition of Rh NPs over ZIF-8, a zeolitic imidazolate framework based on Zn. The isolated ZIF-8 did not show catalytic activity for the hydroformylation of 1-heptene, otherwise the deposition of Rh reaches yields higher than 80% for the production of linear and branched aldehydes, being 1-hexene and 1-styrene the reactants that promote larger yields.

Moreover, the catalysts were easily separated from the products, promoting their reuse without a decrease in the catalytic activity (five times of reutilization). Rh single atom was proposed as well as active site for POPs in the hydroformylation of olefins (Table 2). Li et al.<sup>[60]</sup> used a ligand with steric hindrance, vinyl functionalized biphephos, to be copolymerized with tris(4-vinylphenyl)phosphane, which allow high dispersion of Rh single atoms and a high binding energy between P and Rh. The use of biphosphoamidite bidentate ligands was studied by Wang and Yang,<sup>[62]</sup> to anchor and support the Rh metal catalyst, showing an excellent activity for the olefin hydroformylation without solvent, highlighting the excellent regioselectivity towards linear aldehydes and the capability to be reused without losing the catalytic properties. Zhang et al.<sup>[61]</sup> analysed several POPs displaying anchored Rh single atom for the hydroformylation reaction, being the Rh/CPOL-BINAP&PPh<sub>3</sub> the material that exhibits the highest catalytic activity and regioselectivity for linear aldehydes. The coordination of PPh<sub>3</sub> to the Rh active site enhances the activity of Rh-H species, as supported by DFT calculations and experimental analyses using NMR and FT-IR. Jiang et al.<sup>[64]</sup> synthesized a series of POPs containing P and N as support of Rh single sites, being the Rh-N-POP the system that exhibited larger surface area and larger pore volume. Furthermore, this system showed the better hydroformylation results using 1-octene as substrate, while POPs with P and both P and N exhibited low catalytic activity towards hydroformylation but excellent isomerization activities. The authors hypothesize that this behaviour was related to the partial oxidation of P atoms, the stronger alkalinity, and the fact



**Table 2.** Hydroformylation using single-atom catalysts based on POPs and SILPs.

Catalyst	Substrate	TOF (h <sup>-1</sup> )	Selectivity (%)	I:b	Reaction conditions	Ref.
0.25%Rh/POPs	ethylene	4300	98	–	250 mg of catalyst, 0.1 MPa C <sub>2</sub> H <sub>4</sub> /CO/H <sub>2</sub> 1:1:1, 120 °C; fixed bed reactor	65
0.25%Rh/POPs	ethylene	229	99	–	250 mg of catalyst, 0.1 MPa C <sub>2</sub> H <sub>4</sub> /CO/H <sub>2</sub> 1:1:1, (1000 ppm H <sub>2</sub> S), 120 °C; fixed bed reactor	65
0.13%Rh/CPOL-1bp&10P <sup>a</sup>	propene	1209	93	24	300 mg of catalyst, 5 MPa C <sub>3</sub> H <sub>6</sub> /CO/H <sub>2</sub> 1:1:1, gas hourly space velocity (GHSV) = 1500 h <sup>-1</sup> , 12 h, 70 °C; fixed bed reactor	60
0.14%Rh/CPOL-bp&P(OPh) <sub>3</sub> <sup>a</sup>	1-butene	2490	82	40	100 mg of catalyst, 2 MPa CO/H <sub>2</sub> 1:1, GHSV = 1000 h <sup>-1</sup> , 24 h, 80 °C; fixed bed reactor	61
SILP 0.20%Rh <sub>1</sub> /N-doped PBSAC [EMIM][NTf <sub>2</sub> ]	ethylene	600	100	–	2.5×10 <sup>3</sup> mg of catalyst, 8 MPa C <sub>2</sub> H <sub>4</sub> /CO/H <sub>2</sub> 0.1:1:2, total flow of 310 mL min <sup>-1</sup> GHSV = 1000 h <sup>-1</sup> , 15 h, 120 °C; fixed bed reactor	71
SILP 0.25%Ru/SiO <sub>2</sub> [C <sub>2</sub> C <sub>1</sub> Im]Cl	propene	16.9	66.1	–	2.1×10 <sup>3</sup> mg of catalyst, 8.6 MPa C <sub>3</sub> H <sub>6</sub> /CO <sub>2</sub> /H <sub>2</sub> 0.17:1:3, total flow of 42.5 mL min <sup>-1</sup> GHSV = 1280 h <sup>-1</sup> , 8 h, 170 °C; fixed bed reactor	89
SILP 0.20%Rh/SiO <sub>2</sub> [BMIM][PF <sub>6</sub> ]	propene	16.7	100	23.7	1 MPa C <sub>3</sub> H <sub>6</sub> /CO <sub>2</sub> /H <sub>2</sub> 1:1:1, total flow of 42.5 mL min <sup>-1</sup> GHSV = 7000 h <sup>-1</sup> , 5 h, 100 °C; fixed bed reactor	70
SILP Rh-bpp/SiO <sub>2</sub> [C <sub>2</sub> C <sub>1</sub> Im][NTf <sub>2</sub> ]	1-butene	1090	50	–	5×10 <sup>2</sup> or 2×10 <sup>3</sup> mg of catalyst 0.09 g/min of substrate, 1 MPa CO <sub>2</sub> /H <sub>2</sub> 1:1; fixed bed reactor	67
SILP 0.20%Rh-sxp complex [C <sub>4</sub> C <sub>1</sub> Im][C <sub>8</sub> OSO <sub>3</sub> ]	1-butene	120	–	–	2.3×10 <sup>3</sup> mg of catalyst, 0.09 g/min of substrate, 1.2 MPa CO <sub>2</sub> /H <sub>2</sub> 1:1, 0.3 MPa C <sub>4</sub> H <sub>8</sub> , 100 °C; fixed bed reactor	69

<sup>a</sup> CPOL is copolymer; bp is biphosphos and P is PPh<sub>3</sub>

that the Rh–P interaction restricted the ligand association and dissociation, decreasing the performance towards the hydroformylation reaction. On the other hand, Feng et al.<sup>[65]</sup> revealed the self-recovery of Rh single atom on POPs. Despite sulfur poisoned the active site for the hydroformylation reaction, the activity of Rh remained unaltered after the H<sub>2</sub>S removal. Initially, the formation of Rh-SH species inhibited the coordination of ethylene, with the subsequent poor catalytic activity. However, the Rh-SH can evolve to Rh–H without any action in the CO/H<sub>2</sub> atmosphere. Furthermore, DFT simulations were employed to investigate the catalytic activity of Rh single atoms supported in a polymer (3 V-PPh<sub>3</sub>) for the propionaldehyde obtention,<sup>[57]</sup> unveiling the role of the Rh–P bond strength. Calculations showed that the CO insertion stabilize the structure that contains the Rh atom and two skeleton P atoms in a coplanar plane. The Mulliken charge and density of states analysis revealed a heightened electronegativity of Rh during CO coordination and H<sub>2</sub> oxidative addition, thereby enhancing the reaction activity. In contrast, in the steps involving the insertion of the Rh–C bond through CO coordination and reduction elimination, the electronegativity of Rh is diminished, resulting in a poor performance in hydroformylation reaction. Thus, MOFs and POPs displaying high tuneability in their structure allow a fine control of the catalysis outcome, particularly the attained regioselectivity, a weak point of SACs based on solid supports, nevertheless at the expenses of robustness, P degrades for instance in POPs, and synthetic investment.

### Supported Ionic Liquid Phase

Ionic liquids (ILs) have been widely investigated as novel solvents, electrolytes, and soft functional materials. Supporting them can overcome the issues due to their liquid state, and open the door to further modifications and, thus, properties.<sup>[90]</sup> Supported ionic liquid phase (SILP) typically consist of ionic liquid species immobilized on a solid support material, where the ionic liquid serves as both the solvent and the catalyst. Moreover, it can be anchored to the isolated single metal atoms dispersed on a solid support matrix, where the metal atoms act as active sites for catalysis. The immobilization of ionic liquids onto solid supports enhances their stability and facilitates catalyst recovery. SILPs offer tuneable properties such as polarity, acidity, and solubility, allowing for fine-tuning of the catalytic environment to optimize reaction conditions and specially the selectivity. In the case of the presented catalyst in this review, the support containing Rh, is combined with the ionic liquids (Table 2). Thus, the nature of IL allows per se a high degree of functionalization,<sup>[91,92]</sup> and their immobilization on solids, SILP, confers them other properties, such robustness, which is essential for carbonylation reactions.<sup>[93]</sup> An early example of SILP for hydroformylation application by Riisager et al.<sup>[70]</sup> consists in Rh modified with a sulfonated xantphos ligand impregnated on silica, followed by the impregnation of an IL. The gas-phase hydroformylation of propene proceed with these catalysts, reaching I:b ratios up to 23.7 (96%). Nevertheless, a loss of activity and regioselectivity was observed for



prolonged reaction periods. Recent examples focus in the modification of the support and/or the IL on SILPs.<sup>[67–71]</sup> The N-doping of the carbonaceous support of a SILP based on Rh for the gas-phase hydroformylation of ethylene provided higher activity than the corresponding undoped carbon support.<sup>[71]</sup> The pore of the silica also influenced the catalytic performances of Rh SILP for the gas-phase hydroformylation of 1-butene.<sup>[67]</sup> The hydrothermal treatment of the silica permitted the enlargement of the median pore size, from 2 nm to 27 nm, improving the kinetics of the reaction. Schörner et al.<sup>[69]</sup> proceeded recently with the modification of the nature of the IL on SILP for hydroformylation applications. The activity on the gas-phase hydroformylation of 1-butene was found to correlate with the substrate solubility in the IL. It emerges that SACs based on SILPs provide, similar to MOFs and POPs, a high degree of functionalisation, in both the IL and the support, and could thus provide enhanced stability, and address regioselectivity challenges found in SACs based on solid supports.

The latest examples of SACs for hydroformylation, based mainly in Rh, but some works describe successful examples based on Co and Ru, focus in the tailoring of the support to increase the catalytic properties and the robustness of the materials. Modification of the electronics of Rh atoms have proven in some cases to enhance also the activity or supports that allow it, heteroatoms were introduced in their structure, mainly P and N, with similar results in activity, dispersibility, and robustness than desired and obtained with oxygen or metal vacancies in reducible oxides. In most of the reported single-atom supported metal oxides, CO insertion appears to be the rate-determining step. For instance, in systems such as Rh/MgO, Rh/ReO<sub>x</sub>-Al<sub>2</sub>O<sub>3</sub>, and Rh/WO<sub>x</sub>-Al<sub>2</sub>O<sub>3</sub>, the negative reaction order of CO in olefin hydroformylation has been observed due to the strong adsorption of CO on Rh single sites. Strategies to modulate the CO adsorption strength to facilitate its desorption and enhance attack on hydrogenated olefins have been suggested as essential. For instance, a direct correlation has been found between CO stretching mode and TOF in propene hydroformylation when CeO<sub>2</sub> is modified by adding Xantphos ligands, inducing oxygen vacancies, or adding a promoter such as MnO<sub>x</sub> (Figure 7). Surrounding atoms capable to strongly withdraw electrons from Rh, weaken the CO adsorption strength, resulting in an improvement in the TOF. Thus, for supports based on oxides, the fine-tuning of the oxygen vacancies or the addition of promoters has been shown to be efficient. This modification increases the anchoring sites, thus enhancing the dispersibility of the active metal, and simultaneously increasing the robustness of its coordination, being postulate as the most approachable strategy to improve the catalytic performance in olefin hydroformylation. Regioselectivity appears to be the Achilles' heel of single-atom supported oxides, with mostly low values observed due to the low steric hindrance experienced by the atomic Rh on oxides. Although regioselectivity is understood to depend on several experimental settings, the addition of phosphine organic ligands capable of introducing steric hindrance, or in situ generation of H<sub>2</sub> using H<sub>2</sub>O or other solvents, could help overcome this issue. However, the support is not innocent during the catalytic process. This

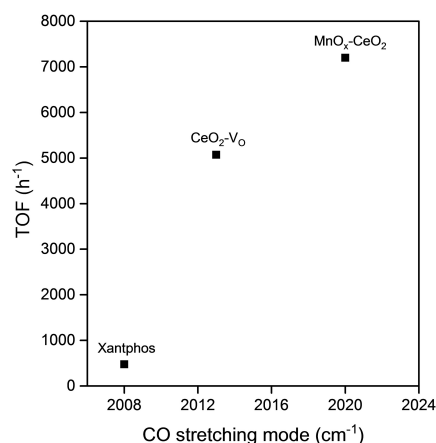


Figure 7. Correlation between between CO stretching modes and TOF in propene hydroformylation for Xantphos-modified Rh/CeO<sub>2</sub>,<sup>[79]</sup> Rh/CeO<sub>2</sub>-V<sub>o</sub><sup>[55]</sup> and Rh/1 %MnO<sub>x</sub>-CeO<sub>2</sub>.<sup>[78]</sup>

phenomenon has been observed in SACs based on zeolites, where the acidic sites can activate olefins. The synergy metal-support is currently underexplored and not fully understood, as typically the effect of the support is analysed in terms of properties conferred to the metallic centre. Supports which allow a high degree of modification, the ones containing organic species such MOFs, POPs, and SILPs, similar observations have been done. In addition, for POPs issues like regioselectivity and even enantioselectivity can be more easily solved; this aspect, is pending to be solved for other supports.

## Methanol, Ethanol and Dimethyl Ether Carbonylations

The production of acetic acid using methanol carbonylation (Figure 8) relies in homogeneous catalysts based on Rh and Ir, specifically [Rh(CO)<sub>2</sub>I<sub>2</sub>]<sup>-</sup> and [Ir(CO)<sub>2</sub>I<sub>2</sub>]<sup>-</sup>. Leaching of metal species is one of the major drawbacks of these procedures, as well as the use of halides. The features of SACs have attracted attention for application in this reaction to circumvent these disadvantages; recent examples, providing free-halide and robust catalysts, followed by SACs which rely in the use of halides as promoters, are detailed below.

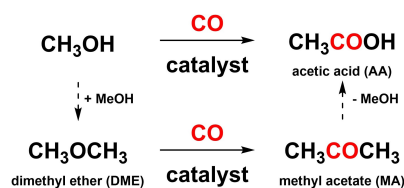


Figure 8. Carbonylation of methanol and dimethyl ether.

### Without Halides

For heterogeneous catalysts, similarly to the homogeneous counterparts, halide additives still remain essential for the carbonylation of methanol and dimethyl ether. Developing halide-free carbonylation catalysts is attractive from both environmental and economic viewpoints. Mordenite (MOR) zeolites have achieved this breakthrough in the past.<sup>[94–98]</sup> The mechanism of the carbonylation by acid zeolites consists in the formation of methoxy species on Brønsted acidic sites, specifically in the 8-membered rings,<sup>[99]</sup> which reacts with CO to form an acylium cation that in turn reacts with H<sub>2</sub>O. These strong acid sites also promote the coupling to methanol to produce dimethyl ether, which in turn can undergo carbonylation to produce methyl acetate, thus diminishing the selectivity of the process (Figure 8). As the reaction of CO with methoxy species was established as the rate-limiting step, a bifunctional catalyst able to activate methanol in acidic sites in combination to a metal to activate CO was proposed to increase the efficiency of the process. The modification of zeolites with Cu was successful

with this aim, and as postulated, improved the carbonylation over the competing condensation, suppressing the production of dimethyl ether. Consequently, the acetic acid selectivity increased.<sup>[100–102]</sup> It is worth noting that modifying zeolites with metals also enhances the carbonylation of dimethyl ether.<sup>[103]</sup> Yet, usually high CO to MeOH ratio is required in the gas-phase carbonylation of methanol using these catalysts. It is important to highlight that the combination a Cu mordenite catalysts, for production of acetic acid from methanol, and a Pd/CeO<sub>2</sub>, to produce CO in situ from methanol, allowed to produce methanol-only halide-free route to acetic acid.<sup>[104]</sup> Taking into consideration these works, SACs could become interesting materials to provide halide-free carbonylation catalysts (Table 3). For instance, Christopher et al. achieved the synthesis of acetic acid from methanol without any additive in the gas-phase using first atomically dispersed Rh on acidic supports,<sup>[105]</sup> and later circumventing the use of Rh, using an atomically dispersed ReO<sub>4</sub> on SiO<sub>2</sub>, yet, when introducing Rh onto the Re based catalyst (Rh-ReO<sub>4</sub>/SiO<sub>2</sub>) increasing considerably the catalytic properties of the ReO<sub>4</sub>/SiO<sub>2</sub> catalyst.<sup>[106]</sup> In this latter work,

**Table 3.** Halide-free methanol and dimethyl ether carbonylation using single-atom catalysts.

Catalyst	Substrate	Selectivity	Rate	Reaction conditions	Ref.
0.2%Rh/ZrO <sub>2</sub>	methanol	~30% AA	~7×10 <sup>-4</sup> mmol <sub>AA</sub> g <sub>cat</sub> <sup>-1</sup> s <sup>-1</sup>	3.3×10 <sup>-3</sup> MPa methanol, 3.3×10 <sup>-3</sup> MPa CO, 300 °C; fixed-bed quartz reactor	105
0.2%Rh/1%Na-ZrO <sub>2</sub>	methanol	~48% AA	~2.5×10 <sup>-4</sup> mmol <sub>AA</sub> g <sub>cat</sub> <sup>-1</sup> s <sup>-1</sup>	3.3×10 <sup>-3</sup> MPa methanol, 3.3×10 <sup>-3</sup> MPa CO, 300 °C; fixed-bed quartz reactor	105
0.2%Rh/5%Na-ZrO <sub>2</sub>	methanol	~54% AA	~2×10 <sup>-4</sup> mmol <sub>AA</sub> g <sub>cat</sub> <sup>-1</sup> s <sup>-1</sup>	3.3×10 <sup>-3</sup> MPa methanol, 3.3×10 <sup>-3</sup> MPa CO, 300 °C; fixed-bed quartz reactor	105
0.2%Rh/10%Na-ZrO <sub>2</sub>	methanol	~40% AA	~1.2×10 <sup>-4</sup> mmol <sub>AA</sub> g <sub>cat</sub> <sup>-1</sup> s <sup>-1</sup>	3.3×10 <sup>-3</sup> MPa methanol, 3.3×10 <sup>-3</sup> MPa CO, 300 °C; fixed-bed quartz reactor	105
1%ReO <sub>4</sub> /SiO <sub>2</sub>	methanol	>90% AA	0.038 mmol <sub>AA</sub> g <sub>Re</sub> <sup>-1</sup> s <sup>-1</sup>	3.3×10 <sup>-3</sup> MPa methanol/CO, 280 °C; fixed-bed quartz reactor	106
5%ReO <sub>4</sub> /SiO <sub>2</sub>	methanol	>90% AA	0.038 mmol <sub>AA</sub> g <sub>Re</sub> <sup>-1</sup> s <sup>-1</sup>	3×10 <sup>-3</sup> MPa methanol/CO, 280 °C; fixed-bed quartz reactor	106
10%ReO <sub>4</sub> /SiO <sub>2</sub>	methanol	>90% AA	0.0285 mmol <sub>AA</sub> g <sub>Re</sub> <sup>-1</sup> s <sup>-1</sup>	3×10 <sup>-3</sup> MPa methanol/CO, 280 °C; fixed-bed quartz reactor	106
20%ReO <sub>4</sub> /SiO <sub>2</sub>	methanol	>20% AA	<0.001 mmol <sub>AA</sub> g <sub>Re</sub> <sup>-1</sup> s <sup>-1</sup>	3×10 <sup>-3</sup> MPa methanol/CO, 280 °C; fixed-bed quartz reactor	106
0.2%Rh/10%ReO <sub>4</sub> /SiO <sub>2</sub>	methanol	~96% AA	~0.2 mmol <sub>AA</sub> g <sub>Re</sub> <sup>-1</sup> s <sup>-1</sup>	3×10 <sup>-3</sup> MPa methanol/CO, 280 °C; fixed-bed quartz reactor	106
0.2%Rh/SiO <sub>2</sub>	methanol	no activity	no activity	3×10 <sup>-3</sup> MPa methanol/CO, 280 °C; fixed-bed quartz reactor	106
Rh/Cs <sub>1</sub> H <sub>2</sub> PW <sub>12</sub>	DME	91% MA	15×10 <sup>-8</sup> mmol <sub>MA</sub> g <sup>-1</sup> s <sup>-1</sup>	CO/DME = 10/1, GHSV = 3000 h <sup>-1</sup> , 1 MPa, 200 °C; flow reactor	109
Rh/Cs <sub>1.5</sub> H <sub>1.5</sub> PW <sub>12</sub>	DME	94% MA	45×10 <sup>-8</sup> mmol <sub>MA</sub> g <sup>-1</sup> s <sup>-1</sup>	CO/DME = 10/1, GHSV = 3000 h <sup>-1</sup> , 1 MPa, 200 °C; flow reactor	109
Rh/Cs <sub>2</sub> H <sub>1</sub> PW <sub>12</sub>	DME	95% MA	43×10 <sup>-8</sup> mmol <sub>MA</sub> g <sup>-1</sup> s <sup>-1</sup>	CO/DME = 10/1, GHSV = 3000 h <sup>-1</sup> , 1 MPa, 200 °C; flow reactor	109
Rh/Cs <sub>2.5</sub> H <sub>0.5</sub> PW <sub>12</sub>	DME	96% MA	9×10 <sup>-8</sup> mmol <sub>MA</sub> g <sup>-1</sup> s <sup>-1</sup>	CO/DME = 10/1, GHSV = 3000 h <sup>-1</sup> , 1 MPa, 200 °C; flow reactor	109
[Rh(CO)(Xantphos)] <sup>+</sup> <sub>0.5</sub> [H <sub>2.5</sub> PW <sub>12</sub> O <sub>40</sub> ] <sup>0.5-</sup> /SiO <sub>2</sub>	methanol	~20% AA	1.5 mmol h <sup>-1</sup>	CO/methanol = 3/1, 0.1 MPa, 200 °C; packed-bed flow micro-reactor	111
[Rh(CO)(Xantphos)] <sup>+</sup> <sub>1</sub> [H <sub>2</sub> PW <sub>12</sub> O <sub>40</sub> ] <sup>-</sup> /SiO <sub>2</sub>	methanol	~55% MA	1.2 mmol h <sup>-1</sup>	CO/methanol = 3/1, 0.1 MPa, 200 °C; packed-bed flow micro-reactor	111
[Rh(CO)(Xantphos)] <sup>+</sup> <sub>2</sub> [H <sub>1</sub> PW <sub>12</sub> O <sub>40</sub> ] <sup>2-</sup> /SiO <sub>2</sub>	methanol	~80% MA	1.2 mmol h <sup>-1</sup>	CO/methanol = 3/1, 0.1 MPa, 200 °C; packed-bed flow micro-reactor	111
[Rh(CO)(Xantphos)] <sup>+</sup> <sub>3</sub> [PW <sub>12</sub> O <sub>40</sub> ] <sup>3-</sup> /SiO <sub>2</sub>	methanol	–	–	CO/methanol = 3/1, 0.1 MPa, 200 °C; packed-bed flow micro-reactor	111
Rh(OAc) <sub>2</sub> /H <sub>3</sub> PW <sub>12</sub> O <sub>40</sub> /SiO <sub>2</sub>	methanol	80% MA	–	CO/methanol = 1/1, 0.1 MPa, 200 °C, GHSV = 1920 h <sup>-1</sup> ; continuous plug-flow microreactor	112

atomically dispersed  $\text{ReO}_4$  species or nanometre sized  $\text{ReO}_x$  species were predominantly produced, respectively, at lower Re loadings (1, 5 and 10% Re) or at higher Re loading (20% Re). The different nature of the Re species having an impact on their catalytic properties, being atomically dispersed  $\text{ReO}_4$  species the more selective towards acetic acid.  $\text{ReO}_x$  clusters and bulk  $\text{Re}_2\text{O}_7$  with stronger acid sites than  $\text{ReO}_4$  species, as determined by TPD- $\text{NH}_3$ , drove to the formation of dimethyl ether, while atomically dispersed  $\text{ReO}_4$  species were selective for the acetic acid production. Mechanistic insights on both Re materials show different rate orders for methanol, and similar for CO. To complete in situ FTIR measurements on atomically dispersed  $\text{ReO}_4$  species showed the formation of  $\text{CH}_3$  in  $-\text{OCH}_3$  bound to  $\text{ReO}_4$ , thus, the authors suggesting in basis of these results, the formation of  $\text{Re}(-\text{O}-\text{Si})(-\text{OH})(=\text{O})_2(-\text{OCH}_3)$  species, Re being in a +7 oxidation state (Figure 9), and further endorsed by in situ XAS. Altogether, the authors propose that the production

of acetic acid occurs through, first, a dissociative methanol adsorption to form  $\text{Re}(-\text{O}-\text{Si})(-\text{OH})(=\text{O})_2(-\text{OCH}_3)$ , followed by CO insertion into the terminal  $\text{CH}_3$  group, which is the rate-determining step. Previously, the same authors showed that dispersed Rh can promote CO insertion into methoxy species;<sup>[105]</sup> thus, introducing Rh to  $\text{ReO}_4$  species should increase the rate of the reaction, taking into consideration their proposed mechanism.  $\text{Rh}-\text{ReO}_x/\text{SiO}_2$  was successfully synthesized, and this modification leading to an increase of both activity and selectivity towards acetic acid (Figure 10).

Heteropoly acids (HPAs), with strong and potentially adjustable acidity, act similarly to zeolites to perform the halide-free carbonylation of methanol and dimethyl ether;<sup>[107]</sup> the addition of a metal also improving their catalytic performances.<sup>[108]</sup> HPAs are polyoxometalate inorganic cage structures with the general formula  $\text{H}_{3(\text{or } 4)}\text{MX}_{12}\text{O}_{40}$ , where M is typically P or Si, and x is usually W or Mo, and for carbonylation reactions, usually

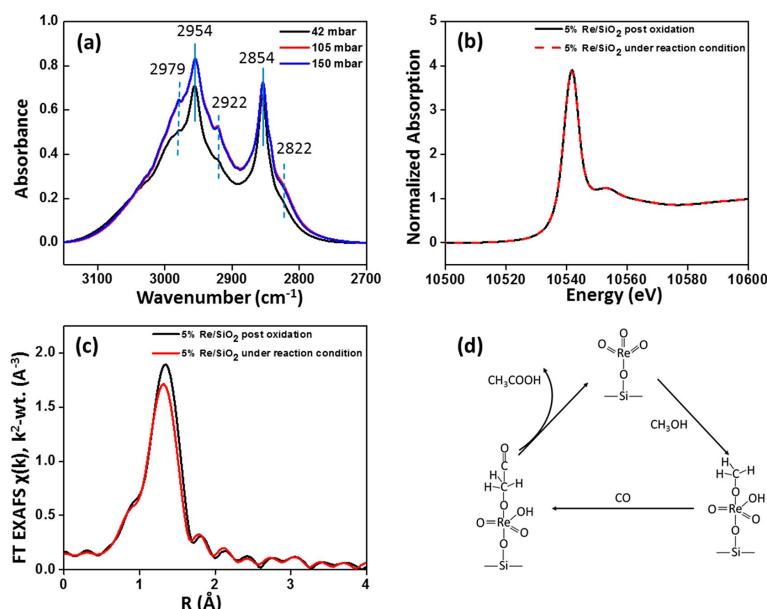


**Figure 9.** (a) In situ FTIR spectra for 5 wt%  $\text{Re}/\text{SiO}_2$ . The samples were oxidized at  $350^\circ\text{C}$  for 1 h before being exposed to  $4.2 \times 10^{-3}$ ,  $10.5 \times 10^{-3}$ , and  $15 \times 10^{-3}$  MPa methanol with a CO partial pressure of  $3 \times 10^{-3}$  MPa (balanced by He). (b) Re  $L_3$ -edge XANES spectra collected under oxidation condition (under  $\text{O}_2$  at  $350^\circ\text{C}$ ) and reaction condition ( $15 \times 10^{-3}$  MPa methanol and  $20 \times 10^{-3}$  MPa CO diluted in He,  $250^\circ\text{C}$ , 1 h) for 5wt% $\text{Re}/\text{SiO}_2$ . (c) EXAFS spectra collected at  $50^\circ\text{C}$  after  $350^\circ\text{C}$  oxidation and  $250^\circ\text{C}$  reaction condition for 5wt% $\text{Re}/\text{SiO}_2$ . (d) Proposed mechanism for acetic acid formation on atomically dispersed  $\text{ReO}_4$  species. Reprinted with permission from *J. Am. Chem. Soc.* 2020, 142 (33), 14178–14189. Copyright 2020 American Chemical Society.<sup>[106]</sup>

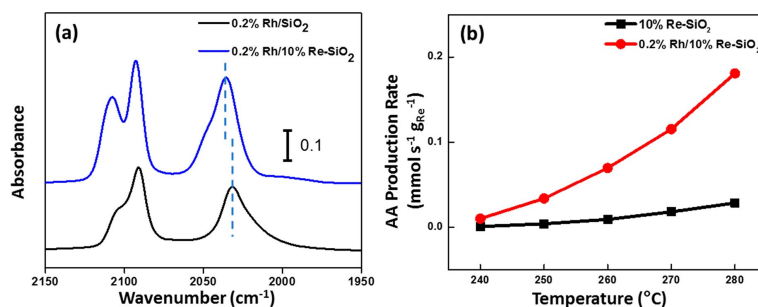


**Figure 10.** (a) CO probe molecule FTIR spectra of  $\text{Rh}/\text{SiO}_2$  and  $\text{Rh}/\text{ReO}_x-\text{SiO}_2$  catalysts. The catalysts were reduced at  $250^\circ\text{C}$  under CO and spectra were collected under Ar. (b) AA production rate comparison between 10wt% $\text{Re}/\text{SiO}_2$  and 0.2wt% $\text{Rh}/10\text{wt}\%\text{Re}-\text{SiO}_2$ . The catalysts were oxidized at  $350^\circ\text{C}$  for 1 h before being exposed to the reaction condition ( $3 \times 10^{-3}$  MPa methanol and CO). Reprinted with permission from *J. Am. Chem. Soc.* 2020, 142 (33), 14178–14189. Copyright 2020 American Chemical Society.<sup>[106]</sup>

modified with Rh. The carbonylation of dimethyl ether to methylacetate has been mainly been studied in early examples in unsupported Rh modified HPAs.<sup>[109,110]</sup> In recent examples, Rh/HPA are supported on oxides and methanol is directly carbonylated. For example,  $[\text{Rh}(\text{CO})(\text{Xantphos})]^+_{-n}[\text{H}_{3-n}\text{PW}_{12}\text{O}_{40}]^{n-}/\text{SiO}_2$  was able to carbonylate methanol under mild reaction conditions (0.1 MPa of CO and 200 °C), to produce a mixture of methyl acetate (MA) and dimethyl ether (DME). Several catalysts displaying various Rh/acid ratio were investigated, the best compromise activity/selectivity found at Rh/acid ratio = 0.5. Nevertheless, this catalyst showed deactivation issues, especially at high temperature.<sup>[111]</sup> In a similar work, the Rh dimer  $\text{Rh}(\text{OAc})_2$  was used as metal source to synthesize via impregnation a  $\text{Rh}(\text{OAc})_2/\text{H}_3\text{PW}_{12}\text{O}_{40}/\text{SiO}_2$  material to perform the methanol carbonylation in the gas phase.<sup>[112]</sup> The condensation of methanol to produce dimethyl ether predominate as seen in the previous work, thus MA and DME were the main products of the reaction. The optimized catalyst produced acetyls with a selectivity up to 90% at 250 °C; with a Rh-to-HPA ratio of 1.6). Nevertheless, high temperatures (350 °C) or absence of CO, deactivate the catalysts due to the formation of Rh NPs.

### With Halides

Many heterogeneous catalysts for methanol carbonylation rely in the use of halides as promoters in the gas- or the liquid-phase, as in homogeneous catalysis. For the later, it appears that their presence is still crucial to be able to carbonylate methanol. The presence of a halide, usually  $\text{CH}_3\text{I}$ , eliminates the need for a strong acidic support, thus opening the door to using various materials as supports for heterogeneous catalysts, specifically for SACs (Table 4). SACs based in Rh on carbonaceous materials are the most explored catalytic systems for this application.<sup>[113–115]</sup> Additionally, a bimetallic Ir–La single sites on carbon demonstrating to be an excellent catalyst for this reaction.<sup>[116,117]</sup>

The synthesis of a Rh SAC on zeolites was achieved through a hydrothermal process, which allowed to produce a stable and efficient catalyst for methanol carbonylation.<sup>[118]</sup> DRIFTS under CO displayed the Rh gem-dicarbonyl species ( $-\text{Rh}(\text{CO})_2$ ) on Rh/ZSM-5 (2095 and 2030  $\text{cm}^{-1}$ ) indicating the presence of well-isolated Rh cation sites on the sample. XPS analyses pointed to the presence of electron deficient  $\text{Rh}^{3+}$  species. All characterisation techniques endorsing the formation of Si–O–Rh bonds. The carbonylation of methanol was performed in the liquid phase in a  $\text{CH}_3\text{OH}/\text{CH}_3\text{I}$  mixture under 2.5 MPa of CO at 1000 rpm. In these conditions, isolated Rh cations stabilized by ZSM-5 zeolite (0.95 wt% Rh), displayed an acetyl formation rate of  $1160 \text{ mol}_{\text{acetyl}} \text{ mol}_{\text{Rh}}^{-1} \text{ h}^{-1}$ , much higher than observed for other Rh impregnated on zeolites catalysts, which exhibited also a considerable Rh leaching, or the commercial homogeneous Rh catalyst (Figure 11). In situ formed  $[\text{Rh}(\text{CO})_2\text{I}]$  analogue species are proposed as the active species in this highly active catalyst. The catalyst was recyclable and a filtration test showed the heterogeneous nature of the operating species,

further characterization of the spent catalysts displayed that it remained essentially the same that the fresh one.

The catalytically active species in the homogeneously catalysed methanol carbonylation,  $[\text{Rh}(\text{CO})_2\text{I}]^-$ , was heterogenized in a covalent triazine framework, a 1,3-bis(pyridyl)imidazolium-based one, which is a dispersible microporous polymer support bearing cationic functionality, to produce a catalysts for the carbonylation of methanol.<sup>[113]</sup> The characterization of the material indicates that Rh is atomically dispersed and coordinated to N atoms. The carbonylation of methanol in the presence of methyl iodide was performed in a 93% conversion with selectivities of 56% for acetic acid and 44% for methyl acetate at 240 °C. However, leaching of Rh was observed, which led to a loss of activity. Rh incorporated in the  $\text{C}_3\text{N}_4$  framework with metal loadings between 1–3 wt% produced mainly acetic acid (84%) together with methyl acetate at full conversion of methanol in the liquid phase (140 °C, 4 MPa of CO,  $\text{CH}_3\text{OH}/\text{CH}_3\text{I}/\text{H}_2\text{O} = 43:34:23$  (molar ratio of  $\text{CH}_3\text{OH}/\text{CH}_3\text{I} = 0.79$ , 7 h).<sup>[114]</sup> Even if it is not clear if 1% Rh loaded catalyst is composed by isolated Rh atoms, for the other samples, XRD patterns show that Rh NPs are present in the fresh catalysts, this could be an explanation about the increase of leaching with higher Rh loading. Only a recycling test was performed at full conversion.

Fine-tuning of the electronic properties of the metal is crucial in SACs. For methanol carbonylation the doping of the support, the introduction of a second metal, or the fine dosing of a theoretical poison of metallic surfaces have been used as strategies to improve catalytic properties of SACs for this application. For instance, the tailoring of activated carbon (AC) with N and S enhanced the carbonylation of methanol using a Rh SAC. Mu et al. synthesized a series of single-Rh-sites on S, N-co-doped AC, Rh/AC–NS, and for comparison purposes their monodoped Rh/AC–S and Rh/AC–N, and undoped AC, Rh/AC (Figure 12).<sup>[115]</sup> The presence of electron donating groups conferred to the Rh atoms an increased electron density compared to Rh on undoped AC. This is illustrated by the XPS analyses, the spectra show that the peaks corresponding the  $\text{Rh}^{1+}$  and  $\text{Rh}^{3+}$  species coexist in all samples, shifted to lower binding energies for all doped materials (Figure 13 (f)). The catalysts tested for the carbonylation of methanol, at 180 °C using syngas ( $\text{CO}/\text{H}_2$  1:1) and a vaporized mixture of  $\text{CH}_3\text{OH}$  and  $\text{CH}_3\text{I}$ , showed an effect of the doping on the rate of the reaction (Figure 13). Methanol was converted to methyl acetate with a rate of  $2731 \text{ h}^{-1}$  for Rh/AC–NS, higher than those of Rh/AC ( $1735 \text{ h}^{-1}$ ), Rh/AC–N ( $1926 \text{ h}^{-1}$ ), and Rh/AC–S ( $850 \text{ h}^{-1}$ ) under the same reaction conditions (Figure 13 (b)). The synergistic effect of N and S was further tuned by changing their ratio ( $\text{S}/\text{N} = 0.27\text{--}2.03$ ). A volcano relationship was found between S/N ratio and activity, with the optimal found at 0.45. Supplementary DFT calculations show that the addition of both N and S decreased the energy barrier of the oxidative addition.

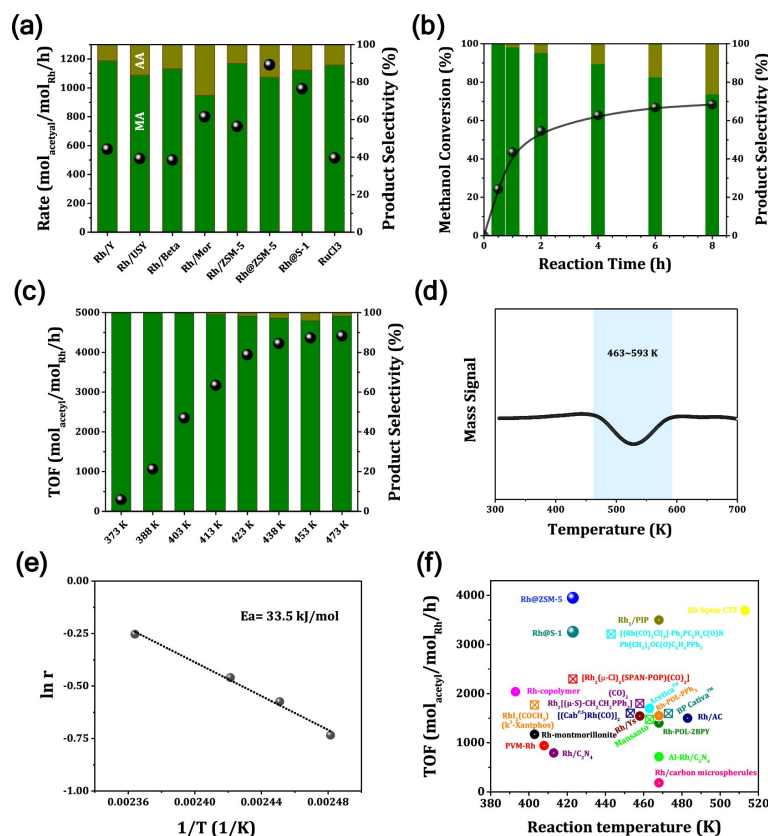
Feng et al. used another strategy to dope a catalyst based on Rh over carbon for this application.<sup>[119]</sup> Three catalysts were synthesised, two consisting in Rh NPs supported in AC or CMK-3 (an ordered carbon), and one in Rh single sites on AC, generated in situ from Rh NPs. The latter SAC being described

Table 4. Methanol carbonylation using single-atom catalysts with additives.					
Catalyst	Conversion	Selectivity	Rate	Reaction conditions	Ref.
Rh/ZSM-5	67%	83% MA 17%AA	1160 mol <sub>acetyl</sub> mol <sub>Rh</sub> <sup>-1</sup> h <sup>-1</sup>	0.03 g of catalyst, 2 mL of CH <sub>3</sub> OH, 316 μL of CH <sub>3</sub> I, 2.5 MPa CO, 6 h, 150 °C	118
Rh/S-1	62%	87% MA 13%AA	994 mol <sub>acetyl</sub> mol <sub>Rh</sub> <sup>-1</sup> h <sup>-1</sup>	0.03 g of catalyst, 2 mL of CH <sub>3</sub> OH, 316 μL of CH <sub>3</sub> I, 2.5 MPa CO, 6 h, 150 °C	118
Rh/ZSM-5 (im- pregnated, NPs)	47%	90% MA 10%AA	773 mol <sub>acetyl</sub> mol <sub>Rh</sub> <sup>-1</sup> h <sup>-1</sup>	0.03 g of catalyst, 2 mL of CH <sub>3</sub> OH, 316 μL of CH <sub>3</sub> I, 2.5 MPa CO, 6 h, 150 °C	118
[Rh(CO) <sub>2</sub> I <sub>2</sub> ] <sup>-</sup> /cova- lent triazine framework	83%	63% MA 37%AA	3693 mol <sub>acetyl</sub> mol <sub>Rh</sub> <sup>-1</sup> h <sup>-1</sup>	0.2 g of catalyst, CH <sub>3</sub> OH/CH <sub>3</sub> I 10:1, 1.5 MPa, 240 °C	113
Rh/C <sub>3</sub> N <sub>4</sub>	> 99%	84 MA 16%AA	–	0.1 g of catalysts, CH <sub>3</sub> OH/CH <sub>3</sub> I/H <sub>2</sub> O 43:34:23, 4 MPa CO, 7 h, 140 °C	114
Rh/AC-NS	88%	85% MA	2731 mol <sub>acetyl</sub> mol <sub>Rh</sub> <sup>-1</sup> h <sup>-1</sup>	0.25 g of catalyst, CH <sub>3</sub> OH = 87 μL min <sup>-1</sup> , CH <sub>3</sub> I = 13 μL min <sup>-1</sup> , 1.7 MPa CO/H <sub>2</sub> 10:1 (60 mL min <sup>-1</sup> ), LHSV = 12 h <sup>-1</sup> , 30 h, 200 °C	115
Rh/AC-S	57%	85% MA	850 mol <sub>acetyl</sub> mol <sub>Rh</sub> <sup>-1</sup> h <sup>-1</sup>	0.25 g of catalyst, CH <sub>3</sub> OH = 87 μL min <sup>-1</sup> , CH <sub>3</sub> I = 13 μL min <sup>-1</sup> , 1.7 MPa CO/H <sub>2</sub> 10:1 (60 mL min <sup>-1</sup> ), LHSV = 12 h <sup>-1</sup> , 30 h, 200 °C	115
Rh/AC-N	79%	83% MA	1926 mol <sub>acetyl</sub> mol <sub>Rh</sub> <sup>-1</sup> h <sup>-1</sup>	0.25 g of catalyst, CH <sub>3</sub> OH = 87 μL min <sup>-1</sup> , CH <sub>3</sub> I = 13 μL min <sup>-1</sup> , 1.7 MPa of CO/H <sub>2</sub> = 10/1 (60 mL min <sup>-1</sup> ), LHSV = 12 h <sup>-1</sup> , 30 h, 200 °C	115
Rh/AC	78%	75% MA	1735 mol <sub>acetyl</sub> mol <sub>Rh</sub> <sup>-1</sup> h <sup>-1</sup>	0.25 g of catalyst, CH <sub>3</sub> OH = 87 μL min <sup>-1</sup> , CH <sub>3</sub> I = 13 μL min <sup>-1</sup> , 1.7 MPa CO/H <sub>2</sub> 10:1 (60 mL min <sup>-1</sup> ), LHSV = 12 h <sup>-1</sup> , 30 h, 200 °C	115
Rh/AC	> 99%	73% MA	3133 mol <sub>acetyl</sub> mol <sub>Rh</sub> <sup>-1</sup> h <sup>-1</sup>	0.25 g of catalyst, 1.7 MPa, 240 °C, CO = 55.4 mL min <sup>-1</sup> , H <sub>2</sub> = 5.5 mL min <sup>-1</sup> , CH <sub>3</sub> OH = 87 μL min <sup>-1</sup> , CH <sub>3</sub> I = 13 μL min <sup>-1</sup>	120
Rh/AC	55%	58% MA	3192 mol <sub>CO</sub> mol <sub>Rh</sub> <sup>-1</sup> h <sup>-1</sup>	0.3 g of catalyst, 1.7 MPa CO/H <sub>2</sub> 10:1, 240 °C, CO = 55.4 mL min <sup>-1</sup> , H <sub>2</sub> = 5.5 mL min <sup>-1</sup> , CH <sub>3</sub> OH = 87 μL min <sup>-1</sup> , CH <sub>3</sub> I = 13 μL min <sup>-1</sup>	119
Rh/AC + H <sub>2</sub> S	71%	36% MA	3974 mol <sub>CO</sub> mol <sub>Rh</sub> <sup>-1</sup> h <sup>-1</sup>	0.3 g of catalyst, H <sub>2</sub> S co-feed, H <sub>2</sub> S 1000 ppm, 1.7 MPa CO/H <sub>2</sub> 10:1, 240 °C, CO = 55.4 mL min <sup>-1</sup> , H <sub>2</sub> = 5.5 mL min <sup>-1</sup> , CH <sub>3</sub> OH = 87 μL min <sup>-1</sup> , CH <sub>3</sub> I = 13 μL min <sup>-1</sup>	119
Rh NPs/AC	53%	27% MA	2921 mol <sub>CO</sub> mol <sub>Rh</sub> <sup>-1</sup> h <sup>-1</sup>	0.3 g of catalyst, 1.7 MPa CO/H <sub>2</sub> 10:1, 240 °C, CO = 55.4 mL min <sup>-1</sup> , H <sub>2</sub> = 5.5 mL min <sup>-1</sup> , CH <sub>3</sub> OH = 87 μL min <sup>-1</sup> , CH <sub>3</sub> I = 13 μL min <sup>-1</sup>	119
Rh NPs/AC + H <sub>2</sub> S	67%	31% MA	3396 mol <sub>CO</sub> mol <sub>Rh</sub> <sup>-1</sup> h <sup>-1</sup>	0.3 g of catalyst, H <sub>2</sub> S co-feed, H <sub>2</sub> S 1000 ppm, 1.7 MPa CO/H <sub>2</sub> 10:1, 240 °C, CO = 55.4 mL min <sup>-1</sup> , H <sub>2</sub> = 5.5 mL min <sup>-1</sup> , CH <sub>3</sub> OH = 87 μL min <sup>-1</sup> , CH <sub>3</sub> I = 13 μL min <sup>-1</sup>	119
Rh NPs/CMK-3	16%	97% MA	395 mol <sub>CO</sub> mol <sub>Rh</sub> <sup>-1</sup> h <sup>-1</sup>	0.3 g of catalyst, 1.7 MPa CO/H <sub>2</sub> 10:1, 240 °C, CO = 55.4 mL min <sup>-1</sup> , H <sub>2</sub> = 5.5 mL min <sup>-1</sup> , CH <sub>3</sub> OH = 87 μL min <sup>-1</sup> , CH <sub>3</sub> I = 13 μL min <sup>-1</sup>	119
Rh NPs/CMK-3 + H <sub>2</sub> S	8%	67% MA	17 mol <sub>CO</sub> mol <sub>Rh</sub> <sup>-1</sup> h <sup>-1</sup>	0.3 g of catalyst, H <sub>2</sub> S co-feed, H <sub>2</sub> S 1000 ppm, 1.7 MPa CO/H <sub>2</sub> 10:1, 240 °C, CO = 55.4 mL min <sup>-1</sup> , H <sub>2</sub> = 5.5 mL min <sup>-1</sup> , CH <sub>3</sub> OH = 87 μL min <sup>-1</sup> , CH <sub>3</sub> I = 13 μL min <sup>-1</sup>	119
Ir–La/AC	~ 45%	90% MA	2200 mol <sub>acetyl</sub> mol <sub>Ir</sub> <sup>-1</sup> h <sup>-1</sup>	240 °C, 2.5 MPa, CO/H <sub>2</sub> 4:1, CO/CH <sub>3</sub> OH = 1 (mole ratio), CH <sub>3</sub> I/CH <sub>3</sub> OH = 1:6 (wt %)	122
Rh/POL-PPh <sub>3</sub>	19%	96% MA	1558 mol <sub>acetyl</sub> mol <sub>Rh</sub> <sup>-1</sup> h <sup>-1</sup>	0.1500 g of catalyst (0.0044 mmol Rh) 2.5 MPa CO flow of 1.34 mmol min <sup>-1</sup> CH <sub>3</sub> OH/ CH <sub>3</sub> I/CO 1:0.16:1.4, 195 °C	125
Rh/PIP-PPh <sub>3</sub>	–	–	3500 mol <sub>acetyl</sub> mol <sub>Rh</sub> <sup>-1</sup> h <sup>-1</sup>	3.5 MPa, 195 °C	126
Rh/POL-2BPY	14%	98% MA	1330 mol <sub>acetyl</sub> mol <sub>Rh</sub> <sup>-1</sup> h <sup>-1</sup>	0.1 g of catalyst (0.0044 mmol Rh) 2.5 MPa CO flow of 1.34 mmol min <sup>-1</sup> CH <sub>3</sub> OH/ CH <sub>3</sub> I/CO 1:0.16:1.4, 195 °C	127

earlier as catalyst for the carbonylation of methanol by the same authors displaying excellent performances for this application.<sup>[120]</sup> In this earlier work, Rh/AC SAC prepared using their methodology of atomic dispersion of supported metal NPs,<sup>[121]</sup> methanol was fully converted at a rate of 3133 mol<sub>acetyl</sub>mol<sub>Rh</sub><sup>-1</sup>h<sup>-1</sup> and a selectivity towards MA of 73%. Later, Rh NPs /AC, Rh NPs /CMK-3 and Rh/AC SAC were submitted to the carbonylation of methanol in the gas-phase in a fixed-bed the reactor and H<sub>2</sub>S was co-fed in the reactor with the syngas (1000 ppm) (Figure 14).<sup>[119]</sup> Rh on AC, NP or single

site, increased its production in presence of H<sub>2</sub>S, while it had a detrimental effect when utilizing Rh NPs/CMK-3. Through spectroscopic techniques, the authors proposed that CH<sub>3</sub>SH and CH<sub>3</sub>SCH<sub>3</sub> were formed in Rh single sites present in both Rh/AC samples, which by their coordination to Rh conferred stable single sites for both materials based on AC. DFT calculations showing that, also, their presence provided a lower Rh energy barrier of CH<sub>3</sub>I oxidative addition and promote the methanol carbonylation. In Rh/CMK-3, the addition of H<sub>2</sub>S to the reaction





**Figure 11.** Catalytic performance of Rh/ZSM-5 in methanol carbonylation. (a) Comparison between Rh-containing zeolites and RhCl<sub>3</sub>. Reaction conditions: 0.03 g of catalyst, 2 mL of CH<sub>3</sub>OH, 316 μL of CH<sub>3</sub>I, 2.5 MPa of CO, 6 h, 150 °C. (b) Time-dependent methanol conversion and production selectivity in methanol carbonylation catalysed by Rh/ZSM-5. Reaction conditions: 0.03 g of catalyst, 2 mL of CH<sub>3</sub>OH, 316 μL of CH<sub>3</sub>I, 2.5 MPa of CO, 150 °C. (c) TOF and production selectivity in methanol carbonylation catalysed by Rh/ZSM-5 at different temperatures. Reaction conditions: 0.03 g of catalyst, 2 mL of CH<sub>3</sub>OH, 316 μL of CH<sub>3</sub>I, 2.5 MPa of CO, 1 h. (d) CO-TPR profile of Rh/ZSM-5. (e) Arrhenius plot of methanol carbonylation catalysed by Rh/ZSM-5. (f) Comparison of Rh-based catalysts for methanol carbonylation: (open symbols) homogeneous catalysts; (closed symbols) heterogeneous catalysts. The TOF value was calculated as the moles of acetyl formed per mole of Rh per hour; data were collected at the first hour of the reaction if available. Adapted with permission from ACS Catal. 2021, 11, 12, 7249–7256. Copyright 2021 American Chemical Society.<sup>[118]</sup>

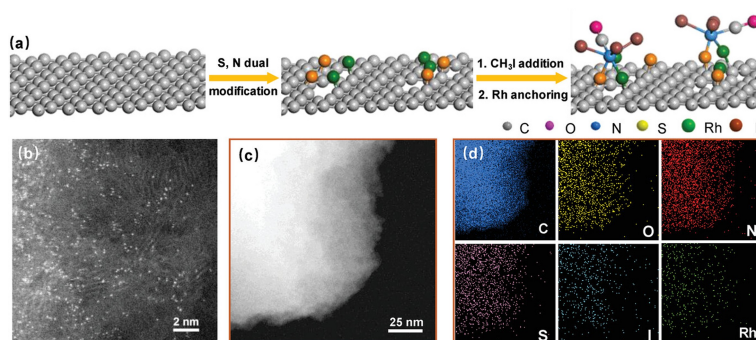


**Figure 12.** Synthesis and structural characterization of Rh/AC-NS. (a) Schematic illustration of the synthesis process of Rh/AC-NS. (b) Aberration-corrected high-angle annular dark-field scanning transmission electron microscopy (AC-HAADF-STEM) image of the Rh/AC-NS. (c), (d) HAADF-STEM image and the corresponding energy dispersive X-ray (EDX) mapping of Rh/AC-NS. Scale bar: 25 nm. Adapted with permission from Adv. Funct. Mater. 2023, 33 (52), 2305823.<sup>[115]</sup>

mixture provoked the formation of a Rh–S layer which blocked the metallic surface.

The introduction of a second metal to an Ir based catalysts also proved to be a good strategy to provide an excellent catalyst for methanol carbonylation. Thus, an Ir based catalyst doped with La on carbon, Ir–La/C, has shown that is able to

carbonylate methanol in the gas-phase at 240 °C under 1.7 MPa of CO/H<sub>2</sub> in the presence of CH<sub>3</sub>I. Characterization of the materials displayed that probably most of the catalyst had an isolated molecular heterobimetallic structure.<sup>[116]</sup> The catalyst provided a high selectivity to acetic acid and methyl acetate (> 99%), for long periods of time (1 month), which highlights the

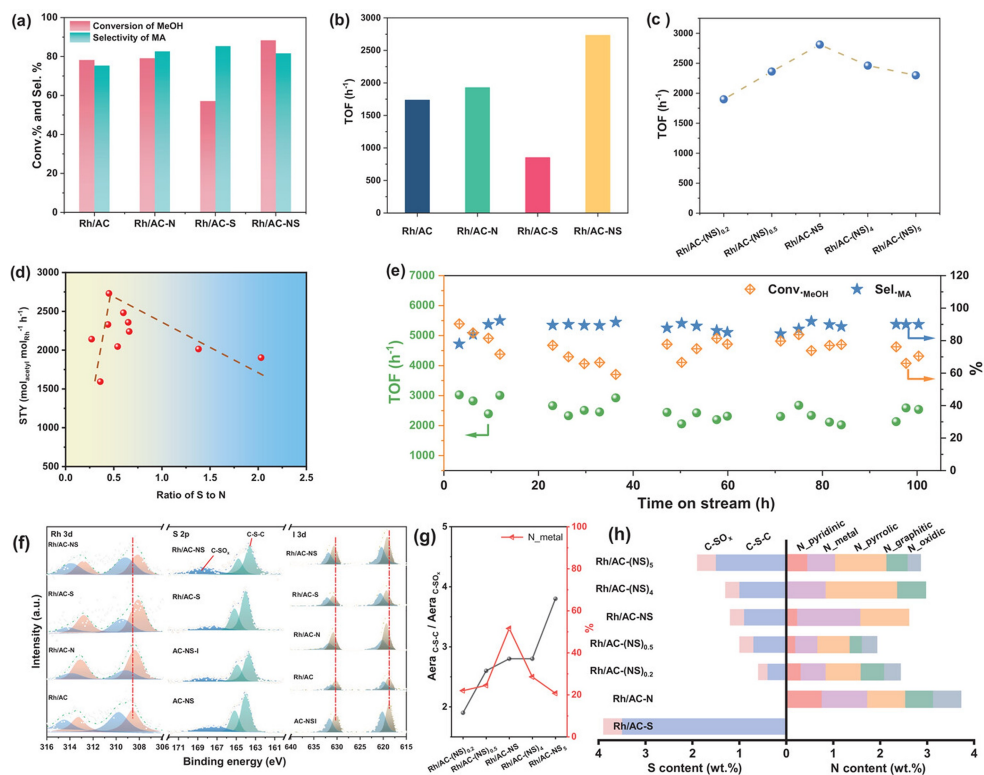


**Figure 13.** Catalytic performance for the methanol carbonylation reaction. (a) Methanol conversion and methyl acetate (MA) selectivity after 23 h reaction on Rh/AC, Rh/AC–N, Rh/AC–S, and Rh/AC–NS catalysts. (b) Acetyl production rate after 23 h reaction on Rh/AC, Rh/AC–N, Rh/AC–S, and Rh/AC–NS. (c) The acetyl production rate for Rh/AC–(NS)<sub>0.2</sub>, Rh/AC–(NS)<sub>0.5</sub>, Rh/AC–NS, Rh/AC–(NS)<sub>4</sub>, and (NS)<sub>5</sub> catalysts after 30 h reaction. (d) Relationship between the ratio of S to N and acetyl production rate after 23 h reaction. (e) Stability test of the Rh/AC–NS catalyst. [Conditions (a, b, c, d, e): m(catalyst) = 0.25 g, P = 1.7 MPa, V(CO/H<sub>2</sub>) = 10/1 = 60 mL min<sup>-1</sup>, CH<sub>3</sub>OH = 87  $\mu$ L min<sup>-1</sup>, CH<sub>3</sub>I = 13  $\mu$ L min<sup>-1</sup>, LHSV = 12 h<sup>-1</sup>, 200 °C.] (f) Rh 3d spectra of the Rh/AC, Rh/AC–N, Rh/AC–S, and Rh/AC–NS; S 2p XPS spectra of the AC–NS, AC–NS–I, Rh/AC–S and Rh/AC–NS; and I 3d XPS spectra of the AC–S–I, Rh/AC, Rh/AC–N, Rh/AC–S and Rh/AC–NS. (g) The ratio of C–S–C to C–SO<sub>x</sub> species was calculated from the deconvolution of the S 2p signal. (h) Content of different S and N species from XPS fitting results. Adapted with permission from *Adv. Funct. Mater.* 2023, 33 (52), 2305823.<sup>[115]</sup>

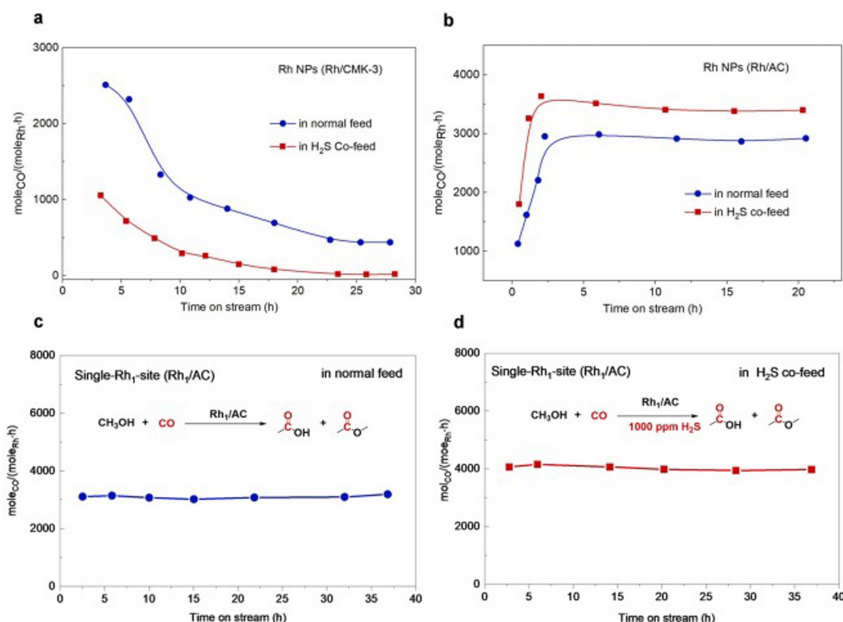


**Figure 14.** Impact of H<sub>2</sub>S on the activity of Rh NPs (Rh NPs/CMK-3 and Rh NPs/AC) and single-Rh-site (Rh/AC) for methanol carbonylation. Conditions: H<sub>2</sub>S co-fed, H<sub>2</sub>S 1000 ppm in syngas (CO/H<sub>2</sub>), 240 °C, 1.7 MPa, CO/CH<sub>3</sub>OH = 1.0 (molar ratio), CO/H<sub>2</sub> = 10 (molar ratio), CH<sub>3</sub>I/CH<sub>3</sub>OH = 3/7 (mass ratio), CO 55.4 mL/min, H<sub>2</sub> 5.5 mL/min, CH<sub>3</sub>OH (liquid) 87.0  $\mu$ L/min, CH<sub>3</sub>I (liquid) 13.0  $\mu$ L/min, 0.3 g Rh/AC or Rh/CMK-3 or Rh<sub>1</sub>/AC in a  $\varnothing$ 6 mm \* 400 mm Hastelloy fixed-bed reactor. Reprinted from *Appl. Catal. B: Environ.* 2023, 325, Feng, S.; Mu, J.; Lin, X.; Song, X.; Liu, S.; Shi, W.; Zhang, W.; Wu, G.; Jiayue, Y.; Dong, W., Sulfur-poisoning on Rh NP but sulfur-promotion on single-Rh<sub>1</sub>-site for methanol carbonylation, 122318, Copyright 2022, with permission from Elsevier.<sup>[119]</sup>

robustness of the catalyst. This is in contrast to the Ir/C prepared for comparative purposes: First, La had a role during the synthesis, as in absence of it, Ir sintered to give NPs instead of forming isolated species; second, the Lewis acidity of La accelerated the reaction rate by favouring the insertion of CO, which could be the rate-determining step. Interestingly, after testing various transition-metal-oxide-promoted Ir/C catalysts, a correlation between activity and electronegativity of transition metals was found, endorsing the hypothesis that La acts as a Lewis acid and accelerates the CO insertion. The authors added more experimental data plus DFT calculations in a following work endorsing further the role of La.<sup>[117]</sup> Similarly, Ir–La/AC was used in a fixed-bed reactor as catalysts for methanol carbonylation.<sup>[122]</sup> The reactor was fed both with mixtures of CO/H<sub>2</sub> and CH<sub>3</sub>OH/CH<sub>3</sub>I to obtain, at best conditions, a TOF of 2200 h<sup>-1</sup> and a selectivity towards methyl acetate over 90%. The addition of La, as in the previous work, helped to produce isolated Ir species and their stabilization under reaction conditions. In a follow up work,<sup>[123]</sup> the authors showed that in the absence of La, Ir/AC SAC, sintered to produce NPs induced by H<sub>2</sub> reduction and carbon deposition. The introduction of La suppressed the reduction of Ir to Ir(0), and provided stability by forming binuclear Ir–La, and decreased the apparent activation energy of methanol carbonylation. Theoretical calculations showed that the introduction of La decreased the energy barrier of the rate determining step, and at same time reduced the carbon deposition on Ir.

The utilization of POPs to obtain SACs has been explored as a strategy for the carbonylation of methanol, similar to their application as catalysts for hydroformylation. POPs bearing P and N functional groups, in order to anchor Rh atoms in isolated manner, have been used as catalysts for this reaction. Rh/POL-PPh<sub>3</sub>, already used as hydroformylation catalyst,<sup>[124]</sup> which polymer is the result of the polymerization of tris(4-vinylphenyl)phosphine, was applied as catalyst for the carbonylation of methanol in fixed-bed reactor (CH<sub>3</sub>OH/CH<sub>3</sub>I/CO = 1:0.16:1.4), displaying a TOF of 1558 h<sup>-1</sup>.<sup>[125]</sup> The catalysts displayed high selectivity towards methyl acetate, up to 97%. Analyses of the spent catalysts did not show any significant change compared to the fresh one. The vinyl-polymerized POP using a methyltris(4-vinylphenyl)phosphonium iodide monomer, displays a cationic nature which allows to anchor efficiently the anionic [Rh(CO)<sub>2</sub>I<sub>2</sub>]<sup>-</sup> species generated in situ (0.28 wt% Rh).<sup>[126]</sup> The authors, using several techniques, concluded that the [Rh(CO)<sub>2</sub>I<sub>2</sub>]<sup>-</sup> species was ionically immobilized onto the cationic framework in the form of [P]<sup>+</sup>–[Rh(CO)<sub>2</sub>I<sub>2</sub>]<sup>-</sup>–[P]<sup>+</sup>. The cationic Rh/POP efficiently catalysed the carbonylation of methanol in the vapour-phase in a fixed-bed reactor (195 °C, 3.5 MPa), displaying a TOF of 3500 h<sup>-1</sup>, outperforming homogeneous catalysts based on [Rh(CO)<sub>2</sub>I<sub>2</sub>]<sup>-</sup> species. Similarly, 6,6'-divinyl-2,2'-bipyridine polymerization, resulted with a POPs able to accommodate Rh single atoms.<sup>[127]</sup> At optimized reaction conditions, the Rh/POL-2BPY catalysts displayed a TOF of 1400 h<sup>-1</sup> for near 400 h under 195 °C and 2.5 MPa for the carbonylation of methanol. Analyses of the catalyst after reaction demonstrating its robustness. A Rh/POP was also used for ethanol carbonylation,<sup>[128]</sup> the catalyst exhibit

to be stable up to 1000 h of reaction, displaying a TOF of 436 h<sup>-1</sup> with a propionyl selectivity of 95 % under 3.5 MPa of CO MPa at 195 °C using a mixture CH<sub>3</sub>CH<sub>2</sub>OH/ CH<sub>3</sub>CH<sub>2</sub>I = 3.39:1.

The use of acidic solid supports combined with a metal allows to perform the carbonylation of methanol in the gas-phase without the addition of halides. The acidic sites are responsible of the activation of methanol, and work together with a metal, usually Rh, responsible to activate the CO. Usually acetic acid is produced from methanol at temperatures > 200 °C in the gas-phase, being the number of acidic sites crucial for the catalytic properties of these materials. The use of CH<sub>3</sub>I allows to explore other manners of modification of the catalytic materials, as acidic sites are not needed to activate methanol. As observed in hydroformylation reactions catalysed by SACs, introducing electron-donor doping atoms onto the support allows to increase the catalytic performances of SACs for methanol carbonylation. Also, bimetallic single sites have demonstrated to be a good strategy with this aim, while providing robustness to the single sites. Finally, introducing H<sub>2</sub>S into the catalytic mixture produced in situ thiol species which provided to Rh single atoms more robustness as well, by producing thiolate species coordinated to the metal. In general, excellent results using Rh as metal pave the way for future work on this area, for which deactivation and selectivity remain critical points. Zeolites and carbonaceous supports are the most studied supports in this application, and for now very few studies deal with the modification of the support, which is key to design new catalysts for this application.

## Oxidative Carbonylation

An alternative to the carbonylation of methanol for the synthesis of acetic acid, a key bulk chemical, is the single-step chemoselective transformation of methane to acetic acid.<sup>[43,44]</sup> Homogeneous catalysts based on Rh and Pt and heterogeneous catalytic systems based on zeolites, Rh and Cu modified, are able to use O<sub>2</sub> as oxidant in the presence of CO to produce acetic acid from methane.<sup>[129,130]</sup> Recently, the production of acetic acid has been achieved without CO, thus, using only CH<sub>4</sub> and O<sub>2</sub> as oxidant, in the presence of Au NPs<sup>[131]</sup> or Cu in a porous cerium MOF.<sup>[132]</sup> These are remarkable results as usually other oxygenates are produced from methane, mainly methanol, in the absence of CO in the reaction mixture.<sup>[133]</sup> The oxidative carbonylation can be catalysed solely by acid zeolites,<sup>[134]</sup> and, as similarly observed for methanol carbonylation, the addition of a metal provides more efficient catalysts for this oxidative reaction (Table 5).<sup>[135]</sup> As alternative to methane, CH<sub>3</sub>Cl can be also oxidatively carbonylated in presence of CO and O<sub>2</sub> in water with zeolites, reaching higher selectivities towards carbonylated products, up to 99% of acetic acid and methyl acetate.<sup>[136]</sup> Brønsted acidic sites of zeolites have been identified as essential for this type of catalysts. Narsimhan et al.<sup>[137]</sup> demonstrated that Cu/MOR, which displays acidic sites, was more active than Cu/ZSM-5, which does not. Furthermore, by decreasing the acidic sites of the mordenite by titration, the catalytic activity decreased (Figure 15). Mechanistic

Table 5. Oxidative carbonylation of methane using single-atom catalysts.						
Catalyst	Production/Conversion	Selectivity	Rate	Reaction conditions	Ref.	
Ce-UiO-Cu(OH)	335 mmol <sub>g<sub>cat</sub></sub> <sup>-1</sup> 400 mol <sub>AA</sub> mol <sub>metal</sub> <sup>-1</sup>	96% AA	–	3.7 mg of Ce-UiO-Cu(OH) (3.1 μmol of Cu), 8 mL H <sub>2</sub> O, 3 MPa CH <sub>4</sub> , 0.6 MPa O <sub>2</sub> , 40 h, 115 °C	132	
Rh/ZSM-5	–	> 65% AA	~ 12 mol <sub>AA</sub> mol <sub>metal</sub> <sup>-1</sup> h <sup>-1</sup>	40 mg catalyst, 0.2 MPa O <sub>2</sub> , 0.5 MPa CO, 2.0 MPa CH <sub>4</sub> , 8 mL H <sub>2</sub> O, 3 h, 150 °C	135	
Rh/ZSM-5	–	70% AA	356 mol mol <sub>Rh</sub> <sup>-1</sup> h <sup>-1</sup>	28 mg of catalyst, 5 MPa CH <sub>4</sub> , 1 MPa CO, 0.8 MPa O <sub>2</sub> , 10 mL, 12 h, 150 °C	139	
Rh/ZSM-5	1.4%	~70% AA	151 mol mol <sub>Rh</sub> <sup>-1</sup> h <sup>-1</sup>	20 mg of catalyst, 2 MPa CH <sub>4</sub> , 0.5 MPa CO, 0.2 MPa O <sub>2</sub> , 20 mL, 2 h, 150 °C	138	
Rh/db-ZSM-5 (hydrophobic)	706 mmol <sub>AA</sub> g <sub>cat</sub> <sup>-1</sup>	~20% AA	–	30 mg catalyst, 0.05 MPa O <sub>2</sub> , 0.1 MPa CO, 0.3 MPa CH <sub>4</sub> , 10 mL H <sub>2</sub> O, 2 h, 150 °C	140	
0.05%Rh/ZrO <sub>2</sub>	–	~18% AA	316.3 mmol kg <sup>-1</sup> h <sup>-1</sup>	10 mg of catalyst, 40 mL H <sub>2</sub> O 0.5 M, 2 MPa (47.5% CH <sub>4</sub> , 47.5% CO), 6 h, 80 °C, 800 rpm	141	
Rh/pMOF	5.22%	65% AA (light) 64% CH <sub>3</sub> OH (dark)	23.62 mmol g <sub>cat</sub> <sup>-1</sup> h <sup>-1</sup> (light) 48.24 mol mol <sub>Rh</sub> <sup>-1</sup> h <sup>-1</sup> (light)	20 mg of catalyst, 0.4 MPa O <sub>2</sub> , 0.5 MPa CO, 1.5 MPa CH <sub>4</sub> , 20 mL H <sub>2</sub> O, 150 °C, 3 h, light: 100 mW/cm <sup>2</sup> , AM 1.5G	142	
Rh-Cu/POPs	–	< 4% AA 9% CH <sub>3</sub> OH 86% CH <sub>2</sub> (OH) <sub>2</sub>	36 mol mol <sub>Rh</sub> <sup>-1</sup> h <sup>-1</sup>	50 mg of catalyst, 20 mL H <sub>2</sub> O, 3 MPa CH <sub>4</sub> , 1 MPa CO, 0.5 MPa O <sub>2</sub> , 2 h, 150 °C	143	
Rh-Cu/POPs + C <sub>6</sub> H <sub>5</sub> I	–	< 7% AA 11% CH <sub>3</sub> OH 53% CH <sub>2</sub> (OH) <sub>2</sub>	80 mol mol <sub>Rh</sub> <sup>-1</sup> h <sup>-1</sup>	50 mg of catalyst, 45 mg C <sub>6</sub> H <sub>5</sub> I, 20 mL H <sub>2</sub> O, 3 MPa CH <sub>4</sub> , 1 MPa CO, 0.5 MPa O <sub>2</sub> , 2 h, 150 °C	143	
Ir <sub>dimer</sub> /SBA-15	10.16 mmol <sub>AA</sub> g <sub>cat</sub> <sup>-1</sup>	62% AA	21.27 mol mol <sub>Ir</sub> <sup>-1</sup> h <sup>-1</sup>	15 mg of catalyst, 0.4 MPa O <sub>2</sub> , 0.5 MPa CO, 1.9 MPa CH <sub>4</sub> , 15 mL H <sub>2</sub> O, 3 h, 150 °C, 700 rpm	144	
Pd/ZSM-5	0.08%	78% AA	131 h <sup>-1</sup>	25 mg catalyst, 2 MPa CH <sub>4</sub> , 2 MPa CO, 15 mL 0.6 M H <sub>2</sub> O <sub>2</sub> , 0.5 h, 25 °C	145	
Fe-Fe/ZSM	0.22%	59% AA	200 μmol <sub>AA</sub> g <sub>cat</sub> <sup>-1</sup> h <sup>-1</sup>	30 mg of catalyst, 0.5 MPa 97% CO/N <sub>2</sub> , 2.5 MPa 95% CH <sub>4</sub> /Ar, 654 mmol H <sub>2</sub> O <sub>2</sub> , 20 mL H <sub>2</sub> O, 6 h, 50 °C	39	
Fe/ZSM-5	6.01 mmol g <sub>cat</sub> <sup>-1</sup>	63% AA	19.00 mmol <sub>CH<sub>4</sub></sub> g <sub>cat</sub> <sup>-1</sup> h <sup>-1</sup> 61.26 mmol <sub>CO</sub> g <sub>cat</sub> <sup>-1</sup> h <sup>-1</sup> 162.83 mmol <sub>H<sub>2</sub>O<sub>2</sub></sub> g <sub>cat</sub> <sup>-1</sup> h <sup>-1</sup>	30 mg of Fe/ZSM-5, 10 mL of 0.5 mol L <sup>-1</sup> H <sub>2</sub> O <sub>2</sub> , 4.0 MPa CH <sub>4</sub> , 4.0 MPa CO, 0.5 h, 50 °C	146	
Ni/ZSM-5	4956 μmol/g <sub>cat</sub>	82% AA	–	20 mg of catalyst, 20 mL H <sub>2</sub> O, 50 μL (0.654 mmol) H <sub>2</sub> O <sub>2</sub> (30 wt %), 3 MPa (97% CO/N <sub>2</sub> and 95% CH <sub>4</sub> /Ar), 50 °C, 1000 rpm	147	

studies demonstrated that the number of Brønsted acid sites dictated the types of Cu<sup>2+</sup> species present on the catalyst and the selectivity of the reaction; also, that methoxy species formed on Cu, after CH<sub>4</sub> oxidation, migrated to the acidic sites to undergo carbonylation. Similar observations were reported for Rh single sites on ZSM-5, but the use of Rh instead of Cu increasing the performance of the catalyst.<sup>[138,139]</sup> Indeed, Rh was found to display the best catalytic performance for this reaction among a series of metal/ZSM-5 catalysts reported by Moteki et al. (Figure 16).<sup>[135]</sup> Single-site Rh on zeolite ZSM-5 demonstrated to efficiently produce acetic acid in the presence of methane, CO and O<sub>2</sub> in water.<sup>[138]</sup> The acidity of the support allowed to fine-tune the reactivity of the reaction. The carbonylation was not observed in the absence of Brønsted acid sites, and methanol was preferentially produced. Mechanistic studies

suggest that CO inserts directly into Rh-CH<sub>3</sub> bonds to form Rh-COCH<sub>3</sub> species, which requires the acidic sites of the zeolite; followed by hydrolysis in water to produce acetic acid. Rh<sub>1</sub>O<sub>5</sub> single site on a ZSM-5 zeolite was also reported successful for the oxidative methane carbonylation to produce acetic acid.<sup>[139]</sup> Rh cations replaced the Brønsted acid sites of H-ZSM-5, giving a stable catalyst. Isotope-labelled experiments and DFT calculations allowed to propose a reaction pathway, in which Rh single sites are responsible of the activation of C–H bonds of CH<sub>4</sub> and O–O bonds of O<sub>2</sub>.

Recent examples focus on the modification of the zeolite on Rh based SACs of this kind,<sup>[140,148–150]</sup> for instance by changing their hydrophobic/hydrophilic properties,<sup>[140]</sup> their Si/Al ratio, i.e. changing their acidity,<sup>[148]</sup> or their mesoporosity.<sup>[149]</sup> It was found that the production of acetic acid is increased by using



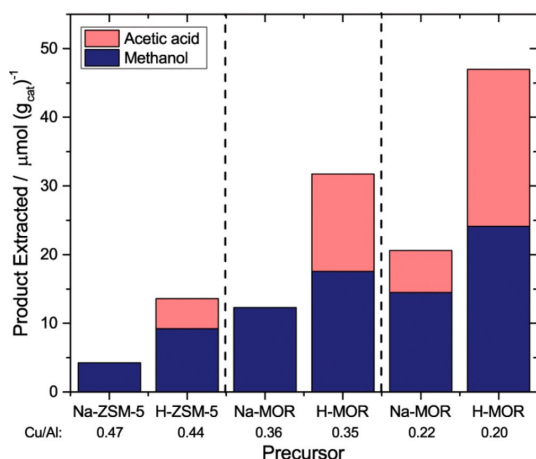


**Figure 15.** Methane oxidation and subsequent carbonylation on Cu-ZSM-5 and Cu-MOR exchanged from sodium and acid precursors. Zeolite precursors and Cu/Al contents are listed for each zeolite. Methane oxidation conditions: Activation at 550 °C under O<sub>2</sub>, 200 °C, 0.5 h. Carbonylation conditions: 200 °C, 0.5 h, 1 MPa CO. Adapted with permission from *J. Am. Chem. Soc.* 2015, 137, 5, 1825–1832. Copyright 2015 American Chemical Society.<sup>[137]</sup>

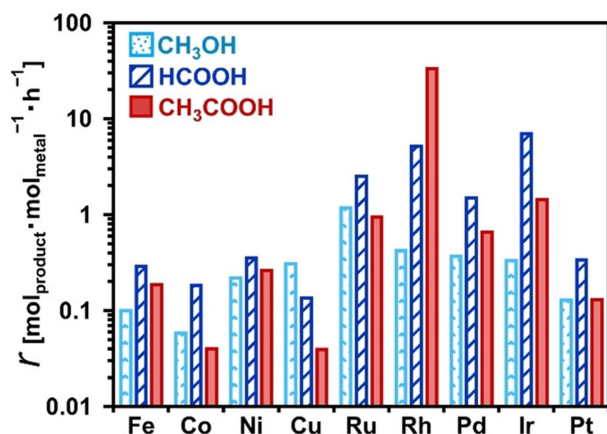


**Figure 16.** Product formation rates [mol<sub>product</sub> mol<sub>metal</sub><sup>-1</sup> h<sup>-1</sup>] of CH<sub>3</sub>OH (light blue dot), HCOOH (blue diagonal line), and CH<sub>3</sub>COOH (red filled) over ZSM-5 supported transition and platinum group metal (Fe, Co, Ni, Cu, Ru, Rh, Pd, Ir, Pt) catalysts (0.2 MPa O<sub>2</sub>, 0.5 MPa CO, 2.0 MPa CH<sub>4</sub>, 8 mL H<sub>2</sub>O, 40 mg catalyst, 150 °C, 3 h). Adapted with permission from *ChemCatChem* 2020, 12 (11), 2957–2961.<sup>[135]</sup>

hydrophobic zeolites, by decreasing the Si/Al ratio, with a highest acetic acid yield (0.53 mmol g<sub>cat</sub><sup>-1</sup>) found on a zeolite with SiO<sub>2</sub>/Al<sub>2</sub>O<sub>3</sub> = 33 modified with 0.5 wt% Rh, and by increasing the mesoporosity of the zeolite.

The effect of CO in the selective oxidation of methane using H<sub>2</sub>O<sub>2</sub> over a Rh based SAC, 0.05% Rh/ZrO<sub>2</sub>, was investigated combining experimental and theoretical calculations.<sup>[141]</sup> The study revealed that Rh/ZrO<sub>2</sub> was able to produce CH<sub>3</sub>COOH from methane in the presence of H<sub>2</sub>O<sub>2</sub> under relatively mild reaction conditions (compared to when using O<sub>2</sub>). Additionally, CO facilitated the CH<sub>4</sub> activation, and prevented the over-oxidation of CH<sub>3</sub> species. Rh, Cu, and Rh–Cu SACs supported on POPs containing PPH<sub>3</sub> moieties, POP-PPH<sub>3</sub>, having demonstrated robust catalysts in other carbonylation reactions, have been used for the methane oxidative carbonylation reaction.<sup>[143]</sup>

Oxygenated products (CH<sub>3</sub>OH, HCOOH, HOCH<sub>2</sub>OH and CH<sub>3</sub>COOH) were obtained from CH<sub>4</sub> in the presence of CO and O<sub>2</sub> at 150 °C in water. The addition of Cu increased the activity of Rh/POP-PPH<sub>3</sub>, and further, the addition of C<sub>6</sub>H<sub>5</sub>I into the reaction media increased the rate of the reaction. The authors concluded that the added iodine species coordinated to the Rh carbonyl species increasing the reaction rate. Even if the oxidation of methane was possible, low amount of acetic acid was obtained. As in their previous works, the polymeric catalyst was found to be stable and recyclable under this reaction conditions.

Li et al.<sup>[142]</sup> recently achieved a further step in controlling the selectivity of methane oxidation in the presence of CO and O<sub>2</sub> as oxidant using a Rh based SAC. The presence or the absence of light triggered a change on the main oxidation product: in the absence of light the carbonylation was not favoured and CH<sub>3</sub>OH was obtained with 64% selectivity, while in the presence of light CH<sub>3</sub>COOH was obtained as main product with a 65% of selectivity (Figure 17). The catalyst consisted of a Rh SAC with high metal content (5%) synthesised using a porphyrin-based MOF as a support. The porphyrin provided the binding sites that allowed the unusual high metal loading for a SAC. DFT calculations indicate that a different coordination of Rh to the porphyrin, either in-plane or out-of-plane depending on the exposure to light, enhances CO activation, under light, thus favouring the production of acetic acid (Figure 17).

Along with Rh, other precious-metal SACs have been successfully used for this application. An Ir dimer complex ([Ir(pyalc)(H<sub>2</sub>O)<sub>2</sub>(μ-O)]<sub>2</sub><sup>2+</sup>, (pyalc = 2-(2'-pyridyl)-2-propanoate)) impregnated on an SBA-15 silica, when submitted to 1.9 MPa of CH<sub>4</sub>, 0.5 MPa of CO and 0.4 MPa of O<sub>2</sub> in water at 150 °C produced preferentially CH<sub>3</sub>COOH in a 21.27 mol mol<sub>Ir</sub><sup>-1</sup> h<sup>-1</sup> rate, the catalyst being robust and recyclable. In another work, several SACs on ZSM-5 based on Ru, Rh, Fe, and Pd, were tested as catalyst for this selective carbonylation, using H<sub>2</sub>O<sub>2</sub> as oxidant.<sup>[145]</sup> At room temperature, a production of oxygenates of 279–653 mmol g<sub>metal</sub><sup>-1</sup> h<sup>-1</sup> were observed when the catalysts were submitted to 2 MPa of CH<sub>4</sub>, 0.1 MPa of CO for 30 min. Among them, Pd/ZSM-5 SAC was the most competitive, displaying a TOF of 131 h<sup>-1</sup>, 1236 mmol g<sub>Pd</sub><sup>-1</sup> h<sup>-1</sup> under 2 MPa of CO, with a 78% AA selectivity. It is worth noting that Fe/ZSM-5 displayed a selectivity of 89% towards acetic acid under the same reaction conditions, even if the activity was much lower (471 mmol g<sub>Fe</sub><sup>-1</sup> h<sup>-1</sup>). DFT calculation show the role of CO is key, increasing the activity of methane conversion, compared on the absence of it, as observed experimentally using Pd/ZSM-5 as catalyst.

Besides the dominant role of Rh and other precious metal-based SACs for this application, examples of oxidative carbonylation of methane catalysed by non-noble metal-based SACs have been recently reported. The use of H<sub>2</sub>O<sub>2</sub> as an oxidant and the radical based mechanism which operates in this kind of catalysts allows to use relatively mild reaction conditions. Fe<sup>[39,146]</sup> and Ni<sup>[147]</sup> single sites successfully produced CH<sub>3</sub>COOH from methane using H<sub>2</sub>O<sub>2</sub> as oxidant. In a first example, the impregnation of FeCl<sub>3</sub>·6H<sub>2</sub>O on calcinated ZSM-5 produced Fe binuclear sites, Fe clusters or Fe NPs depending on the metal



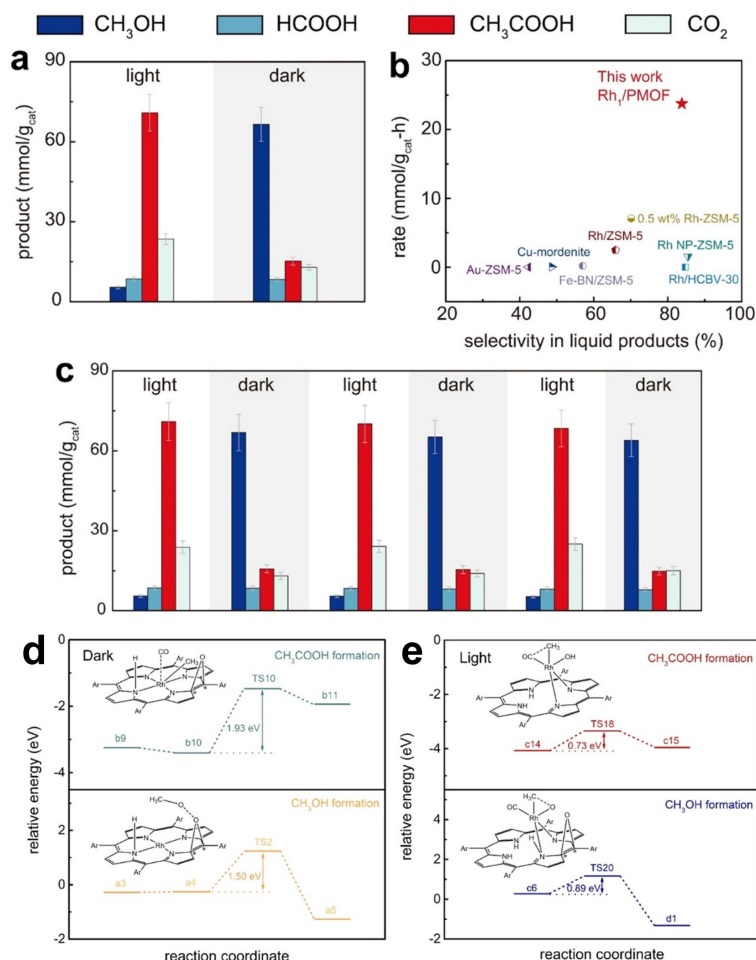


**Figure 17.** (a) Catalytic performance in light (left) and dark (right) showing the dominant products of  $\text{CH}_3\text{COOH}$  and  $\text{CH}_3\text{OH}$ , respectively. (b) Literature comparison of the formation rate of  $\text{CH}_3\text{COOH}$  by  $\text{CH}_4$  oxidation on heterogeneous catalysts. References are as follows: Au-ZSM-5;<sup>[131]</sup> Cu-mordenite;<sup>[137]</sup> Fe-Fe/ZSM-5;<sup>[39]</sup> Rh/ZSM-5;<sup>[139]</sup> 0.5 wt% Rh/ZSM-5;<sup>[138]</sup> Rh NP/ZSM-5;<sup>[135]</sup> and Rh/HCBV-30.<sup>[148]</sup> (c) Reversible selectivity switch between  $\text{CH}_3\text{COOH}$  and  $\text{CH}_3\text{OH}$  in light and dark, respectively, with the same batch of catalyst. Each run was conducted for 3 h. Reaction conditions: 20 mg of Rh/pMOF, 0.4 MPa  $\text{O}_2$ , 0.5 MPa  $\text{CO}$ , 1.5 MPa  $\text{CH}_4$ , 20 mL of water, 150 °C as the reaction temperature. Light: 100 mW/cm<sup>2</sup>, AM 1.5G. Error bars represent the standard deviations of at least three repeated experiments under the same conditions. (d) Preinsertion step of CO for the formation of  $\text{CH}_3\text{COOH}$  (upper) and the  $\text{O}_2$  dissociation step for the formation of  $\text{CH}_3\text{OH}$  (bottom) at the in-plane  $\text{Rh}_1$  site. (e) Methyl migration to CO for the formation of  $\text{CH}_3\text{COOH}$  (upper) and methyl migration to O for the formation of  $\text{CH}_3\text{OH}$  (bottom) at the out-of-plane Rh site. Inset structures in d and e show the corresponding transition states. Adapted with permission from *J. Am. Chem. Soc.* 2023, 145, 20, 11415–11419. Copyright 2023 American Chemical Society.<sup>[142]</sup>

loading (0.31, 0.94, and 3.64%, respectively).<sup>[39]</sup> Fe binuclear species showed the best performances among these catalysts, and also other metal/ZSM-5 prepared for comparative purposes, at low temperature (30 or 50 °C) under 30 MPa of a  $\text{CH}_4/\text{CO}$  mixture. The authors evidenced, experimentally and theoretically, that a  $[\text{Fe}(\text{III})-(\mu\text{O})_2-\text{Fe}(\text{III})-(\text{OH})_2]$  species are responsible of the enhanced catalytic activity, and propose that it favoured the direct coupling of methyl radicals ( $\cdot\text{CH}_3$ ) and adsorbed  $\text{CO}^*$  and  $\text{OH}^*$  species to form  $\text{CH}_3\text{COOH}$ .  $[\text{Fe}(\text{acac})_3]$  was used as metal source to produce a Fe/ZSM-5 SAC, which displayed atomically dispersed Fe.<sup>[146]</sup> This catalyst demonstrated to be active for this reaction, as the bimetallic Fe–Fe SAC, using  $\text{H}_2\text{O}_2$  as oxidant at low temperature (50 °C); yet, using higher pressure (4.0 MPa  $\text{CH}_4$ , 4.0 MPa  $\text{CO}$ ). The authors attributed the  $\text{CH}_3\text{COOH}$  yield to the presence of mononuclear  $\text{Fe}^{3+}$ , located in the zeolite replacing Brønsted acid sites. It is proposed that  $-\text{Fe}-\text{OCH}_3$  species is a possible intermediate, generated from the

reaction of methane and the  $-\text{Fe}-\text{OOH}$  species. Another SAC based on Ni supported on ZSM-5 produced acetic acid in a 82% selectivity using  $\text{H}_2\text{O}_2$  as oxidant.<sup>[147]</sup> As observed for the previous Fe based SAC, the Ni loading had an impact on the catalytic performances, and 1.2% Ni loaded SAC was the best among them, which displayed a high amount of atomically dispersed Ni. Spectroscopic analyses evidenced also for Ni, that radical species are involved in the reaction mechanism;  $\cdot\text{CH}_3$  and  $\cdot\text{OH}$  radicals were observed suggesting that  $\text{H}_2\text{O}_2$  can activate the C–H bond of methane. Taking into consideration all the results collected the authors propose that acetic acid is produced directly from the coupling of  $\text{CH}_4$  and  $\text{CO}$ .

Production of acetic acid from the oxidative carbonylation of methane is an interesting alternative to the carbonylation of methanol. The suitable catalyst should have a fine tuning on their properties to activate C–H from methane, avoid over-oxidation, as well as promoting the CO insertion. Zeolites, with

their acidic sites, have proven to be effective for this purpose, particularly when paired with metals, especially Rh. Rh on ZSM-5 has been the most studied catalytic system, usually using O<sub>2</sub> as oxidant and using high temperatures. Changing the oxidant for H<sub>2</sub>O<sub>2</sub> allows to use milder reaction conditions, due to the different mechanism operating. Notably acetic acid could be obtained at room temperature and using earth-abundant based SACs using H<sub>2</sub>O<sub>2</sub>. As most of the works rely in the use of zeolites as support, it is difficult to drive conclusions about the role of supports in this catalysed reaction, thus, works investigating this effect, crucial on SACs, are needed in the future.

## Alkoxy- and Hydroxycarbonylation of Unsaturated Compounds

Carbonylations of unsaturated compounds in the presence of a nucleophile permit efficiently the formation of carboxylic acids, esters, and amides in one step combining three products, the substrate, the CO and the nucleophile (Figure 18).

Alkoxy-carbonylation is usually catalysed by Pd homogeneous species modified with phosphorus ligands.<sup>[151]</sup> Industrial applications include the methoxycarbonylation of ethylene to provide methyl propionate, a key intermediate to produce polymers, using a homogeneous Pd catalyst.<sup>[152]</sup> Thus, as mentioned before for other carbonylation reactions homogeneously catalysed, providing heterogeneous alternatives is of high interest, and SACs are emerging as interesting candidates. In the methoxycarbonylation of ethylene, the homogeneous process typically relies on the

presence of strong acids. Using SACs could offer an alternative approach to eliminate this need, as seen in methanol carbonylation where SACs enable halide-free gas-phase reactions by working via a different mechanism. For instance, acid free ethylene methoxycarbonylation was achieved over Ru NPs/CeO<sub>2</sub>.<sup>[153]</sup> This work demonstrated that the synergy between the support and the metal was essential for the high catalytic activity without the presence of an acid. Subsequently, SACs have been tested as well for this application (Table 6). Wang et al. recently used a Pt SAC, using as a support MoS<sub>2</sub> nanosheets, for the methoxycarbonylation of ethylene.<sup>[154]</sup> The reaction was performed at 160 °C under 1–2 MPa of CO and 1 MPa of C<sub>2</sub>H<sub>4</sub> displaying at higher CO pressure a TOF of 320.1 h<sup>-1</sup>. For comparative purposes other metallic SACs of Pd, Rh, and Ru on MoS<sub>2</sub>, and Pt on CeO<sub>2</sub>, Al<sub>2</sub>O<sub>3</sub>, MoO<sub>3</sub>, or HZSM-5, were prepared, tested, and found most of them inactive. The authors propose that the origin of the activity is related to the formation of single site Mo–S–Pt–S–Mo species. Supporting this hypothesis, HRTEM analyses show that Pt single atoms are located at the Mo sites along the MoS<sub>2</sub> edges. Additionally, XAFS and XPS analyses conclude that Pt is in an oxidation state of +4 and coordinated to S atoms with a coordination number (CN) of 3.7. DFT calculations and in situ characterization, display the multisite character of the mechanism proposed by the authors (Figure 19). The catalysts were recycled with a significant loss of activity and some residual leaching of Pt and Mo was detected in the filtrates.

Pd single sites on polyoxometalates, [(n-C<sub>4</sub>H<sub>9</sub>)<sub>4</sub>N]<sub>6</sub>[SiW<sub>11</sub>O<sub>39</sub>Pd] and [(n-C<sub>4</sub>H<sub>9</sub>)<sub>4</sub>N]<sub>5</sub>[PW<sub>11</sub>O<sub>39</sub>Pd], were successfully synthesized and employed as catalysts for the hydroxycarbonylation of several olefins.<sup>[155]</sup> The catalysis was

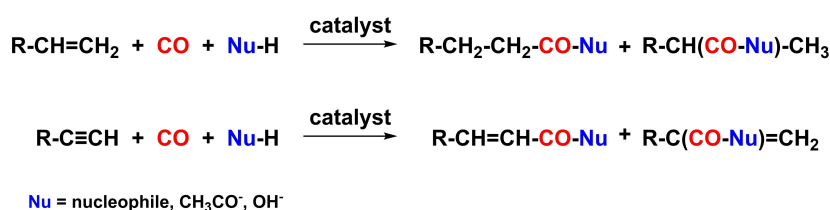
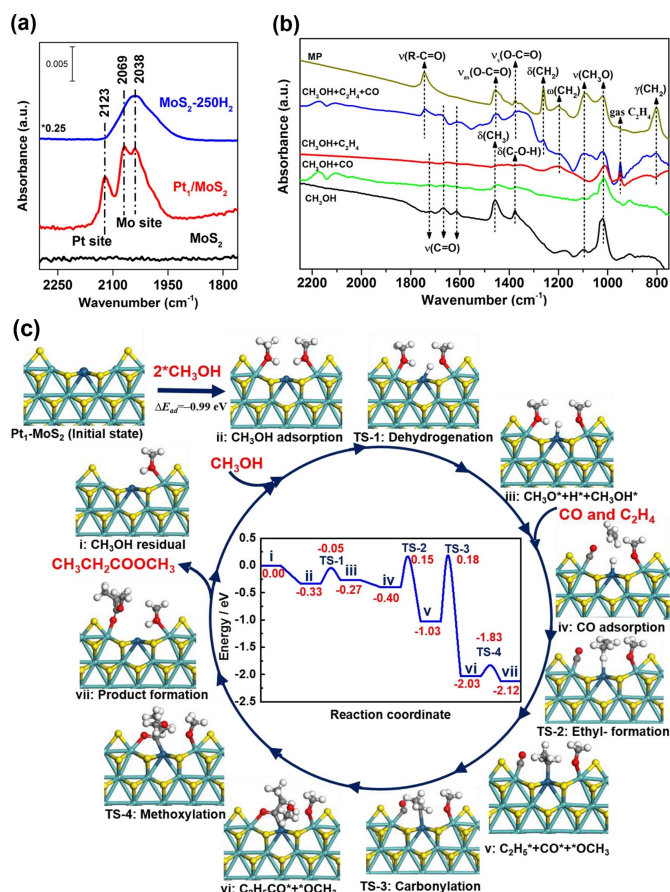


Figure 18. Carbonylation of unsaturated bonds in the presence of a nucleophile.

Table 6. Methoxycarbonylation of ethylene using single-atom catalysts.					
Catalyst	Production rate	Selectivity to methyl propanoate (MP)	Rate	Reaction conditions	Ref.
Pt/MoS <sub>2</sub>	0.35 g <sub>MP</sub> g <sub>cat</sub> <sup>-1</sup> h <sup>-1</sup>	91 % MP	151 mol <sub>MP</sub> mol <sub>Pt</sub> <sup>-1</sup> h <sup>-1</sup>	50 mg catalyst, 1 MPa C <sub>2</sub> H <sub>4</sub> , 1 MPa CO, 5 mL of CH <sub>3</sub> OH, 1 h, 160 °C	154
Pt/MoS <sub>2</sub>	0.74 g <sub>MP</sub> g <sub>cat</sub> <sup>-1</sup> h <sup>-1</sup>	83 % MP	320 mol <sub>MP</sub> mol <sub>Pt</sub> <sup>-1</sup> h <sup>-1</sup>	50 mg catalyst, 1 MPa C <sub>2</sub> H <sub>4</sub> , 1 MPa CO, 5 mL of CH <sub>3</sub> OH, 1 h, 160 °C	154
Pt NPs/ MoS <sub>2</sub>	0.06 g <sub>MP</sub> g <sub>cat</sub> <sup>-1</sup> h <sup>-1</sup>	45 % MP	–	50 mg catalyst, 1 MPa C <sub>2</sub> H <sub>4</sub> , 1 MPa CO, 5 mL of CH <sub>3</sub> OH, 1 h, 160 °C	154
Pd/MoS <sub>2</sub>	0.06 g <sub>MP</sub> g <sub>cat</sub> <sup>-1</sup> h <sup>-1</sup>	92 % MP	–	50 mg catalyst, 1 MPa C <sub>2</sub> H <sub>4</sub> , 1 MPa CO, 5 mL of CH <sub>3</sub> OH, 1 h, 160 °C	154
Ru/MoS <sub>2</sub>	–	–	no activity	50 mg catalyst, 1 MPa C <sub>2</sub> H <sub>4</sub> , 1 MPa CO, 5 mL of CH <sub>3</sub> OH, 1 h, 160 °C	154
Rh/MoS <sub>2</sub>	0.06 g <sub>MP</sub> g <sub>cat</sub> <sup>-1</sup> h <sup>-1</sup>	89 % MP	–	50 mg catalyst, 1 MPa C <sub>2</sub> H <sub>4</sub> , 1 MPa CO, 5 mL of CH <sub>3</sub> OH, 1 h, 160 °C	154



**Figure 19.** (a) DRIFT spectra of CO adsorption on different samples. (b) In situ ATR-IR spectra of the Pt/MoS<sub>2</sub> SAC upon exposure to CH<sub>3</sub>OH, C<sub>2</sub>H<sub>4</sub>, and C<sub>2</sub>H<sub>4</sub>/CH<sub>3</sub>OH, CO/CH<sub>3</sub>OH, C<sub>2</sub>H<sub>4</sub>/CO/CH<sub>3</sub>OH mixtures at the reaction temperature of 160 °C with a total pressure of 1 MPa. First, when Pt/MoS<sub>2</sub> SAC was treated by CH<sub>3</sub>OH, three groups of absorption bands appeared: the bands at 1458 and 1380 cm<sup>-1</sup> ascribed to δ(-CH<sub>2</sub>) and δ(C-OH) in CH<sub>3</sub>OH, the bands at 1100 and 1020 cm<sup>-1</sup> ascribed to ν(-OCH<sub>3</sub>), and the bands at 1720, 1680, and 1610 cm<sup>-1</sup> due to ν(C=O) in HCHO. (c) Calculated mechanism of the methoxycarbonylation reaction of ethylene over Pt/MoS<sub>2</sub> SAC. Adapted with permission from *J. Am. Chem. Soc.* 2024, 146, 1, 695–706. Copyright 2023 American Chemical Society.<sup>[154]</sup>

performed in water using *p*-toluene sulfonic acid, tetrabutylammonium bromide, at 110 °C under 2 MPa of CO. Under these conditions, several alkenes were successfully hydroxycarbonylated giving the corresponding carboxylic acids in high yields (up to 98%), displaying I:b from 0.6 to 2 depending on the nature of the substrate. Under optimized conditions, the catalyst was recycled, but the conversion decreased after several runs, probably due to the formation of Pd NPs; also, the presence of tetrabutylammonium bromide was found crucial to avoid the formation of them; thus, overall, demonstrating that Pd single sites were not that stable under the conditions employed.

Rh SACs based on POPS containing PPh<sub>3</sub> as a coordinating moiety, previously described to be successful for other carbonylation reactions (see above), have also been tested for the hydroxycarbonylation of olefins.<sup>[156]</sup> For the cyclohexene hydroxycarbonylation using *p*-TsOH·H<sub>2</sub>O, acetic acid, CH<sub>3</sub>I under 1 MPa of CO at 180 °C, the catalysts converted up to 97% of the alkene

with a selectivity up to 92% towards cyclohexanecarboxylic acid. As for other carbonylation reactions using this kind of polymeric SACs, the catalyst was robust and reusable. In a follow up work,<sup>[157]</sup> the authors introduced H<sub>2</sub>S in the reactor using same reaction conditions. The H<sub>2</sub>S concentration on the reactor had a volcano-type relationship with activity, with the optimum found at 1000 ppm. The active species shifted from [Rh(CO)<sub>3</sub>]<sup>2-</sup>, under CO, to [(CH<sub>3</sub>)<sub>2</sub>SRh(CO)<sub>3</sub>]<sup>2-</sup>, under CO and H<sub>2</sub>S, as observed spectroscopically. DFT calculations show that this species displays relatively lower energy barriers of several transition states, thus explaining the increase of activity with the addition of H<sub>2</sub>S. Acetylene dialkoxycarbonylation was also achieved using SACs based on a porous polymer.<sup>[158]</sup> The polymerization of the methyltris(4-vinylphenyl) phosphonium iodide monomer produced an ionic POPs which was further decorated with Pd and Ru to give a bimetallic single-site catalysts. Pd–Ru/POP–PPh<sub>3</sub> displayed improved catalytic with respect to the monometallic Pd counterpart (Ru monometallic was inactive), in terms of activity, selectivity and stability. The starting bimetallic single site was identified [Pd<sub>3</sub>–RuCl<sub>2</sub>(CO)<sub>3</sub>]<sup>-</sup> by EXAFS. DFT calculations revealed that the presence of Ru decreased key energy barriers.

SACs have demonstrated that are interesting materials for applications on alkoxy carbonylation, proving to provide an acid-free alternative to homogeneous catalytic systems. This area remains relatively unexplored, offering numerous opportunities for future research. Drawing conclusions from studies on other carbonylation reactions, developing robust and efficient catalysts involves engineering SACs through modifications to either the metal (introduction of a second metal, use of earth-abundant metals) or the support (acidic sites, doping of the support with heteroatoms).

## Miscellaneous Reactions

Using a Rh/CeO<sub>2</sub> SAC 3-pentanone was synthesized through ethylene carbonylation in tandem with alcohol transfer hydrogenation.<sup>[159]</sup> The reaction took place using ethylene, an alcohol, under 1.4 MPa of CO at 160 °C. The synergy of the support and the metal were found key to be able to activate both reactions; the presence of both acidic and basic sites activates the alcohol while Rh sites activated CO and ethylene.

Zn single sites on N-doped porous carbon, Zn/NC, were successfully prepared and used as catalysts in the for glycerol carbonylation with urea.<sup>[160]</sup> XAS analyses confirming the anchoring of a Zn<sup>2+</sup> in N- and/or O-containing functional groups of the carbon support, displaying a CN of 5.7. Glycerol carbonate was produced from glycerol and urea with high yields and selectivity, outperforming Zn NPs, or Zn homogeneous catalyst at relatively low temperature, 120 °C, the catalysts was successfully recycled without loss of activity.

## Summary and Outlook Section

SACs are emerging as powerful catalysts for many applications, including for carbonylation reactions, which their demanding

reaction conditions, presence of CO, elevated temperature and pressure, etc., require robust catalysts. Hydroformylation is the most studied reaction using SACs, and various types of materials have been employed, from more conventional supports, such as oxides or carbon materials, to phosphates or carbides, as well as ionic liquids and functionalized porous materials. In contrast, for other carbonylation reactions, the range of suitable supports tends to be more limited. Addressing the challenges inherent in SACs for carbonylation reactions requires targeted strategies to enhance metal atom stability, catalytic activity and selectivity. Rh is the most commonly used metal for carbonylation reactions in general, although successful examples of other metal SACs have also been reported, such as Ru and Co single atoms for hydroformylation, Ir, Cu, and Re for methanol carbonylation, and Fe and Ni for oxidative carbonylation. The high cost and limited availability of Rh present significant challenges for industrial applications. Exploration of alternative transition metals, along with the development of innovative synthetic strategies and support materials, offers promising avenues for mitigating the economic constraints associated with Rh-based catalysts. Nevertheless, strategies such as support modification and ligand design that could enhance the stability and activity of all these promising single-atom alternative catalysts are still in development, since Rh has paid all the attention owing to its superior catalytic activity. For instance, Fe has been used as catalysts for a carbonylation reaction<sup>[161]</sup> although the research about the use as a single atom is scarce. Besides the nature of the metallic single site, other parameters in the design of these materials should be considered. The amount and spacing of single sites, for example, are important parameters as low metallic loadings for SACs are often needed to prevent metallic sintering, but this can limit cooperative catalysis between metallic centres and real applications in industry, where higher loadings are preferred. Therefore, it is essential to develop supports and synthetic methodologies to modulate the direct coordination environment of single sites to control the electronic properties of the metal, in order to increase their robustness, their catalytic performances, their metal loading, to allow the introduction of bimetallic isolated sites in a controlled manner, and also to facilitate metal-support cooperation. Thus, supports are being modified with these aims. Successful strategies for now focussing in the tailoring of the metal-support interaction to enhance robustness, to generate strong metal-support interactions, and fine-tuning of the electronic environment of the single site, to increase the site-support synergy to selectively bind reaction intermediates and stabilize transition states, along with thorough exploration of reaction conditions and kinetics. Examples include, the modification of non-reducible supports with tethered organic compounds or the addition of reducible oxides, fine-tuning of the number of oxygen vacancies in reducible oxides, which increase metal-support interaction and provide specific electronic properties to the metal. In addition, heteroatoms, usually N and P, are introduced in several supports, carbonaceous, oxides; or different substituents are introduced in polymeric compounds. All these strategies are demonstrating to give interesting catalytic properties to SACs. Nevertheless, regioselectivity and enantioselectivity are still unsolved problems, specifically for hydroformylation. The use of porous organic polymers has demonstrated to solve

this key point, although their use suffers from a high cost in their synthesis. Leaching and sintering issues in both gas- and liquid-phase are also inherent to heterogeneous catalysts. By modification of the supports, this question is being solved for gas-phase hydroformylation, yet, for liquid-phase, leaching of metal species into solution, which are usually highly active and also drives to metal losses, remains a major concern. For other carbonylation reactions including methanol carbonylation, alkoxy- and hydroxycarbonylation, and the oxidative carbonylation of methane, similar conclusions can be drawn as for hydroformylation. The specificity of this series of reactions is that the use of the suitable support circumvents the use of promoters, halides for methanol carbonylation, strong acids for alkoxy- and hydroxycarbonylations, in the gas-phase. These reactions are less studied in comparison to hydroformylation, leaving plenty of room for the potential application of SACs to be further explored. Besides the modification of the support, other strategies to control the activity and selectivity have been explored: the use of LWGS coupled to hydroformylation to change the regioselectivity of the reaction, the introduction of ppm of H<sub>2</sub>S to subtly change the active species, or the introduction of a second metal to create bimetallic sites with the aim to increase their activity and prevent deactivation and leaching pathways. Thus, for the future, the precise combination of reaction conditions, the tailoring of the support and the metallic centres seems to be key to provide interesting SACs for carbonylation reactions. Also, CO<sub>2</sub>-based carbonylations, in which CO<sub>2</sub> acts as a CO surrogate, could circumvent the problems associated with the handling of a highly toxic and flammable molecule such as CO.<sup>[162–164]</sup> Some examples<sup>[89,165–167]</sup> are appearing in the literature, which will pave the way in this interesting and challenging topic.

Advanced characterization techniques, which should include operando/in situ techniques, combined to theoretical calculations are indispensable for elucidating the structural dynamics to correlate the catalytic activity with the coordination environment of the single atom, with the goal to obtain patterns and descriptors to discern between suitable and non-suitable supports for single metal atoms catalysts. Investigating the electronic and geometric effects of different metal-support interactions could offer insights into enhancing catalytic activity and selectivity. Employing advanced characterization techniques and computational modelling to elucidate the structure-function relationships of single-atom catalysts could guide the rational design of improved catalysts. Exploring alternative reaction mechanisms and pathways, coupled with interdisciplinary collaboration across materials science, catalysis, computational chemistry, and chemical engineering, promises innovative solutions and accelerated progress in overcoming the challenges of SACs in carbonylation reactions.

## Acknowledgements

This work was supported by the CNRS, which we gratefully acknowledge. The authors acknowledge the financial support from EMERGENCE@INC2021 for L.J. grant. S.P.-P. appreciates the economic support of Marie Curie fellowship.



## Conflict of Interests

The authors declare no conflict of interest.

**Keywords:** Carbonylation · single site · single atom · catalysts · SAC

- [1] J.-B. Peng, H.-Q. Geng, X.-F. Wu, *Chem* **2019**, *5* (3), 526–552. DOI: 10.1016/j.chempr.2018.11.006.
- [2] P. Kalck, C. Le Berre, P. Serp, *Coord. Chem. Rev.* **2020**, *402*, 213078. DOI: 10.1016/j.ccr.2019.213078.
- [3] X.-F. Wu, X. Fang, L. Wu, R. Jackstell, H. Neumann, M. Beller, *Acc. Chem. Res.* **2014**, *47* (4), 1041–1053. DOI: 10.1021/ar400222k.
- [4] Y. Li, Y. Hu, X.-F. Wu, *Chem. Soc. Rev.* **2018**, *47* (1), 172–194. DOI: 10.1039/c7cs00529f.
- [5] O. D. Roelen, Process for the preparation of oxygen-containing compounds. Germany 1938.
- [6] F. Fischer, H. Tropsch, *Berichte der deutschen chemischen Gesellschaft (A and B Series)* **1926**, *59* (4), 830–831. DOI: 10.1002/cber.19260590442.
- [7] B. Cornils, A. Börner, R. Franke, B. Zhang, E. Wiebus, K. Schmid, In *Applied homogeneous catalysis with organometallic compounds*, Cornils, B. Herrmann, W. A. Beller, M. Paciello, R. Eds.; 2017.
- [8] R. Franke, D. Selent, A. Börner, *Chem. Rev.* **2012**, *112* (11), 5675–5732. DOI: 10.1021/cr3001803.
- [9] *Rhodium catalyzed hydroformylation*; Springer Dordrecht, 2000. DOI: 10.1007/0-306-46947-2.
- [10] A. Haynes, **2022**, 333–362. DOI: 10.1002/9783527829354.ch10.
- [11] Z. Ren, L. Yuan, X. Song, Y. Ding, *Appl. Catal. A* **2020**, *595*, 117488. DOI: 10.1016/j.apcata.2020.117488.
- [12] B. Zhang, D. Peña Fuentes, A. Börner, *ChemTexts* **2022**, *8*, 1–26. DOI: 10.1007/s40828-021-00154-x.
- [13] A. Haynes, P. M. Maitlis, G. E. Morris, G. J. Sunley, H. Adams, P. W. Badger, C. M. Bowers, D. B. Cook, P. I. P. Elliott, T. Ghaffar, *J. Am. Chem. Soc.* **2004**, *126* (9), 2847–2861. DOI: 10.1021/ja039464y.
- [14] Y. Liu, Y.-H. Chen, H. Yi, A. Lei, *ACS Catal.* **2022**, *12* (13), 7470–7485. DOI: 10.1021/acscatal.2c01639.
- [15] Z. Yin, J.-X. Xu, X.-F. Wu, *ACS Catal.* **2020**, *10* (11), 6510–6531. DOI: 10.1021/acscatal.0c01479.
- [16] J. Herwig, R. Fischer, Aqueous biphasic hydroformylation. In *Rhodium catalyzed hydroformylation. Catalysis by metal complexes, vol 22.*, Van Leeuwen, P. W. N. M., Claver, C. Eds.; Springer, Dordrecht, 2000.
- [17] W. Alsalahi, A. M. Trzeciak, *Coord. Chem. Rev.* **2021**, *430*, 213732. DOI: 10.1016/j.ccr.2020.213732.
- [18] S. Tao, D. Yang, M. Wang, G. Sun, G. Xiong, W. Gao, Y. Zhang, Y. Pan, *iScience* **2023**, *26* (3), 106183. DOI: 10.1016/j.isci.2023.106183.
- [19] B. Liu, Y. Wang, N. Huang, X. Lan, Z. Xie, J. G. Chen, T. Wang, *Chem* **2022**, *8* (10), 2630–2658. DOI: 10.1016/j.chempr.2022.07.020.
- [20] D. P. Zhuchkov, M. V. Nenasheva, M. V. Terenina, Y. S. Kardasheva, D. N. Gorbunov, E. A. Karakhanov, *Pet. Chem.* **2021**, *61* (1), 1–14. DOI: 10.1134/s0965544121010011.
- [21] M. R. Axet, S. Castillon, C. Claver, K. Philippot, P. Lecante, B. Chaudret, *Eur. J. Inorg. Chem.* **2008**, 3460–3466. DOI: 10.1002/ejic.200800421.
- [22] T. Li, F. Chen, R. Lang, H. Wang, Y. Su, B. Qiao, A. Wang, T. Zhang, *Angew. Chem. Int. Ed.* **2020**, *59* (19), 7430–7434. DOI: 10.1002/anie.202000998.
- [23] P. Gao, G. Liang, M. Wang, X. Liu, H. Qi, A. Wang, F.-E. Chen, *Nat. Commun.* **2021**, *12* (1), 4698. DOI: 10.1038/s41467-021-25061-0.
- [24] S. Ding, M. J. Hulsey, H. An, Q. He, H. Asakura, M. Gao, J. Y. Hasegawa, T. Tanaka, N. Yan, *CCS Chem.* **2021**, *3* (10), 1814–1822. DOI: 10.31635/ccschem.021.202101063.
- [25] X. Wei, Y. Jiang, Y. Ma, J. Fang, Q. Peng, W. Xu, H. Liao, F. Zhang, S. Dai, Z. Hou, *Chem. Eur. J.* **2022**, *28*, e202200374. DOI: 10.1002/chem.202200374.
- [26] S. K. Kaiser, Z. Chen, D. Faust Akl, S. Mitchell, J. Perez-Ramirez, *Chem. Rev.* **2020**, *120* (21), 11703–11809. DOI: 10.1021/acs.chemrev.0c00576.
- [27] R. Lang, X. Du, Y. Huang, X. Jiang, Q. Zhang, Y. Guo, K. Liu, B. Qiao, A. Wang, T. Zhang, *Chem. Rev.* **2020**, *120* (21), 11986–12043. DOI: 10.1021/acs.chemrev.0c00797.
- [28] S. Ji, Y. Chen, X. Wang, Z. Zhang, D. Wang, Y. Li, *Chem. Rev.* **2020**, *120* (21), 11900–11955. DOI: 10.1021/acs.chemrev.9b00818.
- [29] B. B. Sarma, F. Maurer, D. E. Doronkin, J.-D. Grunwaldt, *Chem. Rev.* **2022**, *123* (1), 379–444. DOI: 10.1021/acs.chemrev.2c00495.
- [30] L. Li, X. Chang, X. Lin, Z.-J. Zhao, J. Gong, *Chem. Soc. Rev.* **2020**, *49* (22), 8156–8178. DOI: 10.1039/d0cs00795a.
- [31] S. Mitchell, E. Vorobyeva, J. Perez-Ramirez, *Angew. Chem. Int. Ed.* **2018**, *57* (47), 15316–15329. DOI: 10.1002/anie.201806936.
- [32] Z. Li, S. Ji, Y. Liu, X. Cao, S. Tian, Y. Chen, Z. Niu, Y. Li, *Chem. Rev.* **2020**, *120* (2), 623–682. DOI: 10.1021/acs.chemrev.9b00311.
- [33] R. Qin, K. Liu, Q. Wu, N. Zheng, *Chem. Rev.* **2020**, *120* (21), 11810–11899. DOI: 10.1021/acs.chemrev.0c00094.
- [34] X. Li, Y. Huang, B. Liu, *Chem* **2019**, *5* (11), 2733–2735. DOI: 10.1016/j.chempr.2019.10.004.
- [35] M. Babucci, A. Guntida, B. C. Gates, *Chem. Rev.* **2020**, *120* (21), 11956–11985. DOI: 10.1021/acs.chemrev.0c00864.
- [36] A. Iemhoff, M. Vennewald, R. Palkovits, *Angew. Chem. Int. Ed.* **2023**, *62* (7), e202212015. DOI: 10.1002/anie.202212015.
- [37] Y. J. Sa, D.-J. Seo, J. Woo, J. T. Lim, J. Y. Cheon, S. Y. Yang, J. M. Lee, D. Kang, T. J. Shin, H. S. Shin, et al., *J. Am. Chem. Soc.* **2016**, *138* (45), 15046–15056. DOI: 10.1021/jacs.6b09470.
- [38] F. J. Escobar-Bedia, M. Lopez-Haro, J. J. Calvino, V. Martin-Diaconescu, L. Simonelli, V. Perez-Dieste, M. J. Sabater, P. Concepcion, A. Corma, *ACS Catal.* **2022**, *12* (7), 4182–4193. DOI: 10.1021/acscatal.1c05737.
- [39] B. Wu, T. Lin, Z. Lu, X. Yu, M. Huang, R. Yang, C. Wang, C. Tian, J. Li, Y. Sun, et al. *Chem* **2022**, *8* (6), 1658–1672. DOI: 10.1016/j.chempr.2022.02.001.
- [40] M. G. Farpon, W. Henao, P. N. Plessow, E. Andres, R. Arenal, C. Marini, G. Agostini, F. Studt, G. Prieto, *Angew. Chem. Int. Ed.* **2023**, *62* (1), e202214048. DOI: 10.1002/anie.202214048.
- [41] J. Hulva, M. Meier, R. Bliem, Z. Jakub, F. Kraushofer, M. Schmid, U. Diebold, C. Franchini, G. S. Parkinson, *Science* **2021**, *371* (6527), 375–379. DOI: 10.1126/science.abe5757.
- [42] M. J. Hulsey, B. Zhang, Z. Ma, H. Asakura, D. A. Do, W. Chen, T. Tanaka, P. Zhang, Z. Wu, N. Yan, *Nat. Commun.* **2019**, *10* (1), 1–10. DOI: 10.1038/s41467-019-09188-9.
- [43] L. Yang, H. Lin, Z. Fang, Y. Yang, X. Liu, G. Ouyang, *Sustainable Energy Rev.* **2023**, *184*, 113561. DOI: 10.1016/j.suser.2023.113561.
- [44] C. Tu, X. Nie, J. G. Chen, *ACS Catal.* **2021**, *11* (6), 3384–3401. DOI: 10.1021/acscatal.0c05492.
- [45] L. Liu, A. Corma, *Chem. Rev.* **2018**, *118*, 4981–5079. DOI: 10.1021/acs.chemrev.7b00776.
- [46] J. Liu, L. Yan, Y. Ding, M. Jiang, W. Dong, X. Song, T. Liu, H. Zhu, *Appl. Catal. A* **2015**, *492*, 127–132. DOI: 10.1016/j.apcata.2014.12.011.
- [47] R. Lang, T. Li, D. Matsumura, S. Miao, Y. Ren, Y.-T. Cui, Y. Tan, B. Qiao, L. Li, A. Wang, et al., *Angew. Chem. Int. Ed.* **2016**, *55* (52), 16054–16058. DOI: 10.1002/anie.201607885.
- [48] L. Wang, W. Zhang, S. Wang, Z. Gao, Z. Luo, X. Wang, R. Zeng, A. Li, H. Li, M. Wang, et al., *Nat. Commun.* **2016**, *7*, 14036. DOI: 10.1038/ncomms14036.
- [49] I. Ro, M. Xu, G. W. Graham, X. Pan, P. Christopher, *ACS Catal.* **2019**, *9* (12), 10899–10912. DOI: 10.1021/acscatal.9b02111.
- [50] J. Amsler, B. B. Sarma, G. Agostini, G. Prieto, P. N. Plessow, F. Studt, *J. Am. Chem. Soc.* **2020**, *142* (11), 5087–5096. DOI: 10.1021/jacs.9b12171.
- [51] S. Lee, A. Patra, P. Christopher, D. G. Vlachos, S. Caratzoulas, *ACS Catal.* **2021**, *11* (15), 9506–9518. DOI: 10.1021/acscatal.1c00705.
- [52] M. Chen, G. Gupta, C. W. Ordzone, A. R. Lamkins, C. J. Ward, C. A. Abolafia, B. Zhang, L. T. Roling, W. Huang, *J. Am. Chem. Soc.* **2021**, *143* (49), 20907–20915. DOI: 10.1021/jacs.1c09665.
- [53] B. Wei, X. Liu, K. Hua, Y. Deng, H. Wang, Y. Sun, *ACS Appl. Mater. Interfaces* **2021**, *13* (13), 15113–15121. DOI: 10.1021/acsmi.0c21749.
- [54] I. Ro, J. Qi, S. Lee, M. Xu, X. Yan, Z. Xie, G. Zakem, A. Morales, J. G. Chen, X. Pan, et al., *Nature* **2022**, *609* (7926), 287–292. DOI: 10.1038/s41586-022-05075-4.
- [55] Y. Zheng, Q. Wang, Q. Yang, S. Wang, M. J. Hulsey, S. Ding, S. Furukawa, M. Li, N. Yan, X. Ma, *ACS Catal.* **2023**, *13* (11), 7243–7255. DOI: 10.1021/acscatal.3c00810.
- [56] J. Zhang, P. Sun, G. Gao, J. Wang, Z. Zhao, Y. Muhammad, F. Li, *J. Catal.* **2020**, *387*, 196–206. DOI: 10.1016/j.jcat.2020.03.032.
- [57] W. Shang, B. Qin, M. Gao, X. Qin, Y. Chai, G. Wu, N. Guan, D. Ma, L. Li, *CCS Chem.* **2023**, *5* (7), 1526–1539. DOI: 10.31635/ccschem.022.202202043.
- [58] M. Zhao, C. Li, D. Gomez, F. Gonell, V. M. Diaconescu, L. Simonelli, M. L. Haro, J. J. Calvino, D. M. Meira, P. Concepcion, et al. *Nat. Commun.* **2023**, *14* (1), 7174. DOI: 10.1038/s41467-023-42938-4.
- [59] C. Hou, G. Zhao, Y. Ji, Z. Niu, D. Wang, Y. Li, *Nano Res.* **2014**, *7* (9), 1364–1369. DOI: 10.1007/s12274-014-0501-4.



- [60] C. Li, L. Yan, L. Lu, K. Xiong, W. Wang, M. Jiang, J. Liu, X. Song, Z. Zhan, Z. Jiang, et al., *Green Chem.* **2016**, *18* (10), 2995–3005. DOI: 10.1039/c6gc00728g.
- [61] W. Wang, L. Yan, C. Li, M. Jiang, Z. Zhao, G. Hou, Y. Ding, *J. Catal.* **2018**, *368*, 197–206. DOI: 10.1016/j.jcat.2018.10.012.
- [62] Z. Wang, Y. Yang, *RSC Adv.* **2020**, *10* (49), 29263–29267. DOI: 10.1039/d0ra04816j.
- [63] J. Ma, M. Liu, M. Zhu, Y. Wang, Y. Zhou, B. Wang, *Catal. Sci. Technol.* **2022**, *12* (22), 6740–6750. DOI: 10.1039/D2CY00924B.
- [64] W. Jiang, J. Li, M. Wu, L. He, G. Zhou, Z. Wang, *Fuel* **2023**, *338*, 127291. DOI: 10.1016/j.fuel.2022.127291.
- [65] S. Feng, M. Jiang, X. Song, P. Qiao, L. Yan, Y. Cai, B. Li, C. Li, L. Ning, S. Liu, et al. *Angew. Chem. Int. Ed.* **2023**, *62* (30), e202304282. DOI: 10.1002/anie.202304282.
- [66] L. Jurado, J. Esvan, L. A. Luque-Alvarez, L. F. Bobadilla, J. A. Odriozola, S. Posada-Perez, A. Poater, A. Comas-Vives, M. R. Axet, *Catal. Sci. Technol.* **2023**, *13* (5), 1425–1436. DOI: 10.1039/d2cy02094g.
- [67] M. Schörner, P. Rothgänger, K. Mitländer, D. Wisser, M. Thommes, M. Haumann, *ChemCatChem* **2021**, *13* (19), 4192–4200. DOI: 10.1002/cctc.202100743.
- [68] M. Hatanaka, T. Yasuda, E. Uchiage, M. Nishida, K.-I. Tominaga, *ACS Sustainable Chem. Eng.* **2021**, *9* (35), 11674–11680. DOI: 10.1021/acssuschemeng.1c02084.
- [69] M. Schörner, A. Schönweiz, S. Vignesh, L. Mokrushina, M. Thommes, R. Franke, M. Haumann, *J. Ionic Liquids* **2023**, *3* (2), 100061. DOI: 10.1016/j.jil.2023.100061.
- [70] A. Riisager, P. Wasserscheid, R. van Hal, R. Fehrmann, *J. Catal.* **2003**, *219* (2), 452–455. DOI: 10.1016/S0021-9517(03)00223-9.
- [71] A. Weiß, M. Giese, M. Lijewski, R. Franke, P. Wasserscheid, M. Haumann, *Catal. Sci. Technol.* **2017**, *7* (23), 5562–5571. DOI: 10.1039/C7CY01346A.
- [72] H. Gong, X. Zhao, Y. Qin, W. Xu, X. Wei, Q. Peng, Y. Ma, S. Dai, P. An, Z. Hou, *J. Catal.* **2022**, *408*, 245–260. DOI: 10.1016/j.jcat.2022.03.011.
- [73] B. Wei, X. Liu, Y. Deng, K. Hua, J. Chen, H. Wang, S. Sun, *Catal.* **2021**, *11* (23), 14319–14327. DOI: 10.1021/acscatal.1c04022.
- [74] F. Wang, J. Ma, S. Xin, Q. Wang, J. Xu, C. Zhang, H. He, C. Z. Xiao, *Nat. Commun.* **2020**, *11* (1), 529. DOI: 10.1038/s41467-019-13937-1.
- [75] R. Li, L. Luo, X. Ma, W. Wu, M. Wang, J. Zeng, *J. Mater. Chem. A* **2022**, *10* (11), 5717–5742. DOI: 10.1039/d1ta08016d.
- [76] A. Ruiz Puigdollers, P. Schlexer, S. Tosoni, G. Pacchioni, *ACS Catal.* **2017**, *7* (10), 6493–6513. DOI: 10.1021/acscatal.7b01913.
- [77] J. Jupille, G. Thornton, *Defects at oxide surfaces*; Springer: Heidelberg, Germany, 2015. DOI: 10.1007/978-3-319-14367-5.
- [78] Y. Zheng, Q. Yang, S. Wang, S. Furukawa, M. Li, N. Yan, X. Ma, *Appl. Catal. B* **2024**, *350*, 123923. DOI: 10.1016/j.apcatb.2024.123923.
- [79] Y. Zheng, Q. Yang, S. Wang, S. Furukawa, P. Wang, M. Li, N. Yan, X. Ma, *J. Catal.* **2024**, *431*, 115394. DOI: 10.1016/j.jcat.2024.115394.
- [80] Y. Liu, Z. Li, Q. Yu, Y. Chen, Z. Chai, G. Zhao, S. Liu, W.-C. Cheong, Y. Pan, Q. Zhang, et al., *J. Am. Chem. Soc.* **2019**, *141* (23), 9305–9311. DOI: 10.1021/jacs.9b02936.
- [81] Y. Liu, Z. Liu, Y. Hui, L. Wang, J. Zhang, X. Yi, W. Chen, C. Wang, H. Wang, Y. Qin, et al., *Nat. Commun.* **2023**, *14* (1), 2531. DOI: 10.1038/s41467-023-38181-6.
- [82] Z. Mao, Z. Xie, J. G. Chen, *ACS Catal.* **2021**, *11* (23), 14575–14585. DOI: 10.1021/acscatal.1c04359.
- [83] B. F. Machado, M. Oubenali, M. R. Axet, T. T. Nguyen, M. Tunckol, M. Girleanu, O. Ersen, I. C. Gerber, P. Serp, *J. Catal.* **2014**, *309*, 185–198. DOI: 10.1016/j.jcat.2013.09.016.
- [84] M. R. Axet, J. Durand, M. Gouygou, P. Serp, *Adv. Organomet. Chem.* **2019**, *71*, 53–174. DOI: 10.1016/bs.adomc.2019.01.002 From American Chemical Society. All Rights Reserved.
- [85] M. R. Axet, O. Dechy-Cabaret, J. Durand, M. Gouygou, P. Serp, Coordination chemistry on carbon surfaces. In *Coord. Chem. Rev.*, Vol. 308; 2016; pp 236–345.
- [86] I. C. Gerber, P. Serp, *Chem. Rev.* **2020**, *120* (2), 1250–1349. DOI: 10.1021/acscchemrev.9b00209.
- [87] H. Zhang, W. Liu, D. Cao, D. Cheng, *iScience* **2022**, *25* (6), DOI: 10.1016/j.isci.2022.104367.
- [88] W. Shang, B. Qin, M. Gao, X. Qin, Y. Chai, G. Wu, N. Guan, D. Ma, L. Li, *CCS Chem.* **2023**, *5* (7), 1526–1539. DOI: 10.1039/c3cc02020a3.
- [89] M. Hatanaka, T. Yasuda, E. Uchiage, M. Nishida, K.-I. Tominaga, *ACS Sustainable Chem. Eng.* **2021**, *9* (35), 11674–11680. DOI: 10.1021/acssuschemeng.1c02084.
- [90] S. Zhang, J. Zhang, Y. Zhang, Y. Deng, *Chem. Rev.* **2017**, *117* (10), 6755–6833. DOI: 10.1021/acs.chemrev.6b00509.
- [91] D. Krishnan, L. Schill, M. R. Axet, K. Philippot, A. Riisager, *Nanomaterials* **2023**, *13* (9), 1459. DOI: 10.3390/nano13091459.
- [92] D. Krishnan, L. Schill, M. R. Axet, K. Philippot, A. Riisager, *ChemCatChem* **2024**, *16*, e202301441. DOI: 10.1002/cctc.202301441.
- [93] M. Haumann, A. Riisager, *Chem. Rev.* **2008**, *108* (4), 1474–1497. DOI: 10.1021/cr078374z.
- [94] K. Fujimoto, T. Shikada, K. Omata, H. Tominaga, *Chem. Lett.* **1984**, *12*, 2047–2050. DOI: 10.1246/cl.1984.2047.
- [95] A. G. Stepanov, M. V. Luzgin, V. N. Romannikov, K. I. Zamaraev, *J. Am. Chem. Soc.* **1995**, *117* (12), 3615–3616. DOI: 10.1021/ja00117a032.
- [96] Q. Xu, S. Inoue, N. Tsumori, H. Mori, M. Kameda, M. Tanaka, M. Fujiwara, Y. Souma, *J. Mol. Catal. A* **2001**, *170* (1–2), 147–153. DOI: 10.1016/s1381-1169(01)00054-1.
- [97] P. Cheung, A. Bhan, G. J. Sunley, E. Iglesia, *Angew. Chem. Int. Ed.* **2006**, *45* (10), 1617–1620. DOI: 10.1002/anie.200503898.
- [98] Y. Ni, L. Shi, H. Liu, W. Zhang, Y. Liu, W. Zhu, Z. Liu, *Catal. Sci. Technol.* **2017**, *7* (20), 4818–4822. DOI: 10.1039/c7cy01621b.
- [99] M. Boronat, C. Martínez-Sánchez, D. Law, A. Corma, *J. Am. Chem. Soc.* **2008**, *130* (48), 16316–16323. DOI: 10.1021/ja805607m.
- [100] T. Blasco, M. Boronat, P. Concepcion, A. Corma, D. Law, J. A. Vidal-Moya, *Angew. Chem. Int. Ed.* **2007**, *46* (21), 3938–3941. DOI: 10.1002/anie.200700029.
- [101] B. Ellis, M. J. Howard, R. W. Joyner, K. N. Reddy, M. B. Padley, W. J. Smith, *Stud. Surf. Sci. Catal.* **1996**, *101* (Pt. B), 771–779.
- [102] L. Zhou, S. Li, G. Qi, Y. Su, J. Li, A. Zheng, X. Yi, Q. Wang, F. Deng, *Solid State Nucl. Magn. Reson.* **2016**, *80*, 1–6. DOI: 10.1016/j.ssnmr.2016.10.003.
- [103] S. Wang, W. Guo, L. Zhu, H. Wang, K. Qiu, K. Cen, *J. Phys. Chem. C* **2015**, *119* (1), 524–533. DOI: 10.1021/jp511543x.
- [104] G. Ormsby, J. S. J. Hargreaves, E. J. Ditzel, *Catal. Commun.* **2009**, *10* (9), 1292–1295. DOI: 10.1016/j.catcom.2009.02.005.
- [105] J. Qi, P. Christopher, *Ind. Eng. Chem. Res.* **2019**, *58* (28), 12632–12641. DOI: 10.1021/acs.iecr.9b02289.
- [106] J. Qi, J. Finzel, H. Robotjazi, M. Xu, A. S. Hoffman, S. R. Bare, X. Pan, P. Christopher, *J. Am. Chem. Soc.* **2020**, *142* (33), 14178–14189. DOI: 10.1021/jacs.0c05026.
- [107] I. V. Kozhevnikov, *Chem. Rev.* **1998**, *98* (1), 171–198. DOI: 10.1021/cr960400y.
- [108] R. W. Wegman, *J. Chem. Soc. Chem. Commun.* **1994**, *8*, 947–948. DOI: 10.1039/c39940000947.
- [109] G. G. Volkova, L. M. Plyasova, A. N. Salanov, G. N. Kustova, T. M. Yurieva, V. A. Likhobolov, *Catal. Lett.* **2002**, *80* (3–4), 175–179. DOI: 10.1023/A:1015420828251.
- [110] M. V. Luzgin, M. S. Kazantsev, G. G. Volkova, W. Wang, A. G. Stepanov, *J. Catal.* **2011**, *277* (1), 72–79. DOI: 10.1016/j.jcat.2010.10.015.
- [111] L. D. Dingwall, A. F. Lee, J. M. Lynam, K. Wilson, L. Olivi, J. M. S. Deeley, S. Gaemers, G. J. Sunley, *ACS Catal.* **2012**, *2* (7), 1368–1376. DOI: 10.1021/cs3000528.
- [112] A. D. Newman, Y. Wang, S. A. Orr, K. Wilson, A. F. Lee, *Catal. Sci. Technol.* **2022**, *12* (12), 3886–3897. DOI: 10.1039/d2cy00254j.
- [113] K. Park, S. Lim, J. H. Baik, H. Kim, K.-D. Jung, S. Yoon, *Catal. Sci. Technol.* **2018**, *8* (11), 2894–2900. DOI: 10.1039/c8cy00294k.
- [114] J. S. Nam, A. R. Kim, D. M. Kim, T. S. Chang, B. S. Kim, J. W. Bae, *Catal. Commun.* **2017**, *99*, 141–145. DOI: 10.1016/j.catcom.2017.06.007.
- [115] J. Mu, G. Long, X. Song, S. Feng, X. Li, Q. Yuan, B. Li, Z. Jiang, L. Yan, Y. Ding, *Adv. Funct. Mater.* **2023**, *33* (52), 2305823. DOI: 10.1002/adfm.202305823.
- [116] J. H. Kwak, R. Dagle, G. C. Tustin, J. R. Zoeller, L. F. Allard, Y. Wang, *J. Phys. Chem. Lett.* **2014**, *5* (3), 566–572. DOI: 10.1021/jz402728e.
- [117] A. J. R. Hensley, J. Zhang, I. Vincon, X. Pereira Hernandez, D. Tranca, G. Seifert, J.-S. McEwen, Y. Wang, *J. Catal.* **2018**, *361*, 414–422. DOI: 10.1016/j.jcat.2018.02.022.
- [118] W. Shang, M. Gao, Y. Chai, G. Wu, N. Guan, L. Li, *ACS Catal.* **2021**, *11* (12), 7249–7256. DOI: 10.1021/acscatal.1c00950.
- [119] S. Feng, J. Mu, X. Lin, X. Song, S. Liu, W. Shi, W. Zhang, G. Wu, Y. Jiayue, W. Dong, *Appl. Catal. B* **2023**, *325*, 122318. DOI: 10.1016/j.apcatb.2022.122318.
- [120] S. Feng, X. Lin, X. Song, B. Mei, J. Mu, J. Li, Y. Liu, Z. Jiang, Y. Ding, *ACS Catal.* **2021**, *11* (2), 682–690. DOI: 10.1021/acscatal.0c03933.
- [121] S. Feng, X. Song, Y. Liu, X. Lin, L. Yan, S. Liu, W. Dong, X. Yang, Z. Jiang, Y. Ding, *Nat. Commun.* **2019**, *10* (1), 1–9. DOI: 10.1038/s41467-019-12965-1.
- [122] S. Feng, X. Song, Z. Ren, Y. Ding, *Ind. Eng. Chem. Res.* **2019**, *58* (12), 4755–4763. DOI: 10.1021/acs.iecr.8b05402.

- [123] S. Feng, X. Lin, X. Song, Y. Liu, Z. Jiang, Y. Ding, *J. Catal.* **2019**, *377*, 400–408. DOI: 10.1016/j.jcat.2019.06.050.
- [124] M. Jiang, L. Yan, Y. Ding, Q. Sun, J. Liu, H. Zhu, R. Lin, F. Xiao, Z. Jiang, J. Liu, *J. Mol. Catal. A* **2015**, *404–405*, 211–217. DOI: 10.1016/j.molcata.2015.05.008.
- [125] Z. Ren, Y. Lyu, S. Feng, X. Song, Y. Ding, *J. Mol. Catal.* **2017**, *442*, 83–88. DOI: 10.1016/j.mcat.2017.09.007.
- [126] Z. Ren, Y. Lyu, X. Song, Y. Liu, Z. Jiang, R. Lin, Y. Ding, *Adv. Mater.* **2019**, *31* (50), 1904976. DOI: 10.1002/adma.201904976.
- [127] Z. Ren, Y. Liu, L. Yuan, X. Song, C. Zheng, S. Feng, Z. Jiang, Y. Ding, *J. Catal.* **2019**, *369*, 249–256. DOI: 10.1016/j.jcat.2018.11.015.
- [128] Zhou Ren, Yang Liu, Yuan Lyu, Xiangan Song, Changyong Zheng, Zhong Jiang, D. Yunjie, *Chin. J. Catal.* **2021**, *42* (4), 606–617. DOI: 10.1016/S1872-2067(20)63676-2.
- [129] N. F. Dummer, D. J. Willock, Q. He, M. J. Howard, R. J. Lewis, G. Qi, S. H. Taylor, J. Xu, D. Bethell, C. J. Kiely, *Chem. Rev.* **2022**, *123* (9), 6359–6411. DOI: 10.1021/acs.chemrev.2c00439.
- [130] N. J. Gunsalus, A. Koppaka, S. H. Park, S. M. Bischof, B. G. Hashiguchi, R. A. Periana, *Chem. Rev.* **2017**, *117* (13), 8521–8573. DOI: 10.1021/acs.chemrev.6b00739.
- [131] G. Qi, T. E. Davies, A. Nasrallah, M. A. Sainna, A. G. R. Howe, R. J. Lewis, M. Quesne, C. R. A. Catlow, D. J. Willock, Q. He, *Nature Catalysis* **2022**, *5* (1), 45–54. DOI: 10.1038/s41929-021-00725-8.
- [132] N. Antil, M. Chauhan, N. Akhtar, R. Kalita, K. Manna, *J. Am. Chem. Soc.* **2023**, *145* (11), 6156–6165. DOI: 10.1021/jacs.2c12042.
- [133] P. Kumar, T. A. Al-Attas, J. Hu, G. M. Kibria, *ACS Nano* **2022**, *16* (6), 8557–8618. DOI: 10.1021/acsnano.2c02464.
- [134] K. B. Golubev, O. V. Yashina, N. N. Ezhova, N. N. Kolesnichenko, *Mendeleev Commun.* **2021**, *31* (5), 712–714. DOI: 10.1016/j.mencom.2021.09.040.
- [135] T. Moteki, N. Tominaga, M. Ogura, *ChemCatChem* **2020**, *12* (11), 2957–2961. DOI: 10.1002/cctc.202000168.
- [136] X. Fang, F. Wen, X. Ding, H. Liu, Z. Chen, Z. Liu, H. Liu, W. Zhu, Z. Liu, *Angew. Chem. Int. Ed.* **2022**, *61* (31), e202203859. DOI: 10.1002/ange.202203859.
- [137] K. Narsimhan, V. K. Michaelis, G. Mathies, W. R. Gunther, R. G. Griffin, Y. Roman-Leshkov, *J. Am. Chem. Soc.* **2015**, *137* (5), 1825–1832. DOI: 10.1021/ja5106927.
- [138] J. Shan, M. Li, L. F. Allard, S. Lee, M. Flytzani-Stephanopoulos, *Nature* **2017**, *551* (7682), 605–608. DOI: 10.1038/nature24640.
- [139] Y. Tang, Y. Li, V. Fun, D.-e. Jiang, W. Huang, S. Zhang, Y. Iwasawa, T. Sakata, L. Nguyen, X. Zhang, *Nat. Commun.* **2018**, *9* (1), 1231. DOI: 10.1038/s41467-018-03235-7.
- [140] H. Wang, W. Xin, Q. Wang, X. Zheng, Z. Lu, R. Pei, P. He, X. Dong, *Catal. Commun.* **2022**, *162*, 106374. DOI: 10.1016/j.catcom.2021.106374.
- [141] B. Liu, M. Huang, Z. Fang, L. Kong, Y. Xu, Z. Li, X. Liu, *J. Catal.* **2022**, *416*, 68–84. DOI: 10.1016/j.jcat.2022.10.012.
- [142] H. Li, C. Xiong, M. Fei, L. Ma, H. Zhang, X. Yan, P. Tieu, Y. Yuan, Y. Zhang, J. Nyakuchena, et al., *J. Am. Chem. Appl. Catal. B: Environ.* **2021**, *293*, 120208. DOI: 10.1016/j.apcatb.2021.120208.
- [143] B. Li, X. Song, S. Feng, Q. Yuan, M. Jiang, L. Yan, Y. Ding, *Appl. Catal. B: Environ.* **2021**, *293*, 120208. DOI: 10.1016/j.apcatb.2021.120208.
- [144] H. Li, M. Fei, J. L. Troiano, L. Ma, X. Yan, P. Tieu, Y. Yuan, Y. Zhang, T. Liu, X. Pan, et al., *J. Am. Chem. Soc.* **2023**, *145* (2), 769–773. DOI: 10.1021/jacs.2c09434.
- [145] W. Xu, H.-X. Liu, Y. Hu, Z. Wang, Z.-Q. Huang, C. Huang, J. Lin, C.-R. Chang, A. Wang, X. Wang, et al., *Angew. Chem. Int. Ed.* **2024**, *63* (16), e202315343. DOI: 10.1002/anie.202315343.
- [146] C.-W. Wang, Y. Sun, L.-J. Wang, W.-H. Feng, Y.-T. Miao, M.-M. Yu, Y.-X. Wang, X.-D. Gao, Q. Zhao, Z. Ding, et al., *Appl. Catal. B* **2023**, *329*, 122549. DOI: 10.1016/j.apcatb.2023.122549.
- [147] J. Liu, Y. Wei, R. Li, Y. Liu, H. Yu, X. Zhou, B. Wu, T. Lin, L. Zhong, *Appl. Catal. B* **2024**, *350*, 123951. DOI: 10.1016/j.apcatb.2024.123951.
- [148] K. B. Golubev, O. V. Yashina, T. I. Batova, N. V. Kolesnichenko, N. N. Ezhova, *Pet. Chem.* **2021**, *61*, 663–669. DOI: 10.1134/S0965544121040058.
- [149] N. V. Kolesnichenko, Y. M. Snatenkova, T. I. Batova, O. V. Yashina, K. B. Golubev, *Microporous Mesoporous Mater.* **2022**, *330*, 111581. DOI: 10.1016/j.micromeso.2021.111581.
- [150] N. V. Kolesnichenko, T. I. Batova, A. N. Stashenko, T. K. Obukhova, E. V. Khramov, A. A. Sadovnikov, D. E. Zavelev, *Microporous Mesoporous Mater.* **2022**, *344*, 112239. DOI: 10.1016/j.micromeso.2022.112239.
- [151] M. Beller, X.-F. Wu, Hydroxy-, alkoxy- and aminocarbonylations of C–X bonds. In *Transition metal catalyzed carbonylation reactions*, Springer Berlin Heidelberg, 2013; pp 13–52.
- [152] J. Vondran, M. R. L. Furst, G. R. Eastham, T. Seidensticker, D. J. Cole-Hamilton, *Chem. Rev.* **2021**, *121* (11), 6610–6653. DOI: 10.1021/acs.chemrev.0c01254.
- [153] J. An, Y. Wang, J. Lu, J. Zhang, Z. Zhang, S. Xu, X. Liu, T. Zhang, M. Gocyla, M. Heggen, *J. Am. Chem. Soc.* **2018**, *140* (11), 4172–4181. DOI: 10.1021/jacs.8b01742.
- [154] A. Wang, L. Zhang, Z. Yu, S. Zhang, L. Li, Y. Ren, J. Yang, X. Liu, W. Liu, X. Yang, et al. *J. Am. Chem. Soc.* **2024**, *146* (1), 695–706. DOI: 10.1021/jacs.3c10551.
- [155] Y. Ma, Y. Jiang, X. Wei, Q. Peng, S. Dai, Z. Hou, *ACS Sustainable Chem. Eng.* **2022**, *10* (47), 15389–15401. DOI: 10.1021/acssuschemeng.2c04089.
- [156] Q. Yuan, X. Song, S. Feng, M. Jiang, L. Yan, J. Li, Y. Ding, *Chem. Commun.* **2021**, *57* (4), 472–475. DOI: 10.1039/d0cc06863b.
- [157] Q. Yuan, Y. Gu, S. Feng, X. Song, J. Mu, B. Li, X. Li, Y. Cai, M. Jiang, L. Yan, et al. *ACS Catal.* **2022**, *12* (7), 4203–4215. DOI: 10.1021/acscatal.1c06039.
- [158] X. Li, J. Wang, Q. Yuan, X. Song, J. Mu, Y. Wei, L. Yan, F. Sun, S. Feng, Y. Cai, *Angew. Chem. Int. Ed.* **2023**, *62* (33), e202307570. DOI: 10.1002/anie.202307570.
- [159] Q. Guo, Y. Wang, J. Han, J. Zhang, F. Wang, *ACS Catal.* **2022**, *12* (6), 3286–3290. DOI: 10.1021/acscatal.2c00346.
- [160] J. Shi, Y. Cui, H. Sun, H. Wang, C. Liu, X. Xue, C. Li, L. Geng, J. Liu, M. Jia, *Chem. Eng. J.* **2023**, *466*, 143317. DOI: 10.1016/j.cej.2023.143317.
- [161] K. M. Driller, H. Klein, R. Jackstell, M. Beller, *Angew. Chem. Int. Ed.* **2009**, *48* (33), 6041–6044. DOI: 10.1002/anie.200902078.
- [162] L. Wu, Q. Liu, R. Jackstell, M. Beller, *Angew. Chem. Int. Ed.* **2014**, *53* (25), 6310–6320. DOI: 10.1002/anie.201400793.
- [163] P. Gautam, B. M. Bhanage, *Catal. Sci. Technol.* **2015**, *5* (10), 4663–4702. DOI: 10.1039/c5cy00691k.
- [164] R. Giovanelli, G. Bertuzzi, M. Bandini, *ChemCatChem* **2023**, *15* (20), e202300827. DOI: 10.1002/cctc.202300827.
- [165] K. Zhang, L. Zong, X. Jia, *Adv. Synth. Catal.* **2021**, *363* (5), 1335–1340. DOI: 10.1002/adsc.202001336.
- [166] Y. Li, Y. Chen, Y.-L. Wan, R.-S. Wang, H. Wang, Y.-Z. Lei, *J. CO<sub>2</sub> Util.* **2022**, *65*, 102214. DOI: 10.1016/j.jcou.2022.102214.
- [167] Y. Shen, Q. Zheng, Z.-N. Chen, D. Wen, J. H. Clark, X. Xu, T. Tu, *Angew. Chem. Int. Ed.* **2021**, *60* (8), 4125–4132. DOI: 10.1002/anie.202011260.

Manuscript received: March 20, 2024

Revised manuscript received: May 21, 2024

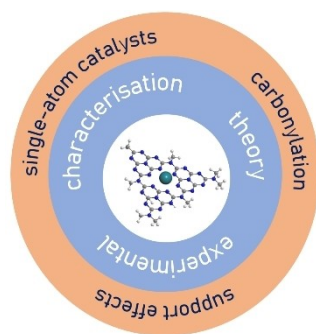
Accepted manuscript online: May 22, 2024

Version of record online: ■■■

## REVIEW

---

This minireview explores recent advances in tailoring solid supports for single-atom catalysts (SACs) to enhance their catalytic performance in carbonylation reactions, including hydroformylation, methanol carbonylation, and oxidative carbonylation as the main reactions. The review underscores the importance of optimizing solid supports for SACs to achieve highly active and selective catalysts in these reactions. It also emphasizes the need to combine advanced in situ/operando characterization techniques and theoretical calculations to gain further insights and provide structure-property correlations, paving the way for future developments in sustainable catalysis.



*L. Jurado, S. Posada-Pérez, M. R. Axet\**

1 – 30

### **Carbonylation Reactions Using Single-Atom Catalysts**